O2 ACTIVATION AT BIOINSPIRED COMPLEXES: DINUCLEAR COPPER SYSTEMS AND MONONUCLEAR NON-HEME IRON COMPOUNDS. MECHANISM AND CATALYTIC APPLICATIONS IN OXIDATIVE TRANSFORMATIONS
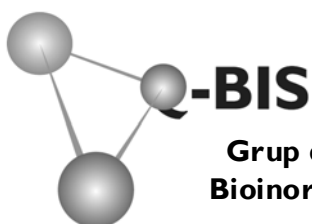
Anna COMPANY CASADEVALL

Q-BIS

Grup de Recerca de Química Bioinorgànica i Supramolecular

Universitat de Girona
Departament de Química
Àrea de Química Inorgànica

O_2 activation at bioinspired complexes: dinuclear copper systems and mononuclear non-heme iron compounds.
Mechanisms and catalytic applications in oxidative transformations

PhD dissertation presented by

ANNA COMPANY CASADEVALL

In candidacy for the degree of

Doctor of Philosophy in Chemistry

Girona, December 2008

El sotasignant Dr. **Miquel Costas Salgueiro**, Professor Titular del Departament de Química de la Universitat de Girona, CERTIFICA que:

La memòria que porta per títol *"O$_2$ activation at bioinspired complexes: dinuclear copper systems and mononuclear non-heme iron compounds. Mechanisms and catalytic applications in oxidative transformations"* recull el treball realitzat sota la seva direcció per l'**Anna Company Casadevall**, Llicenciada en Química per la Universitat de Girona, i que constitueix la seva memòria de Tesi Doctoral per aspirar al grau de Doctora en Ciències, especialitat Química.

I perquè així consti, signa aquest certificat el dia 15 de novembre de 2008.

Dr. Miquel Costas Salgueiro

Agraïments

Ja fa 4 anys des de que vaig començar el doctorat i la veritat és que m'ha passat volant. Suposo que perquè aquesta etapa de la meva vida ha estat, sense cap mena de dubte, una època inoblidable no només per tot el que he après però sobretot per la gent que he conegut.

Primer de tot he de donar les gràcies a en Miquel Costas, el meu director de tesi. Miquel, t'asseguro que m'és molt difícil expressar-te amb poques paraules el meu agraïment. Malgrat que ara ja fa temps que ens coneixem, encara em segueix impressionant el teu entusiasme i la teva implicació en la recerca. M'ha encantat poder treballar amb tu i que m'hagis donat l'oportunitat d'aprendre un munt de coses noves. Gràcies per la teva paciència, pels teus consells i pels teus ànims quan han fet falta. Em sembla que hem fet una molt bona feina amb els recursos que tenim. Estic segura que no hauria pogut trobar enlloc un "jefe" com tu. També vull donar especialment les gràcies a en Xavi Ribas. Xavi, gràcies per ensenyar-me que val la pena fer les coses ben fetes i per donar el toc assenyat i raonable quan a vegades hem volgut accelerar el ritme. Gràcies a tots dos pels vostres consells i les vostres idees però sobretot gràcies per haver-vos preocupat per mi quan les coses a nivell personal s'han complicat una mica més del compte. Us heu convertit en molt més que uns simples "jefes" per mi, us ho puc ben assegurar.

També valoro especialment l'oportunitat que m'ha donat el doctorat per fer dues estades a l'estranger: a la University of Minnesota (Minneapolis) sota la supervisió del Prof. Dr. Lawrence Que Jr. i al Max Planck Institute für Bioanorganische Chemie (Mülheim an der Ruhr) al grup del Prof. Dr. Karl Wieghardt. Ha estat una gran experiència conèixer dos grans laboratoris en els quals es fa recerca de primer nivell i on hi treballa gent amb un gran talent dels quals també he après molt. Per altra banda, també vull destacar que el treball inclòs en aquesta memòria no hagués estat possible sense les múltiples col·laboracions que mantenim tant a nivell nacional com internacional. Els càlculs teòrics han estat realitzats a l'Institut de Química Computacional (Universitat de Girona). L'Albert Poater (sota la supervisió del Dr. Miquel Solà) i la Mireia Güell (dirigida pel Dr. Josep Mª Luis) han fet moltíssima feina per poder calcular estructures i camins de reacció que no són gens fàcils de modelar. Em sembla que aquesta col·laboració ha donat fruits molt interessants i estic segura que encara sortiran alguns treballs més. Moltes gràcies. Per altra banda, també hem col·laborat amb el Prof. Luigi Casella (University of Pavia), la Dra. Elena Rybak-Akimova fent estudis de stopped-flow (Tufts University), en Rubén Mas-Ballesté que ha fet part dels experiments de ressonància Raman (University of Minnesota), el Dr. Teodor Parella fent alguns dels estudis de RMN (Universitat Autònoma de Barcelona) i, finalment, amb el Dr. Jordi Benet-Buchholz (Institut Català d'Investigació Química) i en Xavier Fontrodona (Universitat de Girona) que s'han encarregat de la resolució de les estructures de raigs X.

Gràcies a tots els companys de l'àrea de Química Inorgànica per fer-me el camí tan fàcil: la Marisa, la Montse (la reina de la informàtica), la MªÁngeles, l'Ester, la Cristina, en Raül, en Xavi Sala, la Vero, en Mohammed, en Quim Mola (de Ventdelplà), en Jordi Rich (que ja s'ha convertit en

l'organitzador oficial de sopars) i la Irene (que acaba de començar però a qui segur que li anirà molt bé). Laura, gràcies per ser-hi des de gairebé el primer dia perquè ja saps que els començaments sempre són difícils i sense tu hagués estat tot molt més complicat. Ha estat un plaer tenir-te a la poiata del davant, poder treballar juntes i trobar una bona amiga. Isaac, com ho fas per estar sempre de bon humor i tenir alguna bestiesa per dir a cada moment? Gràcies per fer tanta feina i "amb tanta qualitat" i per fer-nos riure tant. Arnau, per què no pares de queixar-te ni un sol dia de la teva vida? En fi, al final em sembla que m'hi he acostumat. Gràcies per dir-ne sempre de les teves i per ser tan sincer de tant en tant. Ha estat molt bé conèixer un "fenómeno" com tu. Alicia, espero que tinguis èxit en la dura lluita contra el desordre al laboratori. Jo ho he intentat quatre anys però mentre hi hagi l'Arnau no esperis aconseguir gaire res de bo. Isabel, merci per compartir amb mi molts cotilleos, per escoltar-me, per ser una companyia tan agradable i... "porque tu lo vales". Molts de vosaltres no heu estat simples companys de feina i m'heu ajudat molt més del que us podeu imaginar quan m'heu fet riure i també quan m'heu preguntat que com em va. Moltíssimes gràcies.

Gràcies també als becaris de química orgànica amb els quals he compartit laboratori i que m'han donat consells en qüestions de síntesi orgànica. I, tampoc em vull oblidar dels químics teòrics (malgrat ser freakies, són bones persones) amb qui he compartit sopars molt divertits.

També vull mencionar especialment a la colla d'amigues de Banyoles amb qui ja portem més de 10 anys juntes: l'Anna, la Magda, la Nuri, l'Imma, la Laura i la Meritxell. Espero que continuem juntes molts anys més, sou genials i m'encanta poder ser amiga vostra.

I finalment, un agraïment molt especial a la meva família i sobretot als meus pares que sempre m'han recolzat en totes les decisions que he pres i s'han preocupat d'entendre quin és el camí que vull seguir. M'heu demostrat que treballant es pot arribar lluny i gràcies a vosaltres he après que en aquesta vida s'ha de ser valent i que els problemes (que a vegades s'acumulen) s'han d'afrontar de cara i sense por. Sou un gran exemple per mi i estic segura que tot anirà bé. I també vull donar les gràcies a la Nuri, la meva germana. Gràcies per compartir amb mi confidències, riures, plors i alguna vegada discussions d'aquelles que fan història. Nuri, tu vals molt i encara que a vegades no t'ho demostri, no sé què faria sense tu. També donar les gràcies a la meva àvia pel seu amor incondicional. I un record especial pel tiu i l'avi a qui sempre tindré presents i que haurien estat molt orgullosos si haguessin pogut veure aquesta tesi. I, finalment, vull donar les gràcies a l'Eduard que ha estat al meu costat durant els darrers anys (que ràpid que passa el temps). Compartir amb tu aquest temps i saber que estàs sempre al meu costat és meravellós. Gràcies per fer-te imprescindible en la meva vida, per tots els moments que hem viscut junts i per tots els que vindran tant si estem a prop com lluny.

Moltes gràcies a tots.

Anna

Als de casa (tant als que hi són com als que ja no hi són),

a l'Edu.

Contents

Supplementary digital material

The material listed below can be found in the attached CD:

- pdf file of the PhD dissertation
- cif files for each crystal structure presented within this thesis

Chapter	Crystal structure	File name
Chapter III.1	$[Cu_2(Me3m)](BArF)_2$	1(BArF)2
	$[Cu_2(\textit{m}\text{-XYL}^{MeAN})](SbF_6)_2$	2(SbF6)2
Chapter III.3	$[Cu_2(^{H}L)](ClO_4)_2$	1ClO4
	$[Cu_2(^{tBu}L)](ClO_4)_2$	2ClO4
	$[Cu_2(^{tBu}L)](CF_3SO_3)_2$	2CF3SO3
	$[Cu_2(^{NO2}L)(CH_3CN)](BArF)_2$	3BArF·CH3CN
Chapter IV.1	$[Fe(PyMe_2tacn)(CH_3CN)_2](PF_6)_2$	[3CH3CN]PF6
	$[Fe(Py(\textit{i}Pr)_2tacn)(CF_3SO_3)_2]$	1CF3SO3
Chapter IV.2	$[Fe(PyMe_2tacn)(CF_3SO_3)_2]$	1
Chapter IV.3	$[Fe(6Me\text{-}PyMe_2tacn)(CH_3CN)_2](ClO_4)_2$	[2CH3CN]ClO4 (100K)
	$[Fe(6Me\text{-}PyMe_2tacn)(CH_3CN)_2](ClO_4)_2$	[2CH3CN]ClO4 (210K)
	$[Fe(6Me\text{-}PyMe_2tacn)(H_2O)_2](CF_3SO_3)_2$	[2H2O]CF3SO3
	$[Fe(6F\text{-}PyMe_2tacn)(CF_3SO_3)_2]$	3CF3SO3
	$[Fe(pinene\text{-}PyMe_2tacn)(CF_3SO_3)_2]$	4CF3SO3
	$[Fe(4Me\text{-}PyMe_2tacn)(CF_3SO_3)_2]$	5CF3SO3
	$[Fe(4,6Me_2\text{-}PyMe_2tacn)(CF_3SO_3)_2]$	6CF3SO3
Chapter IV.6	$[Fe_2(O)(COOCH_3)(PyMe_2tacn)_2](ClO_4)_3$	3ClO4

Chapter I

General introduction

Table of contents

I.1. O$_2$ activation and model systems

I1.1. Molecular O$_2$: biological roles and chemical properties

Dioxygen serves at least two important roles in aerobic life. The most commonly appreciated function is its role as the terminal electron acceptor in processes such as cellular respiration through which electron and proton gradients are generated *via* O$_2$-reduction to water. These gradients are subsequently employed in the biosynthesis of the central energy-rich molecules used throughout the metabolism. The second role played by dioxygen in aerobic organisms involves enzymes that can convert dioxygen to alternative forms that constitute highly specialized oxidizing reagents used to catalyze the synthesis of important biomolecules, and or the degradation of xenobiotics.[1]

The dioxygen molecule has a high potential reactivity that is kept in control by its particular molecular structure. In general, the dioxygen-utilizing reactions involve the cleavage of the oxygen-oxygen bond and the formation of C-O and O-H bonds (usually water is also formed). These processes are energetically very favorable, i.e., exothermic. Despite this strong thermodynamic driving force, the chemical reactivity of dioxygen with organic molecules at ambient temperatures is intrinsically low. If this was not the case, dioxygen would spontaneously oxidize organic compounds to CO$_2$ and water, and life would not exist in its current form. The low kinetic reactivity of dioxygen is due to its unfavorable one-electron reduction potential and more important, to its triplet ground state (S = 1): molecular oxygen is a diradical having two unpaired electrons (Scheme 1). The two oxygen atoms share six electrons in the σ_{2pz}, π_{2px} and π_{2py} molecular orbitals and two unpaired electrons reside in the two degenerate antibonding π_{2px}* and π_{2py}* orbitals, leaving O$_2$ with a formal bond order of two. The triplet ground state of O$_2$ makes the direct reaction with singlet molecules (S = 0), the spin-paired state of most organic molecules representative of biological substrates, a spin-forbidden process.[2]
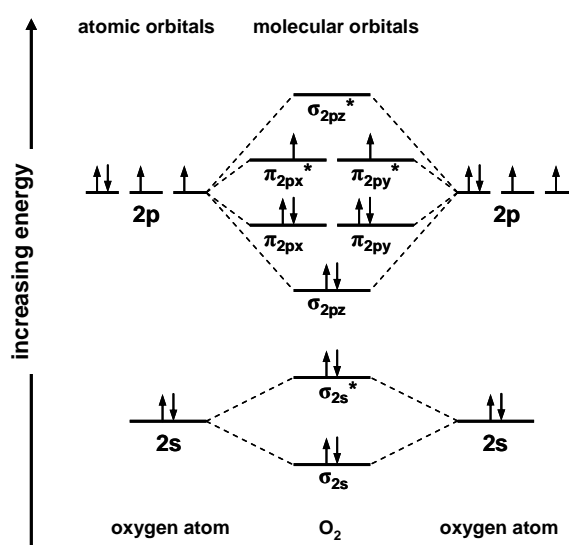
Scheme 1. Molecular orbitals energy diagram for O$_2$.

The central question arising from this observation is how O_2 can react at ambient temperature and with high specificity in natural systems. The answers to this question are of fundamental importance in understanding the wide range of interacting O_2-dependent metabolic processes that make life possible despite living surrounded by oxygen. However, understanding of nature's oxygen activation strategies also has many direct applications, including (a) the design of new pharmaceuticals relevant to a wide variety of diseases, (b) the development of targeted biodegradation systems for the environment, (c) novel technological applications based in oxidation reactions such as pulp bleaching and paper whitening, and (d) the preparation of catalysts for the conversion of abundant molecules to value-added synthons.

In order to overcome the high kinetic barrier inherent to the reactions of triplet O_2, in nature dioxygen is activated from its abundant triplet ground state to reactive singlet or doublet species (O_2^-, O_2^{2-}) by oxidase and oxygenase enzymes. In many cases, these enzymes generate species of even greater reactivity by cleaving the O-O bond. Generally, nature's strategy involves a transition metal (mainly Cu and Fe but also Mn, Ni and Zn), which in the appropriate oxidation state is able to react directly with triplet O_2 to form dioxygen adducts that can participate in reaction pathways leading either to the incorporation of oxygen atoms into organic substrates or to their oxidation. All of these reactions are tightly regulated both spatially and temporally so that specific chemistry occurs and it is compatible with downstream metabolic pathways or specific functions.

In all biological systems, the O_2 molecule needs to be reductively activated because simple inversion of an oxygen electron to yield directly the singlet state is highly endothermic. The source of the activating electrons is quite varied; the list includes the metal, the organic substrate itself, a cosubstrate, a second redox-active metal or cofactor, reduced pyridine nucleotide and for some oxidases, ascorbate.

The understanding of biological oxygen activation mechanisms has been advanced in recent years through the concomitant use of chemical, structural, spectroscopic and computational approaches and by the combined study of enzymes and model systems.[3-7]

I1.2. Metalloenzymes and model compounds

Among the known structurally characterized proteins, one in three contains a metal in their active site. The majority of these metalloproteins are enzymes which are also called "biological catalysts". Metal ions only account for less than 1% of the total protein weight, but their ability to exist in multiple oxidation states and different geometries allows them to promote complex biochemical reactions and participate in highly specialized biological functions such as oxygen activation.[2]

Metalloproteins are involved in many biological processes like electron transport, oxygen storage, metal transport, chemical bond hydrolysis, redox processes or synthesis of biochemical compounds. The reactivity of the active center depends on several factors: the

nature of the metal and the ligand, the coordination geometry of the metal center, the relative disposition of the metal centers in polymetallic systems and the tridimensional configuration of the polypeptidic chain. All these factors determine the ability of the metal ion to stabilize different oxidation states, to react with the substrate, and the formation of cavities capable of controlling the accessibility of the substrate to the metallic center.

The main aim of bioinorganic chemistry is structurally characterize the active site of proteins and study their reactivity. However, several difficulties arise when working with proteins because, apart from being macromolecules with a high molecular weight, they are generally obtained in low quantity by means of complicated processes of isolation and purification. A different strategy to study these biological systems is to take advantage of synthetic model chemistry (biomimetic studies).[8] Its objective is the preparation of synthetic models (small-molecule transition metal complexes) in order to achieve two main goals: mimicking the function of an enzyme that catalyzes an important chemical transformation or gaining scientific insight into the biological system, by providing mechanistic, structural, and spectroscopic data for comparison with the protein. In model chemistry, the accomplishment of these objectives often begins with the preparation of a suitable ligand (organic synthesis) and continues through several steps towards the ultimate goal of catalytic reactivity.

In this thesis we take advantage of the model chemistry approach in order to study O_2-activating proteins. Particularly, the work is centered in developing models for those enzymes containing a dinuclear copper center or a mononuclear non-heme active site.

I.2. O$_2$ activation by copper systems

I2.1. Biological role of copper

Since 1925, it is well known that copper is an essential element, and, in fact, it is found in most living organisms. Despite being present only in trace amounts, it is essential for life. In metalloenzymes, copper exists in mononuclear and coupled multinuclear configurations that have evolved to facilitate redox processes. Besides, copper centers can share the active site with other metal ions like zinc or iron.

Conventional wisdom suggests that biological Cu serves exclusively as 1e⁻ shuttle, alternating between Cu^{I} and Cu^{II}. The Cu^{III} state is generally considered to be inaccessible because of the highly positive Cu^{III}/Cu^{II} redox potentials. However, several reaction mechanisms postulate the existence of intermediates in which the copper center reaches an oxidation state higher than the common. Such state has so far not been detected in biological systems.

The versatility of copper is clearly reflected by the wide range of biological reactions that catalyses. However, in most cases, the role of this metal ion is directly related to two basic functions: electron transfer and O$_2$ activation and transport.[2,9]
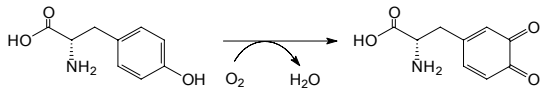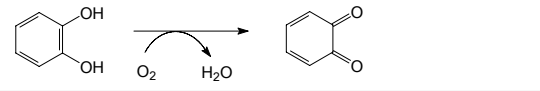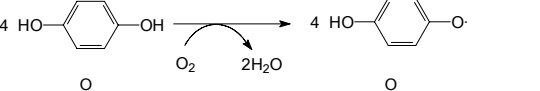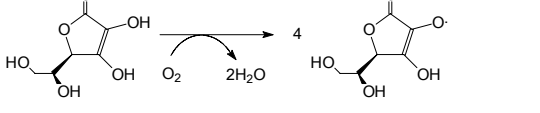
The electron transfer activity is performed by the so called "blue copper proteins". Their characteristic blue color comes from an intense absorption band at $\lambda \sim 600$ nm ($\varepsilon > 3000$M^{-1}cm^{-1}) which is assigned to a thiolate-to-copper charge transfer (LMCT) band.

Transport and activation of O$_2$ is carried out by a wide range of enzymes. In the following section, copper proteins implicated in O$_2$ activation will be described in more detail.

I2.1.1. Copper proteins implicated in O$_2$ activation

Scheme 2 shows the most important copper proteins involved in the interaction with O$_2$ and the reactions they catalyze. These proteins are classified in 5 groups depending on the structure of their active center.[7,10]

	PROTEIN	CATALYTIC REACTION
coupled dinuclear center	Hemocyanin	$deoxyHc[Cu^I Cu^I] + O_2 \rightleftharpoons oxyHc[Cu^{II}\text{-}O_2^{2-}\text{-}Cu^{II}] + O_2$
	Tyrosinase	(L-tyrosine) $\xrightarrow[H_2O]{O_2}$ (dopaquinone)
	Catechol oxidase	(catechol) $\xrightarrow[H_2O]{O_2}$ (o-quinone)
trinuclear center	Laccase	$4\ HO\text{-}C_6H_4\text{-}OH \xrightarrow[2H_2O]{O_2} 4\ HO\text{-}C_6H_4\text{-}O\cdot$
	Ascorbate oxidase	4 (ascorbate) $\xrightarrow[2H_2O]{O_2} 4$ (ascorbate radical)
	Ceruloplasmin, FET3	$4\ Fe^{2+} \xrightarrow[2H_2O]{O_2} 4\ Fe^{3+}$
polymetallic center	Superoxide dismutase: Cu/Zn	$2 O_2^- + 2H^+ \longrightarrow O_2 + H_2O_2$
	Cytochrome c oxidase: Cu/Fe	$O_2 + 4e^- + 4H^+ \longrightarrow H_2O$

Scheme 2. Copper proteins involved in oxygen binding and activation.

The nuclearity (number of metallic centers in the active site) is not directly related to the function of the enzyme. For example, dopamine β-hydroxylase and tyrosinase are monooxygenases and both of them hydroxylate a specific substrate. However, they possess a dinuclear center with completely different structural properties: in dopamine β-hydroxylase the copper atoms are non-coupled (no bridging ligand mediates electronic coupling between the two metallic centers, so that O$_2$ activation only occurs in one center and the second one acts as an electron source) whilst in tyrosinase the two metal centers bind simultaneously to one O$_2$ molecule. On the other hand, a given nuclearity does not determine a specific activity. This is the case of hemocyanin and tyrosinase which have an almost identical active site but they develop completely different functions: hemocyanin reversibly coordinates O$_2$ (transport) but tyrosinase acts as a monooxygenase and oxidase protein. In fact, these two proteins serve as a paradigm for understanding how O$_2$ can be bound and activated at a dicopper site.

I2.1.2. Hemocyanin and tyrosinase

Before any X-ray crystallographic information on hemocyanin or tyrosinase was available, spectroscopic and mechanistic experiments had already shown that the active site of both enzymes is very similar,[11,12] which was further corroborated by X-ray studies.[13,14]

The active site of tyrosinase and hemocyanin is constituted by two copper atoms which are coordinated to three histidine residues per copper. In the reduced form, Cu^I ions show a trigonally distorted coordination geometry and they are separated by 4.6 Å. However, in the oxygenated form, O$_2$ is reduced by 2e$^-$ to form a peroxide ion, which is ligated in a μ-η^2:η^2 mode

(see section I2.2.1). Each five-coordinated Cu^{II} center has a distorted square-pyramidal geometry with one histidine nitrogen atom that is weakly associated; the Cu···Cu separation of *ca.* 3.6 Å is significantly contracted relative to that in the reduced form (Figure 1).
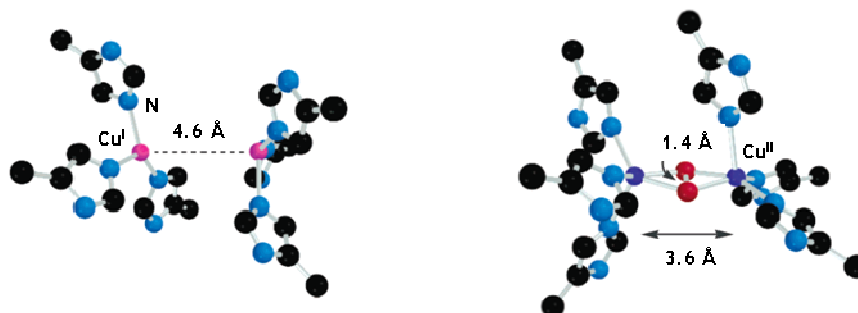
Figure 1. Reduced and oxygenated forms of hemocyanin.

In spite of having an almost identical active center, the different reactivity between hemocyanin and tyrosinase can be explained on the basis of the structure of the polypeptidic chain around the active site. In hemocyanin there is a protein domain that shields the access of substrates to the dicopper center of the protein. Because this domain interferes with the binding of the substrate, hemocyanin can play only one role, namely, that of an oxygen transporter by the reversible coordination of dioxygen to the active site. In fact, hemocyanin serves as oxygen carrier in some arthropods and molluscs, analogous to hemoglobin in vertebrates.[15] On the other hand, tyrosinase is a monooxygenase enzyme that catalyzes the electrophilic hydroxylation of phenol to catechol (*ortho*-diphenol) and the two-electron oxidation of the formed catechol to *ortho*-quinone (Scheme 3). It has been found that the active site of tyrosinase is situated close to the molecular surface, a useful location to ensure the access of the substrate. Moreover, analysis of the crystal structure indicates that the substrate-binding pocket has a large vacant space above the dicopper center which allows direct interaction between the substrate (phenol) and the active site.[14]
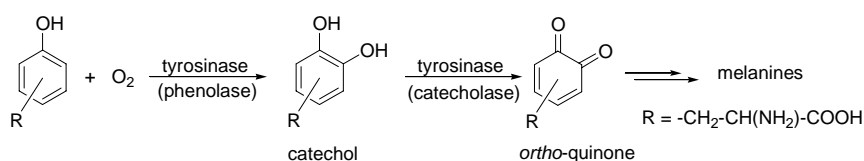
Scheme 3. Biological function of tyrosinase towards the final synthesis of melanines.

A recent work demonstrates that hemocyanin can exhibit efficient monooxygenase activity (phenolase activity) if the polypeptidic chain is altered by treatment with urea. This observation corroborates the identical active center between both proteins and the critical role that plays the folding of the polypeptidic chain to determine the function of a specific enzyme.[16]

The proposed mechanism for the hydroxylation of phenols by tyrosinase is depicted in Scheme 4.[10,17]
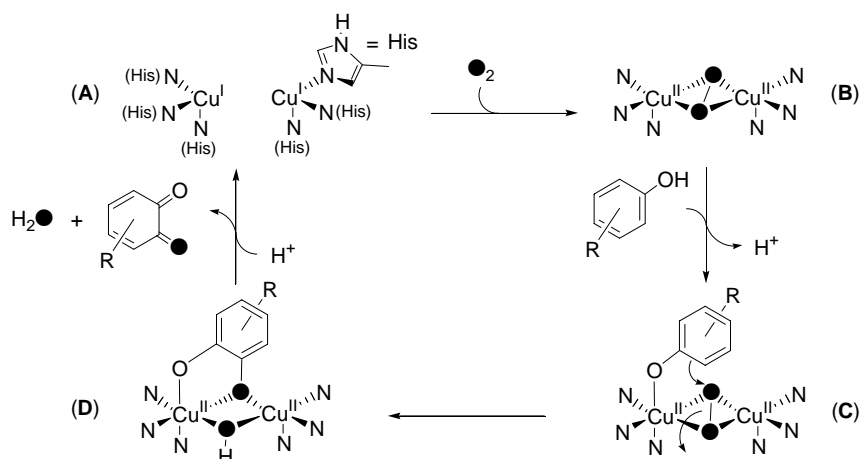
Scheme 4. Hydroxylation of a monophenolic substrate by tyrosinase.

In the first step of the catalytic cycle, the reduced form of tyrosinase (**A**) interacts with molecular O_2 to give the oxygenated intermediate (**B**) in which a peroxo ligand is coordinated in a $\mu\text{-}\eta^2\text{:}\eta^2$ mode to the two Cu^{II} centers. At this point, the substrate approaches the active center and it is preoriented by hydrophobic interactions with the histidine residues that coordinate the metal center and by hydrogen-bonding interactions with nearby protein residues. The substrate binds to one of the metal centers (**C**) and hydroxylation of the aromatic ring occurs. To this end, the O-O axis of the peroxo ligand rotates and it points towards the phenolic ring. The proximity of the *ortho* position of the phenolic ring to the side-on coordinated peroxo group enables an electrophilic attack of the Cu_2O_2 moiety on the aromatic ring, whereby concomitant cleavage of the O-O bond occurs, so that the resulting diphenolic moiety binds in a bidentate fashion (**D**). Finally, release of the *ortho*-quinone product regenerates the reduced form (**A**). Overall, the active center of tyrosinase accommodates important changes during the catalytic cycle which are only possible with a highly flexible dicopper center. Indeed, this flexibility has been clearly evidenced by crystallographic studies.[14]

I2.2. O₂ Binding and activation by biomimetic Cu complexes

The biological importance of the reactions involved in the copper regulated O_2 metabolism and the potential technological utility of the oxidation reactions catalyzed by copper dependent enzymes have fueled great efforts in understanding the reaction mechanisms regulating O_2 activation by these metalloproteins. A particular strategy to achieve these goals has been the study of the reaction of bioinspired synthetic models with O_2.

The study of mono- and dinuclear copper complexes with simple ligands reproducing the coordination environment of the metal center in proteins has allowed the characterization of a wide range of novel chemical species resulting form the interaction of O_2 with copper(I). These Cu:O_2 type of species tend to be highly unstable and, in fact, the advance in stabilizing and characterizing Cu:O_2 species formed by the oxygenation of Cu^I complexes can be attributed

partly to a greater accessibility of appropriate spectroscopic tools and to a better appreciation of the appropriate reaction conditions. Low temperatures (*ca.* 200 K), aprotic solvents (*e.g.*, CH$_2$Cl$_2$, THF, acetone) and weakly coordination anions are now standard conditions. Due to their high instability, these compounds are called the "intermediate species" formed upon Cu^I to Cu^{II} oxidation by O$_2$. The identification and characterization of these intermediates has been crucial to postulate possible reaction mechanisms of natural enzymes.

I2.2.1. Interaction of O$_2$ with copper model complexes

One of the most relevant aspects of the chemistry of Cu^I complexes is their interaction with molecular O$_2$ which causes the total or partial reduction of O$_2$ and the oxidation of the metallic center to Cu^{II} or even Cu^{III}.

Several Cu^I complexes have been synthesized and their reactivity towards O$_2$ has been thoroughly studied which has allowed the determination of different coordination modes in Cu$_n$-O$_2$ type of systems. The most relevant detected and characterized species derived from the interaction of Cu^I model compounds with O$_2$ are presented in Scheme 5. They are classified depending on the Cu:O$_2$ ratio and the copper oxidation state.[7,18]
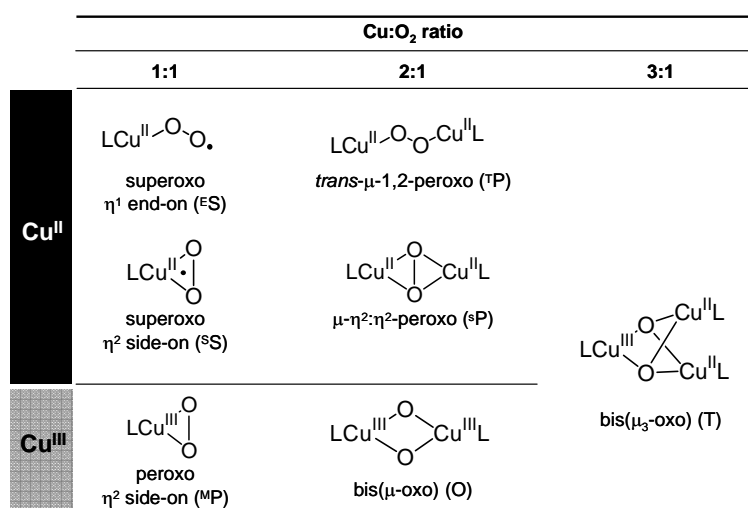
Scheme 5. Cu:O$_2$ species formed by reaction of Cu^I complexes with O$_2$.

I2.2.1.1. Intermediate species Cu:O$_2$ 1:1

Mainly, mononuclear Cu:O$_2$ 1:1 complexes correspond to superoxide species. Most experimental data suggests that oxygenation of copper(I) complexes proceeds *via* formation of Cu^{II}-superoxo species. In several cases, the existence of this type of intermediates has been confirmed by structural and/or spectroscopic means.

In solution, the superoxo species tend to react with a second equivalent of Cu^I complex (Scheme 6) which implies that in most cases, despite being formed, they are difficult to detect due to their high reactivity. Low-temperature stopped-flow UV-vis spectroscopy is a powerful technique for characterizing such transient species.[19]

$$LCu^I + O_2 \rightleftharpoons LCu^{II}\text{-}(O_2^{\bullet -}) \xrightarrow{ LCu^I } LCu^{II}\text{-}(O_2^{2-})\text{-}Cu^{II}L$$
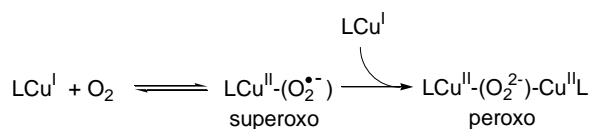
$$ \text{superoxo} \text{peroxo}$$

Scheme 6. Generation of superoxo complexes from mononuclear Cu^I compounds and their reaction with another Cu^I to give a peroxo intermediate.

Despite the predilection of superoxo species to form higher nuclearity $Cu:O_2$ complexes, an increase in the steric hindrance of the ligands and the use of anionic rather than neutral ligands can sufficiently attenuate the second process depicted in Scheme 6, so that 1:1 complexes can be isolated and characterized. Indeed, the crystal structure of three superoxo intermediates exhibiting a side-on coordination mode (^SS)[20-22] and one with an end-on coordination mode (^ES)[23] have been solved by X-Ray crystallography (Figure 2). On the basis of crystallographic and computational studies, the electronic structure of one of these 1:1 adducts is best described as a $Cu^{III}O_2^{2-}$ species (^MP).[24]
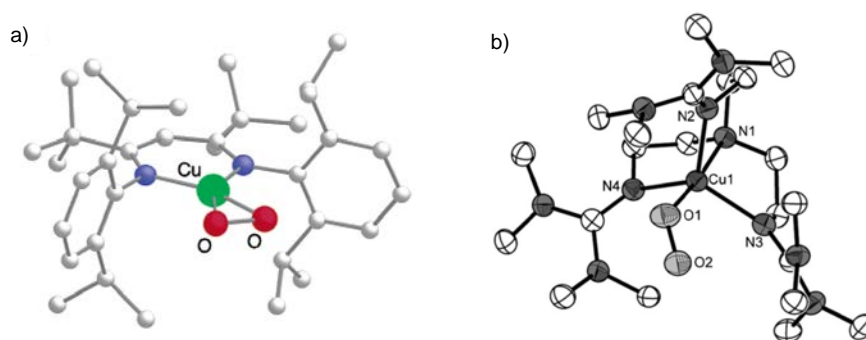
Figure 2. X-Ray structures of 1:1 $Cu:O_2$ complexes: (a) $[Cu^{III}(O_2)(^{H,tBu}Dk^{iPr})]$ species showing a side-on coordination mode (^MP)[24]; (b) $[Cu^{II}(O_2)(TMG_3tren)]^+$ with an end-on coordination mode (^ES).[23]

Superoxide compounds have recently been crystallographically characterized in a precatalytic state of peptidylglycine α-hydroxylating monooxygenase[25] and they are postulated to be key intermediates in the enzymatic cycles of other mononuclear copper enzymes like amine oxidase[26] and dopamine β-hydroxylase.[27]

I2.2.1.2. Intermediate species $Cu:O_2$ 2:1

The reduction of O_2 to peroxide ($2e^-$) is thermodynamically more favorable than to superoxide ($1e^-$) which is clearly evidenced by the abundance of Cu_2O_2 adducts synthetically prepared. Traditionally, the synthesis of Cu_2O_2 intermediate species was performed using mononuclear complexes that self-assemble when reacting with O_2 or, in selected cases, using dinucleating ligands.

The configurations exhibiting a $Cu:O_2$ 2:1 ratio (Cu_2O_2) are basically *trans*-μ-1,2-peroxodicopper(II) (^TP), μ-η^2:η^2-peroxodicopper(II) (^sP) and bis(μ-oxo)dicopper(III) (O).

trans-μ-1,2-peroxodicopper(II) complexes (^TP)

The biological relevance of ^TP intermediates has not been proved yet but they are synthetically accessible through the use of mononuclear copper(I) complexes with tetradentate

ligands which self-assemble upon O$_2$ reaction.[28-31] Their assignment as ^{T}P species is based primarily on distinctive intense UV-vis features that are responsible for their purple colors: *ca.* 530 nm ($\varepsilon \sim$ 10000 M^{-1}cm^{-1}) and *ca.* 600 nm (shoulder, $\varepsilon \sim$ 7000 M^{-1}cm^{-1}). Resonance Raman (rRaman) spectroscopy is also an adequate tool to identify this type of species which are characterized by an O-O stretching vibration at *ca.* 830 cm^{-1} ($\Delta[^{18}O_2] \sim$ 45 cm^{-1}) and a Cu-O stretching vibration at *ca.* 555 cm^{-1} ($\Delta[^{18}O_2] \sim$ 24 cm^{-1}).[7]

[Cu$^{II}_2$(O$_2$)(tpa)$_2$]$^{2+}$ (tpa = tris(2-pyridylmethyl)amine) (Figure 3) constitutes the prototypical example of these compounds and it is obtained by reversible interaction of [Cu^{I}(tpa)(EtCN)]$^{+}$ with O$_2$ at cryogenic temperatures.[28,29]
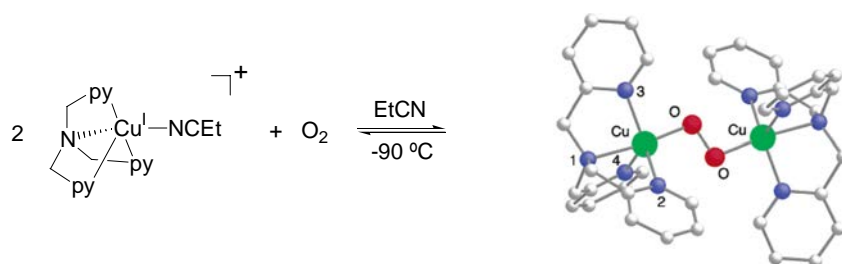
Figure 3. X-Ray structure of the ^{T}P species [Cu$^{II}_2$(O$_2$)(tpa)$_2$]$^{2+}$ formed upon reaction of [Cu^{I}(tpa)(EtCN)]$^{+}$ with O$_2$ in EtCN at -90ºC.[28]

μ-η^2:η^2-peroxodicopper(II) complexes (^{s}P)

^{S}P coordination mode was discovered by Kitajima and coworkers with the resolution of the X-Ray crystal structure of [Cu$^{II}_2$(O$_2$)(Tp^{iPr2})$_2$] (Tp^{iPr2} = tris(3,5-diisopropylpyrazolyl)hydroborate)[32,33] (Figure 4). The similarity between the spectroscopic features of this compound and those of the oxidized form of hemocyanin strongly supported the notion that O$_2$ binding in the oxygenated form of this protein occurred with the same mode, as was later demonstrated by the resolution of the crystal structure of the natural protein.[13] This was a great success of synthetic bioinorganic chemistry because through the characterization of a simple coordination complex, the correct and unprecedented coordination mode of O$_2$ in a natural system could be established.
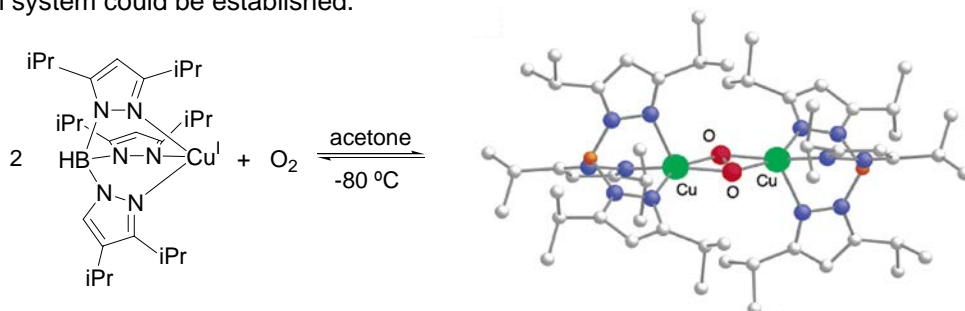
Figure 4. X-Ray structure of the ^{S}P species [Cu$^{II}_2$(O$_2$)(Tp^{iPr2})$_2$] formed upon reaction of [Cu^{I}(Tp^{iPr2})] with O$_2$ in acetone at -80ºC.[32,33]

^{S}P species have very characteristic spectroscopic features. UV-vis spectra exhibit a high-energy charge-transfer band (340 - 380 nm; $\varepsilon \sim$ 18000 - 25000 M^{-1}cm^{-1}) and a weaker lower energy band (510 - 550 nm; $\varepsilon \sim$ 1000 M^{-1}cm^{-1}) conferring their characteristic violet color.

Their resonance Raman spectra display a low-energy O-O stretching vibration at 730 – 760 cm^{-1} ($\Delta[^{18}O_2] \sim 40$ cm^{-1}).[7]

bis(μ-oxo)dicopper(III) complexes (O)

The first $Cu^{III}(\mu\text{-}O)_2\text{-}Cu^{III}$ core was reported by Tolman in 1996[34] and it presents completely different spectroscopic features compared to the rest of Cu:O₂ intermediates.

The first structurally characterized O species was generated with a macrocyclic *fac* triamine ligand, Bz₃tacn (Bz₃tacn = tribenzyl-1,4,7-triazacyclonane),[34,35] and despite its instability above -80ºC, it could be fully characterized by several techniques including X-Ray analysis of its perdeutero-analogue (Figure 5).
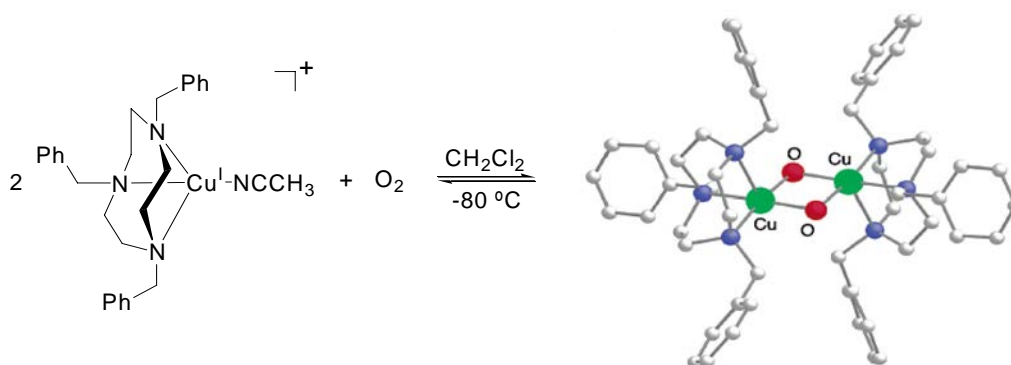
Figure 5. X-Ray structure of the O species $[Cu^{III}_2(O)_2(d_{21}\text{-}Bz_3tacn)_2]^{2+}$ formed upon reaction of $[Cu^I(d_{21}\text{-}Bz_3tacn)(CH_3CN)]^+$ with O₂ in CH₂Cl₂ at -80ºC.[34,35]

Since Tolman's discovery, several O type of intermediates have been spectroscopically and, in selected cases, structurally characterized. With a single exception,[36] all of them arise from the interaction of two mononuclear complexes which self-assemble upon O₂ reaction.[21,24,37,38]

The structural differences between O and ^SP isomers portend different UV-vis and rRaman spectroscopic characteristics. O complexes generally exhibit two intense ligand-to-metal charge transfer absorptions at *ca.* 300 nm ($\varepsilon \sim 20000$ M^{-1}cm^{-1}) and *ca.* 400 nm ($\varepsilon \sim 24000$ M^{-1}cm^{-1}). rRaman experiments reveal a characteristic and intense vibration at *ca.* 600 cm^{-1} that shifts by *ca.* 25 cm^{-1} upon $^{18}O_2$ substitution.[7]

One of the major contributions from Tolman and co-workers was the demonstration of the existence of a rapid equilibrium between ^SP and O isomers thus indicating reversible scission and formation of the dioxygen O-O bond (Scheme 7).[39] This reaction is of technological and scientific interest because it constitutes the key step during the dioxygen formation event that takes place in the oxygen evolving center of photosystem II, albeit catalyzed by Mn centers.[2] Tolman's work constitutes the first precedent of a transition metal complex where the O-O bond is formed and broken reversibly. Because of its significance, this equilibrium has been deeply studied[40-42] and it has been seen that it is influenced primarily by the steric demands of the ligand, although counterion, solvent, and electronic features of the ligand can

also affect its position. In general, sterically not demanding ligands favor the more compact bis-oxo core, while the introduction of steric constraints *via* ligand or binding anions results in ^SP type of species.

$$LCu^{III}\underset{O}{\overset{O}{<}}Cu^{III}L \rightleftharpoons LCu^{II}\underset{O}{\overset{O}{<}}Cu^{II}L$$

bis(μ-oxo) (O)   μ-η^2:η^2-peroxo (^{S}P)
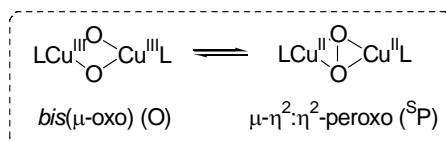
Scheme 7. Equilibrium between bis(μ-oxo) and μ-η^2:η^2-peroxo complexes.

I2.2.1.3. Intermediate species Cu:O$_2$ 3:1

Multi-copper oxidases (ascorbate oxidase, laccase, ceruloplasmin) couple the oxidation of various substrates to achieve the complete 4e$^-$ reduction of O$_2$ to H$_2$O at a trinuclear copper active site. Despite the presence of only three copper centers, the 4e$^-$ reduction can be well understood if it is considered that the fourth reducing equivalent comes from a blue cooper site situated away from the Cu$_3$ cluster (12 Å).

Among model compounds known to date, there are very few ligands capable of holding a trinuclear Cu core bridged by oxide ligands.[43,44] The first example of a discrete 3:1 Cu:O$_2$ species was reported by Stack *et al.* in 1996 (Scheme 8).[43] This compound is a mixed valence complex where the O$_2$ molecule has been fully reduced by 4e$^-$ and it is coordinated to two Cu^{II} and one Cu^{III} center. It is considered that the lack of steric restrictions imposed by the ligands is responsible for the formation of such species.

(a)   (b)

$$3\ [LCu^I(MeCN)]^+ \xrightarrow[\text{O}_2 \quad \text{3 MeCN}]{-80°C,\ CH_2Cl_2} [L_3Cu_3O_2]^{3+}$$

L =

$$LCu^{III}\underset{O-Cu^{II}L}{\overset{O-Cu^{II}L}{<}}$$

bis(μ$_3$-oxo) (T)
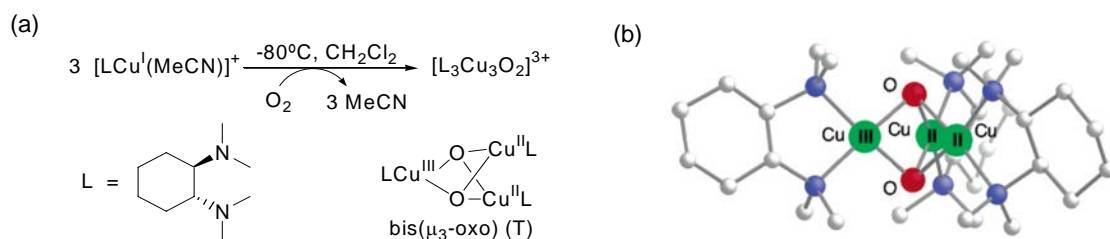
Scheme 8. (a) Formation of a bis(μ$_3$-oxo) species upon reaction of the mononuclear [Cu^{I}L(MeCN)]$^+$ complex with O$_2$ in CH$_2$Cl$_2$ at -80ºC. (b) X-Ray structure of the bis(μ$_3$-oxo) species [Cu$^{II}_2$Cu^{III}(μ$_3$-O)$_2$(L)$_3$]$^{3+}$.[43]

I2.2.2. Use of dinucleating systems

I2.2.2.1. General considerations

In general, biological models of dinuclear copper proteins that activate oxygen consist in mononuclear Cu^I complexes which self-assemble upon reaction with molecular O$_2$. However, in natural systems some active centers are constituted by a dinuclear copper site in which the metallic ions are disposed in a particular configuration favoring a specific interaction with molecular O$_2$. For this reason, an important step towards the mimicking of the natural active sites of dicopper proteins is the synthesis of dinucleating ligands capable of establishing some control over the spatial arrangement of the two metal centers in the synthetic system. These

ligands are constituted by two coordination sites which hold two copper centers close enough to give rise to intramolecular interaction with O$_2$.

The connection between the two coordination sites of a dinucleating ligand has been done basically by an alkyl group[45,46] or an aromatic ring. A particular case of the latter is constituted by *meta*-xylyl linked dinuclear Cu^I complexes and specially remarkable are the works done by Karlin and coworkers[47,48] and Casella and coworkers[49] which are depicted in Scheme 9.
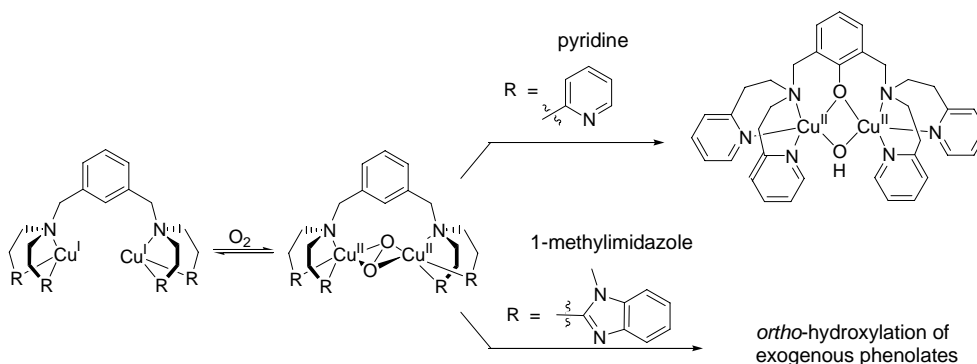
Scheme 9. Both Karlin's (R = pyridine) and Casella's (R = 1-methylimidazole) systems react with O$_2$ to form μ-η^2:η^2-peroxodicopper(II) complexes, but they have completely different reactivity.

In Karlin's system (R = pyridine) a μ-η^2:η^2-peroxodicopper(II) intermediate species has been spectroscopically characterized and it has been proved that its irreversible decomposition to Cu^{II} causes the intramolecular hydroxylation of the aromatic ring (electrophilic aromatic substitution). In sharp contrast, when R is a 1-methylimidazole group, the same type of Cu$_2$O$_2$ compound do not produce aromatic hydroxylation of the ligand but the system is capable of both aromatic *ortho*-hydroxylation and catechol oxidation to quinones of exogenous phenolates (*vide infra*).

I2.2.2.2. Macrocyclic dicopper complexes: properties and limitations.

Another approach towards the O$_2$ activation by dinuclear copper(I) complexes has been achieved by using macrocyclic dinucleating ligands due to its ability of preorganizing two metal centers in a particular Cu···Cu distance. Recent studies with hexaaza dinuclear macrocyclic ligands show that O$_2$ activation can occur intramolecularly and in some cases aromatic hydroxylation of the supporting macrocyclic ligand occurs (Scheme 10).[50-52] However, in these systems no Cu:O$_2$ intermediate species has been detected and the nature of the putative Cu:O$_2$ species has been studied only through the use of DFT calculations.
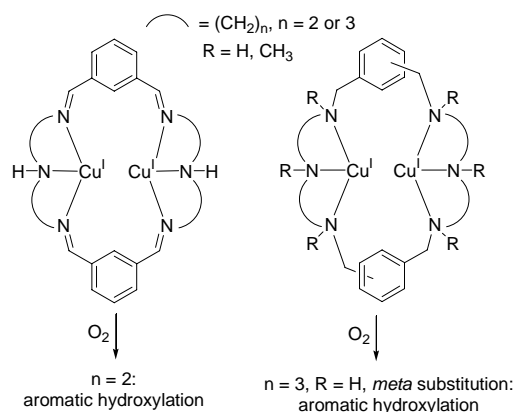
Scheme 10. Dinuclear hexaaza macrocyclic ligands used to activate molecular dioxygen.

I2.2.3. Reactivity of Cu$_2$O$_2$ species

The main function of most O$_2$-activating copper enzymes is the activation of molecular O$_2$ to oxidize a given substrate. Due to the catalytic and synthetic applications of such reactions, several studies have been undertaken to gain further insight into the mechanism of these processes. In this line, the reactivity of some of the Cu:O$_2$ intermediate species described above, specially Cu$_2$O$_2$ species, has been studied and analyzed.

Generally, copper-dioxygen species are only stable at low temperatures (-80ºC) and warming usually causes decomposition, typically to Cu^{II} complexes, *via* processes involving intramolecular oxidation of a supporting ligand. These processes can be considered as destructive and thus they may be undesired from the point of view of catalyst development, but they provide fundamental mechanistic information relevant to Cu:O$_2$ species in enzymatic and other catalytic systems. N-dealkylation,[37,53] aliphatic hydroxylation[54] and arene hydroxylation[47,48,55,56] reactions have been reported to come from the decomposition of bis(μ-oxo)dicopper(III) (O) or μ-η^2:η^2-peroxodicopper(II) (^{S}P) intermediate species. In Scheme 11 some examples of these ligand oxidation processes are illustrated.
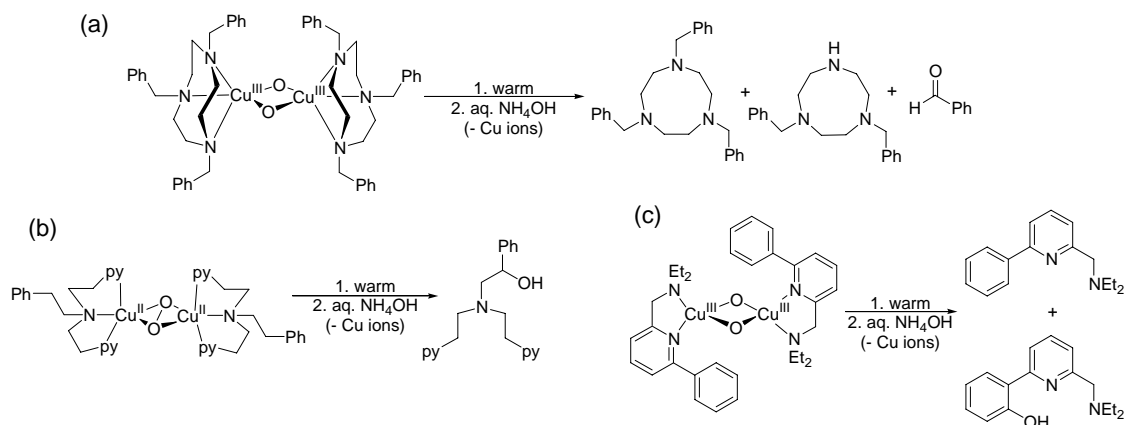
Scheme 11. Decomposition of Cu$_2$O$_2$ species accompanied by ligand oxidation. (a) N-dealkylation,[53] (b) aliphatic hydroxylation[54] and (c) arene hydroxylation.[55]

The reactivity of these Cu$_2$O$_2$ species towards exogenous substrates is especially relevant to catalysis and it has been thoroughly studied. These catalytic reactions include oxygen atom transfer, hydrogen atom abstraction, oxidation of alcohols to aldehydes or ketones[57-59] and conversion of amines to nitriles[60,61] among others. In Scheme 12, some examples of reactivity of copper-dioxygen adducts towards exogenous substrates are depicted.
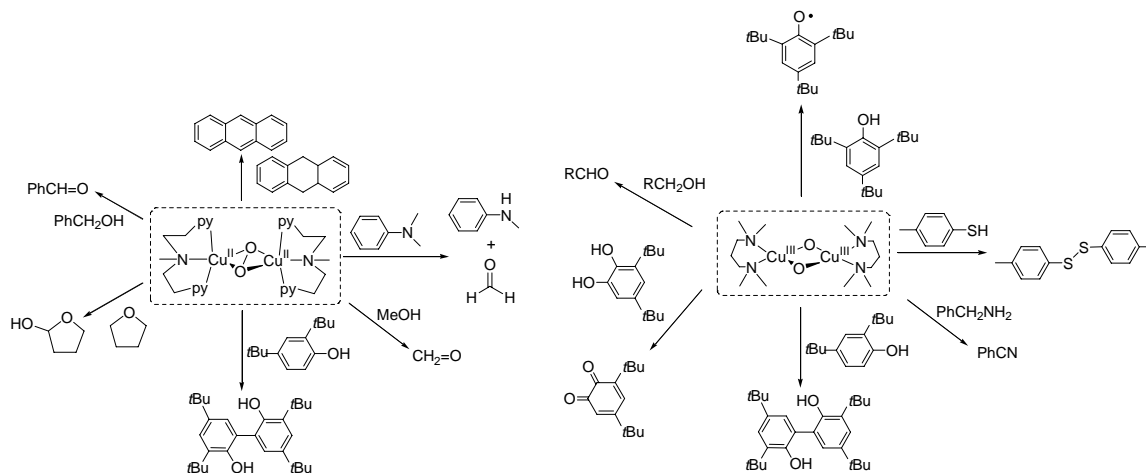
Scheme 12. Reactivity of Cu$_2$O$_2$ adducts towards exogenous substrates.[59,61]

A specially relevant reaction performed by some Cu$_2$O$_2$ adducts is the *ortho*-hydroxylation of phenols or phenolates to catechols or quinones.[62] Its importance is attributed to its direct relevance to the catalytic transformations performed by tyrosinase. In the literature, there are two model systems bearing a μ-η^2:η^2-peroxodicopper(II) (^{S}P) site which are capable of performing the *ortho*-hydroxylation of exogenous phenolates to give catechols or quinones.[49,63] Scheme 13 shows the structure of these model complexes along with the reaction they catalyze. In both cases, Hammett analysis using *para*-substituted phenolates clearly indicates that the hydroxylation of the substrate proceeds through an electrophilic attack analogously to what is observed in tyrosinase which suggests that these systems can be thought as true models for the natural enzyme.[64,65]
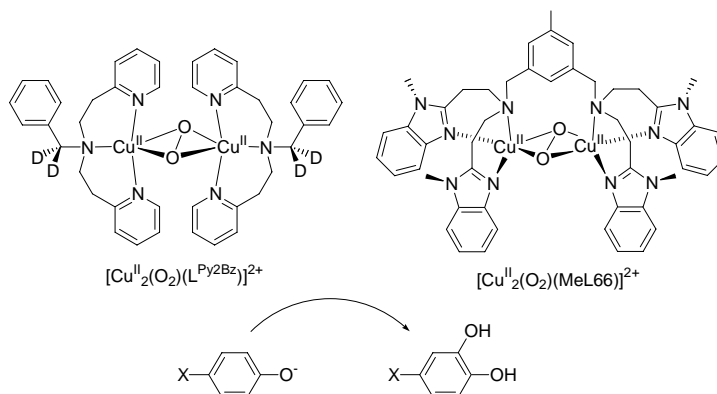
Scheme 13. Model systems capable of performing *ortho*-hydroxylation of exogenous phenolates to form catechols. Both of them bear a μ-η^2:η^2-peroxodicopper(II) site.[63,64]

A μ-η^2:η^2-peroxodicopper(II) site is also present in most of the model systems where intramolecular aromatic hydroxylation occurs,[47,48,56] a reaction which is directly related to the *ortho*-hydroxylation of phenols. As mainly intramolecular and intermolecular aromatic hydroxylation takes place when a side-on peroxo unit (^{S}P) is present, in general it is considered that this is the most suitable Cu$_2$O$_2$ species to carry out the monooxygenase reaction performed by tyrosinase. However, the aromatic hydroxylation mechanism continues being subject of intense discussion because the existence of a rapid equilibrium between μ-η^2:η^2-peroxodicopper(II) (^{S}P) and bis(μ-oxo) (O) species[39] hinders the assignment of the true hydroxylation species in natural systems. In the case of tyrosinase, it is well established that the observed Cu$_2$:O$_2$ intermediate corresponds to a μ-η^2:η^2-peroxodicopper(II) but if the O-O bond breaks prior to, along with or after electrophilic attack by the oxygen to the aromatic ring remains unclear. In this line, a work by Stack and coworkers with a model compound is specially remarkable.[66] In this specific case, it is spectroscopically observed that the O-O cleavage occurs before the hydroxylation reaction (Scheme 14). This observation contradicts the most extended idea which considers that the true hydroxylation species is a side-on peroxo (^{S}P) type of intermediate.
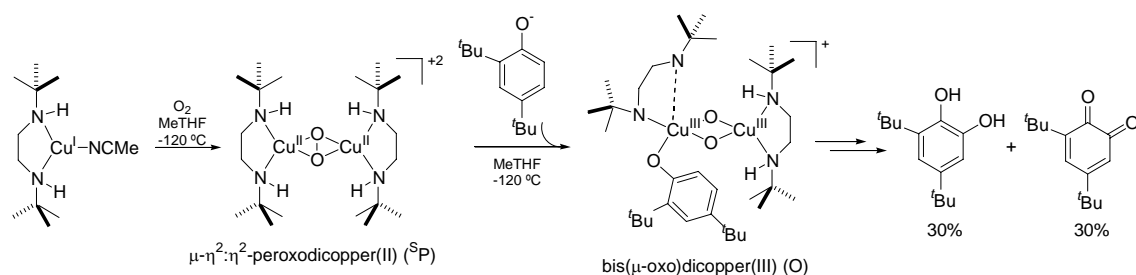
Scheme 14. Schematic representation of the O-O bond breaking prior to substrate hydroxylation.[66]

In conclusion, while extensive work on the last 20 years has resulted in great advances on the comprehension of the interaction between copper and O$_2$, fundamental details on this biologically relevant chemistry remain to be explored.

I.3. O$_2$ activation by iron systems

I3.1. Biological role of iron
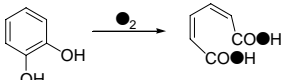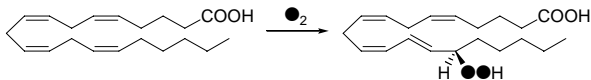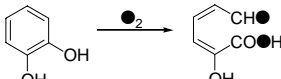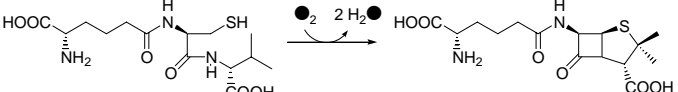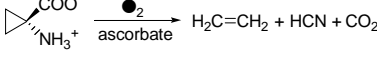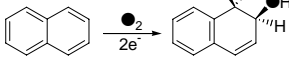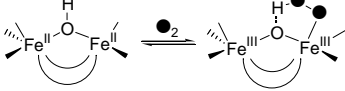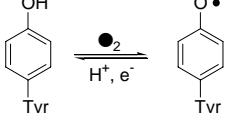
Iron is an ubiquitous element in living systems and its versatility is unique. It is found in the active center of molecules responsible for oxygen transport and electron transfer and also in a diverse range of metalloenzymes such as oxidases, hydrogenases, reductases, dehydrogenases and deoxygenases.[67]

Iron is the 4th most abundant element in the earth's crust (after oxygen, silicium and aluminum) and it has two readily interconverting oxidation states: Fe^{II} and Fe^{III}. However, in natural systems the presence of iron centers in higher oxidation states, such as Fe^{IV} or Fe^{V}, and lower oxidation states such as Fe^{I}, has been postulated in order to explain some biological processes. In fact, Fe^{IV} intermediate species have been directly detected in selected natural systems.

Its high availability and its various attainable oxidation states have led to the evolutionary selection of iron in many life processes. A clear indication of its versatility is the presence of iron in a wide range of metalloenzymes in different configurations: together with a porphyrin ligand to give heme systems, ligated to sulfides to give iron-sulfur clusters and in non-heme mononuclear or dinuclear centers.

I3.1.1. O$_2$-activating iron proteins

Iron proteins implicated in O$_2$ activation are present in nature in a wide range of configurations. They can be classified in three different superfamilies depending on the structure of their active: heme proteins, mononuclear non-heme systems and dinuclear non-heme enzymes. Scheme 15 shows the most important O$_2$-activating iron proteins and the reactions they catalyze.

Scheme 15. Iron proteins implicated in oxygen binding and activation.[4,8,68]

In this introduction, only cytochrome P450 (section I3.1.2) and Rieske dioxygenases (section I3.1.3) will be described in detail as they constitute relevant examples of heme and monuclear non-heme iron enzymes. Understanding their structure and activity serves as inspiration for the work presented in this thesis.

I3.1.2. Cytochrome P450: the heme paradigm

Cytochrome P450s constitute an important "superfamily" of heme-iron enzymes which is spread in all forms all life: from bacteria to mammalians.[69] Due to the critical functions that they play in mammalian metabolism, including the biosynthesis of steroids, the detoxification of xenobiotics and drug metabolism, cytochrome P450s are the most studied and best understood oxygen-activating metalloenzymes.[2,9]

The interest in cytochrome P450s arises not only from a desire to understand its physiological function but also from the unique ability of these enzymes to perform controlled transfer of oxygen atoms from O_2 to non-activated organic chemical substrates, a formidable challenge for synthetic chemistry. Cytochrome P450s are capable of performing a wide variety of oxidation reactions (Scheme 16) ranging from hydroxylation of non-activated carbon-hydrogen bonds, epoxidation, N-, S- and O-dealkylation, N-oxidation, sulfoxidation and dehalogenation.[2]

$$R\text{-}H \;+\; O_2 \;+\; 2\,e^- \;+\; 2\,H^+ \longrightarrow R\text{-}OH \;+\; 2\,H_2O$$

$$\begin{array}{c}\diagup\!\!=\!\!\diagdown\end{array} \;+\; O_2 \;+\; 2\,e^- \;+\; 2\,H^+ \longrightarrow \;\; \overset{O}{\diagup\!\!\triangle\!\!\diagdown} \;+\; 2\,H_2O$$
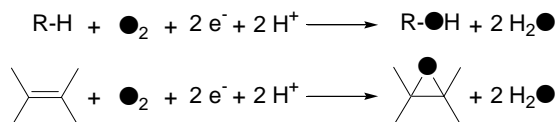
Scheme 16. Hydroxylation and epoxidation reactions catalyzed by cytochrome P450.

Cytochrome P450s were first identified and purified approximately 50 years ago but most of the information about their structure and mechanism was obtained from the several X-ray crystal structures of water-soluble P450-camphor solved during the last two decades.[70] The active center is constituted by an iron center in an octahedral geometry. The four equatorial coordinating positions are occupied by the porphyrin; a cysteine thiolate atom and another ligand assigned as water or hydroxide occupy the two axial positions (Figure 6).
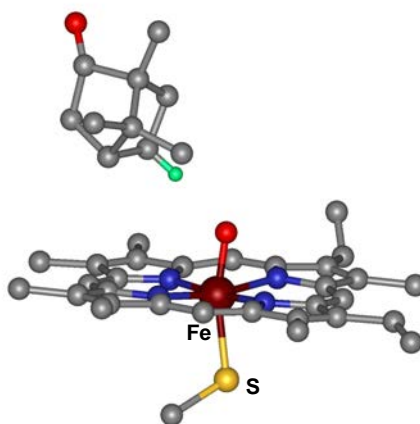
Figure 6. Active site of cytochrome P450-camphor.

The family of cytochrome P450s is considered as the paradigm for oxygen activation and hydrocarbon oxidation by an iron center. For this reason, extensive efforts have been devoted to understand its catalytic mechanism over the past 30 years and nowadays the principal features of the catalytic cycle of cytochrome P450s are well established (Scheme 17).[70,71]
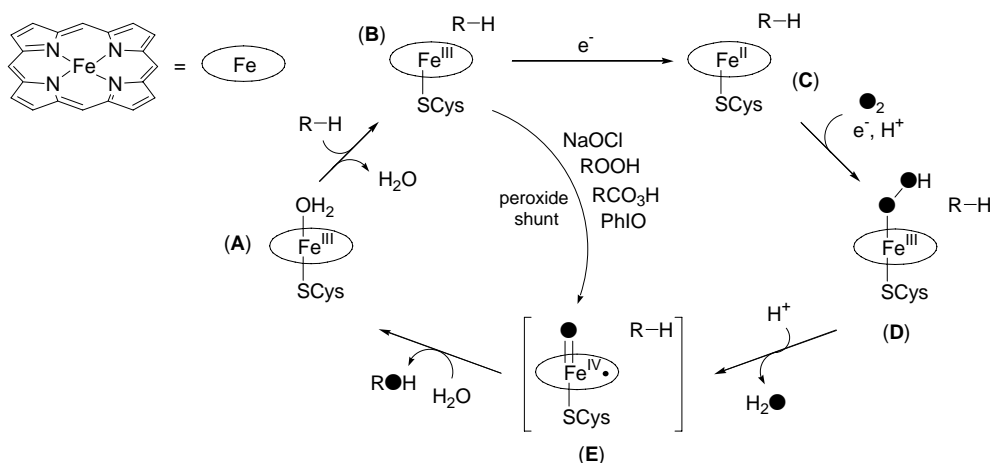
Scheme 17. Catalytic mechanism for cytochrome P450s.

As shown in Scheme 17, starting from the predominant low-spin iron(III) state (**A**), the binding of the substrate at the active site occurs (**B**), which triggers spin crossover and subsequent one-electron reduction to give an Fe^{II} center (**C**). The coordination of O_2 to the Fe^{II} center gives a ferric-superoxide complex which becomes a hydroperoxoiron(III) complex (**D**) after a second one-electron reduction and protonation. This species undergoes proton assisted heterolytic cleavage of the O-O bond to generate a high-valent oxo-Fe^{IV}-porphyryl radical cation (**E**) and a water molecule. The oxygen atom is transferred from this oxo complex to the nearby substrate through a two-step process known as "oxygen rebound" (Scheme 18) This mechanism involves hydrogen-atom abstraction by the iron-oxo species (**E**) to form an iron(IV)-hydroxo species and a short-lived alkyl radical, rapidly followed by the "rebound" to give the new C-O bond. This second step must be faster than the epimerization of the alkyl radical to account for the lack of stereo- and enantioscrambling of the substrate during hydroxylation. Finally, dissociation of the oxidized product completes the catalytic cycle. Direct cycling between the ferric state (**B**) and the high valent oxidant species (**E**) can be done by using oxidants such as hydro and alkylperoxides, NaOCl, PhIO or peracids. This shortcut is known as the "peroxide shunt" (Scheme 17) and it receives use in catalysis.
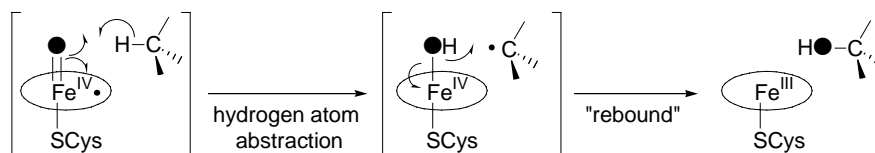
Scheme 18. Postulated "oxygen rebound" mechanism for C-H hydroxylation in cytochrome P450s.

I3.1.3. Rieske dioxygenases

During the past 15 years great efforts have been devoted to the understanding of mononuclear non-heme iron enzymes[4] mainly due to the increasing number of crystal structures available. From these structural studies, it has been found that a common structural motif is found in a great number of these metalloenzymes in which the iron center is coordinated to

three protein residues, two His and one Asp or Glu, constituting one face of an octahedron. This structural motif is known as the 2-His-1-carboxylate facial triad (Scheme 19).[72,73] The triad leaves three free sites on the opposite face of the octahedron available for coordination with exogenous ligands such as solvent molecules, substrate, cosubstrate or molecular oxygen, bringing them into close proximity for subsequent reaction.
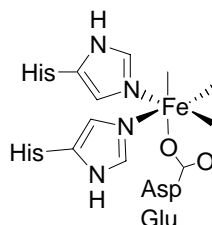
Scheme 19. Schematic representation of the 2-His-1-carboxylate facial triad found in some mononuclear non-heme iron enzymes.

Within this group, Rieske dioxygenases are specially efficient and versatile, even more than the heme-containing cytochrome P450s. In fact, they catalyze a number of oxidations such as benzylic hydroxylation, desaturation, sulfoxidation, and O- and N-dealkylation. However, the technological interest in these enzymes resides on the fact that they are capable of carrying out enantioselective and stereospecific arene and olefin *cis*-dihydroxylation which is a novel transformation not observed thus far in any other enzymatic systems. In natural systems, the *cis*-dihydroxylation of arenes catalyzed by Rieske dioxygenases constitutes the first step in the biodegradation of aromatic molecules by soil bacteria and leads to the formation of catechols which are further degraded by intradiol- and extradiol-cleaving catechol dioxygenases.
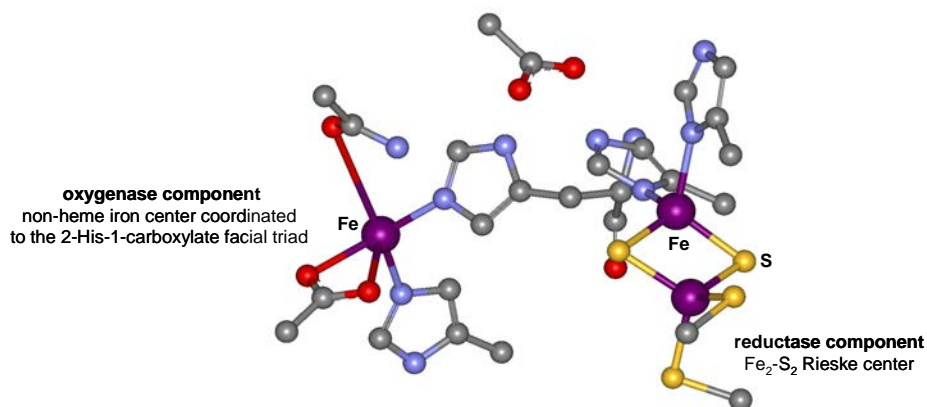
Figure 7. Active center of Rieske dioxygenase showing the oxygenase and reductase component.

Rieske dioxygenases are multicomponent enzymes (Figure 7). The oxygenase component corresponds to the non-heme iron center and it effects the O$_2$ activation and substrate dihydroxylation. The other component is a reductase center constituted by an iron-sulfur cluster (Fe$_2$S$_2$) that delivers electrons to the oxygenase center in a controlled manner during catalysis. Napthalene dioxygenase (NDO) is the only Rieske dioxygenase that has been crystallographically characterized[74] which has allowed the determination of several structural parameters and mechanistic aspects of this family of enzymes.[75] NDO catalyses the *cis*-dihydroxylation of naphthalene (Scheme 20) and it is representative of other *cis*-dihydroxylating

enzymes (*e.g.* benzoate 1,2-dioxygenase,[76] toluene 2,3-dioxygenase,[77] benzene dioxygenase[78] and phthalate dioxygenase[79]). In the course of catalysis both atoms of oxygen from O$_2$ are incorporated into the *cis*-diol product.
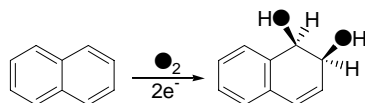
Scheme 20. Naphthalene dioxygenase-catalyzed arene *cis*-dihydroxylation reaction.

Nowadays, it is proposed that the catalytic cycle of Rieske dioxygenase (Scheme 21) starts in the oxidase component when the fully reduced form (**A**) binds the arene substrate to initiate the reaction (**B**). O$_2$ binding followed by electron transfer from the reductase component generates the iron(III)-peroxo intermediate (**C**). Time resolved cryo-crystallographic studies on frozen crystals of NDO exposed to O$_2$ clearly indicate that the peroxo ligand binds in a side-on configuration. This species is the last detectable intermediate before substrate oxidation occurs.[80] Two possible pathways have been proposed in order to explain the *cis*-dihydroxylation starting from Fe^{III}-η^2-OOH (**C**). The first scenario involves the direct attack to the substrate to form the (η^1-alkylperoxo)-iron species (**D**) and the second possibility is based on the cleavage of the O-O bond and conversion into an electrophilic OH-Fe^V=O (**E**) prior to substrate attack. Such a species would be equivalent to OsO$_4$, MnO$_4^-$ or RuO$_4$ which are well-known *cis*-dioxometal species capable of eliciting *cis*-dihydroxylation of olefins.[81,82] The observation that oxygen atoms from H$_2$^{18}O can be incorporated into the naphthalene *cis*-diol product (3-10%)[83] agrees with the mediation of an iron-oxo species. Moreover, it has also been observed that 70% of oxygen was incorporated from H$_2$^{18}O into 1-indanol when toluene 2,3-dioxygenase performed the hydroxylation of indane.[84] These results argue for the involvement of an intermediate that allows solvent to be incorporated into product such as high valent iron-oxo species.
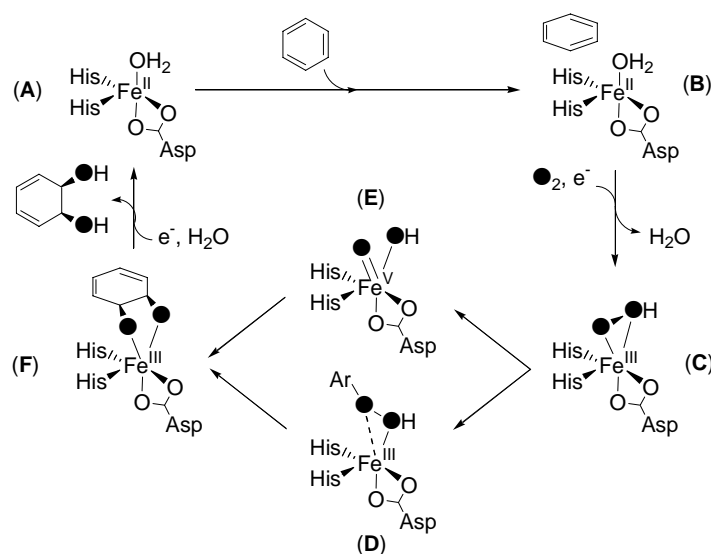
Scheme 21. Rieske dioxygenases catalytic cycle showing the two possible mechanisms for the arene dihydroxylation step.

Recent experiments also reveal that NDO can elicit catalytic chemistry when H_2O_2 is used as oxidant thus resembling the "peroxide shunt" found in cytochrome P450s.[83] This observation together with other similarities with the catalytic cycle of cytochrome P450s suggest that a common mechanistic landscape is operating in heme and non-heme mononuclear iron enzymes. In this line, usually the heme paradigm serves as inspiration for the study of non-heme systems.

I3.1.4. High-valent iron-oxo species: a common feature in biological systems

As can be seen in Scheme 15, O_2-activating iron proteins constitute a heterogeneous group of enzymes in which there is a great variability in the structure of the active site and in the type of reactions that they catalyze. Despite this diversity, there is a common feature in most of these systems: the postulation of high-valent iron-oxo species as the key oxidizing intermediates. In specific cases this type of species are not only postulated but they have also been detected in natural systems (Scheme 22).

As stated above, in the catalytic cycle of cytochrome P450 it has been postulated for years that an iron(IV)-oxo porphyrin π-radical transfers its oxygen atom to the substrate. However, it has not been until very recently, that this type of species has been characterized in the biological system.[70,85] In the same line, for non-heme iron enzymes high-valent iron-oxo species have been trapped in several cases. Within the last three years, $Fe^{IV}=O$ intermediates have been detected and characterized in several mononuclear non-heme iron enzymes: taurine/α-ketoglutarate dioxygenase (TauD),[86,87] prolyl 4-hydroxylase,[88] tyrosine hydroxylase[89] and halogenase CytC3.[90] In all cases, the iron(IV) center possesses a high-spin state (S = 2). For dinuclear non-heme iron proteins, high-valent oxidation states are also postulated as the key oxidant species in most of the proposed mechanistic cycles. In fact, Fe^{III}-O-Fe^{IV} units[91,92] and Fe^{IV}-O-Fe^{IV} cores[93] have been detected for ribonucleotide reductase and methane monooxygenase.
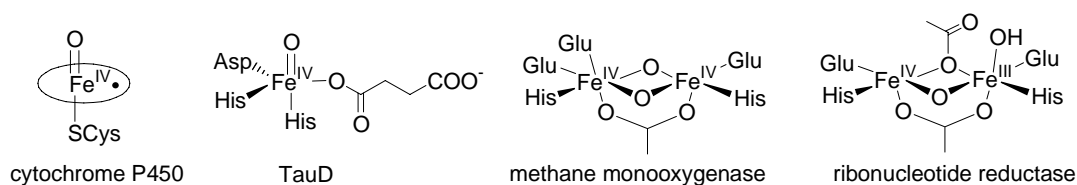
Scheme 22. Structures for high-valent intermediates for cytochrome P450, TauD, methane monoooxygenase and ribonucleotide reductase.

I3.2. O₂ binding and activation by biomimetic iron complexes

The present work is based on the development of synthetic models for mononuclear non-heme iron enzymes such as Rieske dioxygenases. For this reason, the description of model compounds will be focused on those that mimic non-heme mononuclear iron proteins. The description will be divided in two parts: (1) synthetic models that mimic structurally and/or

functionally the active center of the natural systems, and (2) catalytic models which reproduce the activity of the enzymes which allows to get insight into some mechanistic aspects.

I3.2.1. Structural models: mononuclear non-heme Fe^{IV}-oxo and Fe^{V}-oxo

In general, the mechanistic cycles of O$_2$-activating non-heme iron enzymes start with the coordination of O$_2$ to the reduced Fe^{II} center to give iron(III)-peroxo species. Alternatively, in model systems, ferric-peroxo species can be generated *via* reaction of Fe^{II} or Fe^{III} complexes with peroxides.[4] The possible implication of these species in oxidation reactions is controversial. On one hand, a recent computational study has established the presence of low activation barriers for the epoxidation of olefins by [Fe^{III}(OOH)(bpmen)]$^{2+}$ (bpmen = N,N'-dimethyl-N,N'-bis(2-pyridylmethyl)ethylene-1,2-diamine).[94] On the other hand, the reactivity of well-defined synthetic Fe^{III}-OOH species using tpa, N4Py and Bn-tpen ligadns (see Scheme 23 for ligands' structure) has been studied, and it has been concluded that they act as sluggish oxidants.[95]

In biological systems further O-O bond cleavage gives rise to high valent iron(IV) or iron(V)-oxo species, yet evidence for this chemistry has remained elusive until recently. Although the first paper on the synthesis and characterization of an iron(IV)-oxo porphyrin radical appeared in 1981,[96] the first X-ray structure of a mononuclear non-heme iron(IV)-oxo complex was reported only five years ago.[97] The late discovery of non-heme iron(IV) species can be attributed to their high reactivity and the lack of a convenient spectroscopic signature that would readily signal its presence in a reaction mixture. Therefore, evidence for the formation of these species was built on the basis of mechanistic studies[98-100] until the preparation and crystallographic characterization of two synthetic non-heme Fe(IV)-oxo compounds[97,101] allowed the definition of very characteristic spectroscopic features for this type of intermediates, thus facilitating their detection and the development of several model compounds. Finally, the first spectroscopic characterization of an iron(V)-oxo species was accomplished just one year ago[102] and analogously to Fe^{IV} species, its implication had only been evidenced by mechanistic studies in catalytic chemistry. [103]

The following section will focus on the synthetic models for Fe^{IV}=O and Fe^{V}=O species which play a key role in the catalytic cycle of non-heme mononuclear iron enzymes implicated in O$_2$ activation.

I3.2.1.1. Iron(IV)-oxo species

The reaction of the iron(II) complex of tmc (tmc = tetramethylcyclam, Scheme 23) with PhIO afforded [Fe^{IV}(O)(tmc)(NCCH$_3$)](CF$_3$SO$_3$)$_2$, which persists for weeks at -40°C. Its remarkable stability led to its crystallization and constituted the first X-ray crystal structure of a mononuclear non-heme iron(IV)-oxo complex (Figure 8).[97] This pale green species shows an absorption maximum at λ_{max} = 800 nm (ε = 400 M^{-1}cm^{-1}) and Mössbauer spectroscopy affords an isomer shift δ = 0.17(1) mm·s^{-1} and a quadrupole splitting ΔE_Q = 1.24(1) mm·s^{-1}, values consistent with a low spin (S = 1) iron(IV) metal center (d^4 electronic configuration). The crystal structure reveals a Fe-O distance of 1.646(3) Å, a value closely resembling to the distances

measured by EXAFS for iron(IV)-oxo units in synthetic and biological porphyrin complexes.[104,105] This compound was further characterized by electrospray ionization mass spectrometry, EPR, and vibrational spectroscopy.
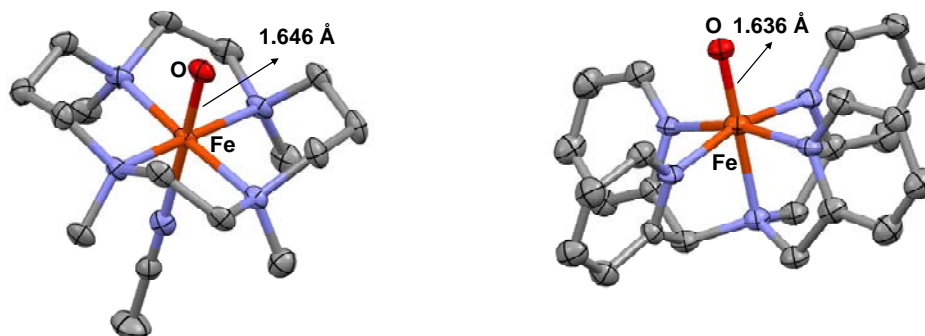
Figure 8. X-ray structures of [Fe^{IV}(O)(tmc)(NCCH$_3$)]$^{2+}$ (left) and [Fe^{IV}(O)(N4Py)]$^{2+}$ (right).

Once the spectroscopic properties of the iron(IV)-oxo unit were established, several other non-heme iron(IV)-oxo complexes have been synthesized using nitrogen based tripodal tetradentate N$_4$ ligands (R-tpa,[106] bpmcn[107]), and pentadentate N$_5$ ligands (N4Py,[101] R-tpen,[108] bispidine[109]) (see Scheme 23 for ligand structures). Diffraction quality crystals for [Fe^{IV}(O)(N4Py)]$^{2+}$ were also obtained[101] (Figure 8). Table 1 summarizes the spectroscopic properties for some synthetically prepared iron(IV)-oxo compounds and those for three biologically detected Fe^{IV}=O intermediates.
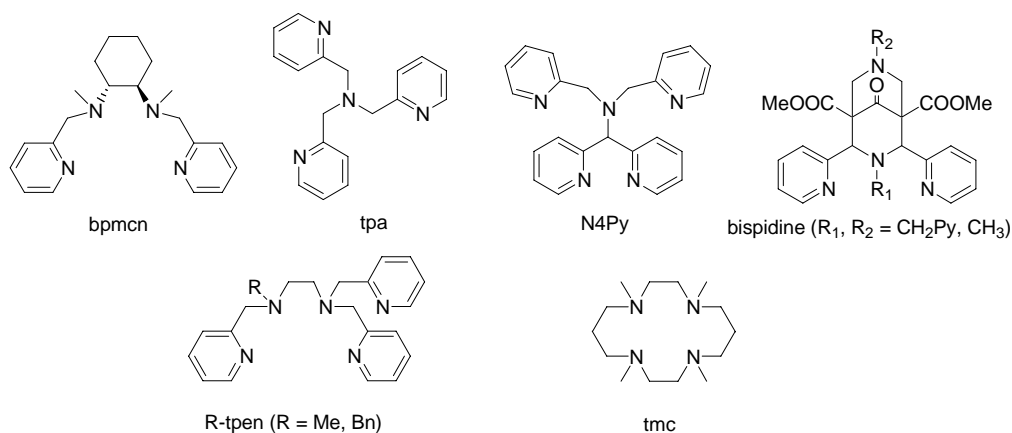
Scheme 23. Ligands used for the preparation of mononuclear non-heme iron(IV)-oxo complexes.

In general, iron(IV)-oxo complexes are prepared by reaction of the starting Fe^{II} complex with oxygen atom donors such as PhIO, peracids (*m*-CPBA, peracetic acid), KHSO$_5$, O$_3$ and NaOX (X = Cl or Br), and in some cases by using hydroperoxides (H$_2$O$_2$, *tert*-butyl hydroperoxide). The stability of non-heme Fe^{IV}=O complexes is highly dependent on the ligand structure. In general, pentadentate ligands (N4Py, Bn-tpen, bispidine) and macrocyclic tetradentate ligands (tmc) afford complexes much more thermally stable than tripodal tetradentate ones (tpa, bpmcn) in which there is a labile position in a *cis* configuration with respect to the oxo group (compare t$_{1/2}$ values in Table 1).

Table 1. Properties of selected non-heme Fe^{IV}=O compounds.

	r(Fe=O) (Å)	λ$_{max}$, nm (ε, M^{-1}·cm^{-1})	δ, mm·s^{-1} (ΔE$_Q$, mm·s^{-1})	multiplicity (S)	t$_{1/2}$ at 25 ºC	ref.
[Fe^{IV}(O)(tmc)(NCMe)]$^{2+}$	1.646(3)^a	820 (400)	0.17 (1.24)	1	10 h	97
[Fe^{IV}(O)(tpa)(NCMe)]$^{2+}$	1.67^b	724 (300)	0.01 (0.92)	1	< 10 min	106
[Fe^{IV}(O)(bpmcn)(NCMe)]$^{2+}$	1.66^b	753 (280)	0.07 (1.02)	1	< 10 min	107
[Fe^{IV}(O)(N4Py)]$^{2+}$	1.636(3)^a	695 (400)	-0.04 (0.39)	1	60 h	101
[Fe^{IV}(O)(Bn-tpen)]$^{2+}$	1.67^b	739 (400)	0.01 (0.87)	1	6 h	108
[Fe^{IV}(O)(bispidine)]$^{2+}$	-	715 (400)	0.015 (0.68)	1	-	109
Fe^{IV}=O TauD	1.62^b	-	0.31 (-0.88)	2	-	87
Fe^{IV}=O propyl hydroxylase	-	-	0.30 (-0.82)	2	-	88
Fe^{IV}=O halogenase CytC3	-	-	0.30 (-1.09)	2	-	90

^{a}Values obtained from X-ray crystallography. ^{b}Values obtained from EXAFS analysis.

Another important aspect to take into account is the spin state of the synthetically prepared Fe^{IV}=O species. While the spin state in the natural systems has been found to be high spin (S = 2), in model compounds always a low spin configuration (S = 1) is detected (Table 1). Thus, preparation of high spin iron(IV)-oxo compounds constitutes an important challenge in modern model chemistry because this achievement would allow to make a decisive step towards the better mimicking of biological Fe^{IV}=O species from an electronic point of view. Indeed, high spin iron(IV) species have been described but they do not contain the biologically relevant terminal oxo ligand, but instead a chloride ion.[110]

Scheme 24 summarizes the wide range of reactions performed by synthetically prepared iron(IV)-oxo species.
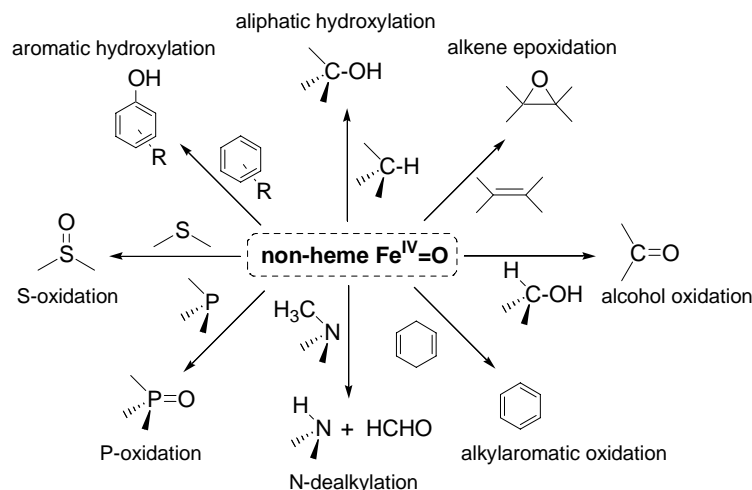
Scheme 24. Oxidation reactions mediated by mononuclear non-heme iron(IV)-oxo complexes.

In several studies, it has been observed that the oxygen atom from the Fe^{IV}=O unit could be transferred to organic substrates such as Ph$_3$P yielding Ph$_3$PO quantitatively[97] or sulfides to give the corresponding sulfoxide products.[111] The oxidation of olefins such as cylcooctene or stilbene was also achieved and it afforded the formation of the respective epoxide products.[106,112] However, the most striking observation made in oxygenation reactions by non-heme iron(IV)-oxo complexes was the hydroxylation of alkanes which was studied for [Fe^{IV}(O)(N4Py)]$^{2+}$ and [Fe^{IV}(O)(Bn-tpen)]$^{2+}$.[108] The oxidation of C-H bonds as strong as those of

cyclohexane was observed. Large kinetic isotope effects (KIE > 30) were measured, a clear indication that C-H bond activation occurs *via* a rate determining step involving hydrogen atom abstraction. High KIE values have also been measured in hydrogen atom abstraction reactions performed by the iron(IV) intermediate of TauD (KIE ~ 37).[113] Other processes like aromatic hydroxylation,[114] alcohol oxidation[115] and N-dealkylation[116] have also been observed for synthetic $Fe^{IV}=O$ species.

On the other hand, since metal-oxo species can in principle exchange their oxygen with water prior to oxo transfer to organic substrates, the incorporation of labeled ^{18}O from $H_2{}^{18}O$ into oxidation products has been considered as an evidence for the participation of high-valent iron-oxo intermediates in different processes. However, the mechanisms of oxygen exchange between high valent metal-oxo species and water are not fully understood. For this reason synthetic iron(IV)-oxo species have provided the opportunity to investigate this mechanism in more detail. The results obtained in these works are in agreement with the existence of an "oxo-hydroxo tautomerism" in order to explain the oxygen exchange with water (*vide infra*).[117]

I3.2.1.2. Iron(V)-oxo species

On the basis of ^{18}O labeling experiments, it has been postulated that an HO-Fe^V-oxo intermediate is the active species in the large family of Rieske dioxygenase enzymes (*vide supra*) and also in several bioinspired non-heme iron catalysts (*vide infra*).[118] Despite their postulated existence, iron(V) complexes are exceedingly rare[119] and preparation and characterization of iron(V)-oxo species was not achieved until very recently[102] by using a tetraamido macrocyclic ligand (TAML, Figure 9). In fact, TAMLs have been widely used to prepare a variety of high-valent iron compounds.[120]
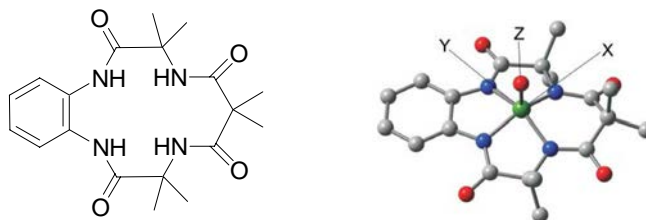
Figure 9. Schematic representation of TAML ligand (left). Geometry-optimized structure of [Fe^V(O)(TAML)]⁻ as obtained from DFT calculations (right).

The characterized Fe^V-oxo compound is a pentacoordinated complex bearing a deprotonated TAML ligand which occupies the equatorial positions and an oxo ligand ligated to one of the axial positions. The complex was obtained by reaction of an Fe^{III} precursor with *m*-chloroperbenzoic acid at low temperatures (-60ºC). Full characterization by UV-vis, electron paramagnetic resonance (EPR), Mössbauer and X-ray absorption spectroscopies, as well as electrospray ionization mass spectrometry (ESI-MS) allowed its assignation as a d^3 iron(V)-oxo complex with a S = 1/2 ground state. DFT calculations were also performed in order to get more insight into the electronic and structural characteristics of the compound (Figure 9). [Fe^V(O)(TAML)]⁻ displays the signature reactivity features of a strongly oxidizing iron-oxo complex. It oxidizes quantitatively Ph_3P to yield Ph_3PO, thioanisole to the corresponding

sulfoxide and cylooctene and styrene to epoxides. Reaction of ethylbenzene afforded a mixture of 1-phenylethanol and acetophenone. More importantly, ^{18}O incorporation into oxidized products was detected when $H_2^{18}O$ was present (25% ^{18}O-incorporation into sulfoxide product), in line with the well-known ability of high-valent metal-oxo species to exchange their oxygen atom with water.

I3.2.2. Bio-inspired oxidation catalysis

The functionalization of hydrocarbons which come from natural gas and crude oil has been of great interest because their abundance in nature makes them a convenient chemical feedstock.[121] However, due to their intrinsic inert nature, hydrocarbons require certain functionalization before being used in the chemical industry. Nature has developed different strategies to perform the stereospecific oxidation of C-H or C=C bonds. Inspired by biological systems, several model compounds have been prepared in order to oxidize hydrocarbons using H_2O_2 as the oxidant. Aside from the design of novel synthetically useful oxidation technologies, bioinspired catalysts also offer a simple structural platform to study the chemistry associated to large and complex molecules such as metalloenzymes. In this regard, bioinspired catalysts can give valuable information about the reaction mechanisms operating in enzymes.

In most common catalytic biomimetic studies, the combination of O_2 and 2e$^-$ is replaced by peroxides, which can be understood as a 2e$^-$ reduced version of O_2. However, the combination of peroxides and transition metal ions is commonly associated to free-diffusing radical chemistry.[122] The reaction between Fe^{II} (but also Cu^I, Mn^{II} and Co^{II}) and H_2O_2 or 'Fenton's reagent' (equations 1 and 2), despite having been studied for over 80 years, still arouses intense disagreements with respect to the species generated in the reaction.[123,124]

(1) $M^n + HOOH \rightarrow M^{n-1} + HOO\cdot + H^+$ $M^n = Cu^{II}, Mn^{III}, Fe^{III}, Co^{III}$

(2) $M^{n-1} + HOOH \rightarrow M^n + HO\cdot + HO^-$
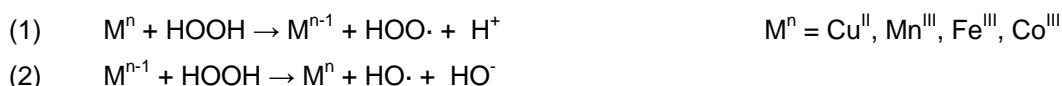
It is the goal of biomimetic studies to identify a catalyst that generates a selective metal-based oxidant analogous to those used in biological systems, rather than HO· or RO· radicals that readily initiate radical chain autooxidations in the presence of O_2.

I3.2.2.1. Mechanistic probes

Because it is often very difficult in catalytic oxidation systems to observe the actual reagent that carries out the key oxidative transformation, indirect probes have been useful to deduce the reaction mechanism.[125] These probes provide insight into the oxidative power of the active species responsible for substrate attack along with the presence of radicals and their lifetime, when generated.

Kinetic isotope effects (KIE). The kinetic isotope effect is a competition reaction between protio- and deuteroalkanes based on the difference of C-H/C-D bond strength. In a radical-chain

reaction initiated by hydroxyl radicals, KIE values between 1 and 2 have been reported[126]. The low discrimination between C-H and C-D bonds is consistent with the strong oxidative power of the oxidant. In some enzymatic reactions, KIE values higher than the theoretical maximum of 7[127] have been reported and explained by tunneling effects; for example, values higher than 11 for cytochrome P450[128] and 50 – 100 for methane monooxygenase[129] have been reported.

Regioselectivity. The nature of the oxidant in a hydroxylation reaction can also be probed by an intramolecular competition reaction in the oxidation of adamantane, which contains both secondary and tertiary C-H bonds (Scheme 25). The regioselectivity is parameterized as a 3°/2° ratio derived from the amount of 1-adamantanol divided by the amount of 2-adamantanol and 2-adamantanone and multiplied by 3 to correct for the higher number of secondary C-H bonds. The indiscriminate hydroxyl radical typically affords values near 2, while *t*BuO· initiated reactions exhibit values around 10.[130] For cytochrome P450s and heme catalysts, the adamantane regioselectivity can achieve values as high as 48.[131]
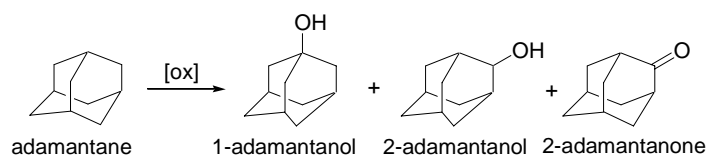
Scheme 25. Possible products obtained in the oxidation of adamantane.

Alcohol/ketone ratio (A/K) The A/K is the simplest test that reflects the lifetime of an alkyl radical. When long-lived alkyl radicals are generated in the oxidation of secondary alkanes such as cyclohexane, O$_2$ traps the radicals at a diffusion-controlled rate and gives alkylperoxyl radicals (Scheme 26). Subsequent reaction of the alkylperoxyl radicals results in a Russell-type termination step leading to the formation of equimolar amounts of alcohol and ketone.[132] When the reaction is performed in the absence of O$_2$, the product yield can decrease dramatically due to a lack of chain propagation. Alkyl radicals formed by some metal-based oxidants, on the other hand, react quickly with the metal center, to form the alcohol product. In this case, alcohol would be expected to be the sole oxidation product, although some ketone may also be formed presumably due to further oxidation of the alcohol product.
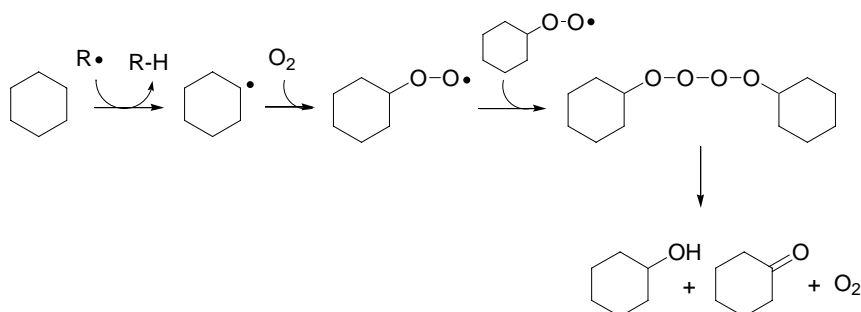
Scheme 26. Alkyl radical trapping by O$_2$ giving equimolar amounts of alcohol and ketone.

Substrate-based probes of radical lifetime. *Cis* and *trans* isomers of 1,2-dimethylcyclohexane and decahydronaphthalene (decalin) have been commonly used to probe

the lifetime of the nascent alkyl radical in the alkane hydroxylation reactions. This test takes advantage of the competition between the epimerization of the putative tertiary alkyl radical intermediate and the formation of the product C-O bonds. This competition determines the ratio of *cis* and *trans* tertiary alcohol products (Scheme 27). It is estimated that the tertiary carbon radical epimerizes with a first-order rate constant of 10^9 s^{-1}.[133,134] Reactions that give rise to long-lived free radicals should afford both *cis* and *trans* alcohols with a *cis*:*trans* ratio of approximately 1.2. On the other hand, short-lived alkyl radicals where the C-O bond formation step is extremely fast should afford a tertiary alcohol where the original configuration is retained. Analogous analysis can be done in oxidation reactions of *cis* and *trans* olefins. Loss of stereoretention in the oxidized products is indicative of the presence of a reaction intermediate capable of undergoing *cis-trans* isomerization and thus, the implication of non-concerted reaction pathways.

retention of configuration   inversion of configuration
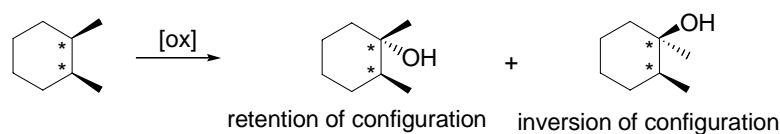
Scheme 27. Possible isomers of the tertiary alcohol obtained in the oxidation of *cis*-1,2-dimethylcyclohexane.

Labeling studies: **Oxo-hydroxo tautomerism.** Labeling studies have been used as a mechanistic tool to unambiguously characterize oxygen atom transfer mechanisms mediated by metal-oxo species in opposition to mechanisms related to free radical oxidation reactions.[103,135] Since O₂ traps carbon centered alkyl radicals at diffusion controlled rates, O₂ incorporation into products indicates that free-diffusing alkyl radicals are generated along the reaction pathway. On the other hand, when the oxidation is performed in water, metal-oxo species are able to transfer an oxygen atom coming from either the oxygen source or bulk water. This fact has been explained by the so called "oxo-hydroxo tautomerism", a mechanism involving a rapid shift of two electrons and one proton from a hydroxo ligand to the oxo group leading to the transformation of the hydroxo ligand into an electrophilic oxo entity (Scheme 28).

heme center   **non-heme center**
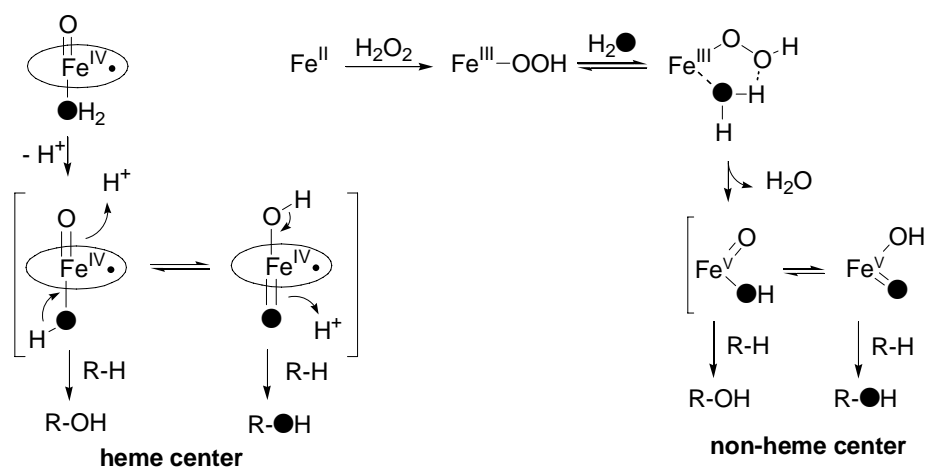
Scheme 28. "Oxo-hydroxo tautomerism" for heme and non-heme centers. This process mediates the incorporation of oxygen from water into the oxidized products.

This phenomenon was initially proposed for heme systems[135] in which the oxo-hydroxo tautomerism takes place between two ligands in a relative *trans* configuration. Afterwards, the idea was extended to non-heme systems in which water was also incorporated into the oxidized products.[83,84] In this case, in general, the two groups implicated in the "oxo-hydroxo tautomerism" are disposed *cis* one to each other. In catalytic model systems, a water-assisted pathway to form a high-valent oxo species responsible for the chemistry is proposed. This fact together with the oxo-hydroxo tautomerism can explain the incorporation of oxygen coming from water into oxidized products.[103,136] Experimentally, the existence of the "oxo-hydroxo tautomerism" can be detected by the addition of ^{18}O-labeled water to the catalytic media. Posterior mass-spectroscopy (MS) analysis of the oxidized products allows the detection and quantification of ^{18}O-labeled compounds.

I3.2.2.2. Oxidation of alkanes (C-H bonds)

Great efforts have been devoted to the preparation of complexes capable of oxidizing hydrocarbons. In this line, several non-heme mononuclear iron complexes have been prepared which are capable of performing stereoselective alkane oxidation to give alcohols. Designing suitable ligands is essential to achieve good results and a schematic representation of the most relevant ones is depicted in Scheme 29. In outline, it has been seen that the most effective non-heme iron(II) catalysts are those possessing nitrogen-based tripodal or linear tetradentate ligands so that two *cis* labile sites available for coordination with exogenous ligands (the oxidant and/or the substrate) are available.
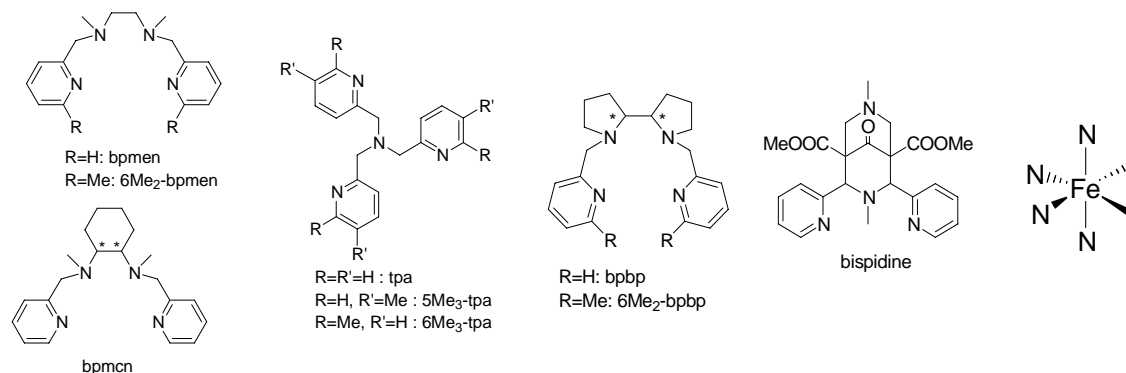
Scheme 29. Schematic representation of the most relevant ligands used to prepare mononuclear iron(II) complexes to perform alkane and olefin oxidations along with the coordination they adopt around the metal center.

Two main families of complexes possessing tetradentate ligands have been studied in the oxidation of alkanes: tpa (tripodal) and bpmen (linear) families.[118] Mononuclear iron(II) complexes derived from these ligands are quite efficient catalysts and the mechanistic probes clearly point towards the mediation of metal-based oxidants (Table 2).[103]

Table 2. Oxidation of alkanes with H_2O_2 catalyzed by different iron(II) complexes.[103]

	cyclohexane		cis-1,2-DMCH	adamantane	oxygen-source
ligand	A + K (A/K)[a]	KIE	RC (%)[b]	3º/2º[c]	H_2O / H_2O_2 / O_2[d]
tpa	3.2 (6)	3.5	100	17	27 / 70 / 3
bpmen	6.3 (5)	3.2	96	15	18 / 84 / 0
5Me₃-tpa	4.0 (5)	3.8	100	21	38 / 69 / 0
6Me₃-tpa	2.9 (2)	3.3	54	15	1 / 22 / 77

Catalyst:H_2O_2:alkane = 1:10:1000. [a]Turnover number (TN, mols of product / mols of catalyst), A = cyclohexanol, K = cyclohexanone. A/K = (mols A / mols K). [b]Retention of configuration in the oxidation of cis-1,2-DMCH. [c]3º/2º = 3x(1-adamantanol)/(2-adamantanol+2-adamantanone). [d]Origin of the oxygen atom (%): from water / hydrogen peroxide / O_2.

As can be seen in Table 2 slight modifications in the ligand architecture can cause important changes in the catalytic results especially when the modification is introduced in the α position of the pyridine ring. This is clearly seen for 6Me₃-tpa which generates a catalyst with some non-metal based character as evidenced by the low percentage of retention of configuration (RC) in the oxidation of cis-1,2-dimethylcyclohexane (cis-1,2-DMCH) and by the high level of O_2 incorporation, a clear indication that autooxidation processes take place. On the other hand, water incorporation into products points towards the mediation of high valent iron-oxo species. Moreover, bpmen and tpa give rise to catalysts which are especially efficient affording high conversions of H_2O_2 into products.

Other mononuclear iron systems capable of oxidizing alkanes using H_2O_2 have been prepared.[137-139] However, none of them can compare to tpa or bpmen systems neither in terms of efficiency nor in metal-based character of the active species.

From a synthetic organic chemistry point of view, it is interesting to refer to a recent work from White et al. in which the oxidation of aliphatic C-H bonds is achieved in high yields and in a selective manner using a combination of H_2O_2 and acetic acid as the oxidant.[140] In this study the catalyst is a mononuclear iron complex with the bpbp ligand (see Scheme 29), a chiral version of bpmen.

I3.2.2.3. Oxidation of alkenes (C=C double bonds)

Concomitantly with the studies of alkane oxidation, the same bio-inspired non-heme iron catalysts were tested in the oxidation of olefins using H_2O_2. These complexes differ from previously reported iron catalysts in their ability to catalyze not only epoxidation but also olefin cis-dihydroxylation analogously to the reaction performed by Rieske dioxygenases.[141] Concurrently to alkane oxidation, the first examples reported of non-heme iron catalysts capable of eliciting olefin epoxidation and cis-dihydroxylation are those containing ligands of the tpa and bpmen family.[142] Afterwards other mononuclear complexes based on bpmcn,[143] bpbp[144] and bispidine[145] ligands have also given good results in this field (Scheme 29).

Table 3. Oxidation of alkenes with H$_2$O$_2$ catalyzed by different iron(II) complexes.

ligand	cyclooctane D + E (D/E)[b]	*cis*-diol 2H$_2$O$_2$/H$_2$O$_2$+H$_2$O/2H$_2$O[c]	epoxide H$_2$O$_2$ / H$_2$O[d]	*cis*-2-heptene RC diol[e] (%)	RC epoxide[f] (%)	ref.
tpa	7.4 (1.2)	3 / 97 / 1	90 / 9	96	80	142
5Me$_3$-tpa	6.7 (1.4)	2 / 98 / 1	93 / 2	94	83	142
6Me$_3$-tpa	7.1 (16.8)	96 / 4 / 0	54 / 3	93	35	142
bpmen	8.4 (0.1)	23 / 73 / 4	73 / 30	79	92	94
6Me$_2$-bpmen	7.9 (4.3)	-	-	78	60	146
α-bpmcn	6.5 (0.1)	4 / 88 / 1	66 / 15	67	85	143
bispidine	2.5 (1.5)	95 / 5 / 0	100 / 0	-	-	145
bpbp[a]	4.3 (0.7)	-	-	-	-	144
6Me$_2$-bpbp[a]	6.5 (64.0)	-	-	95	95	144

Catalyst:H$_2$O$_2$:cyclooctene = 1:10:1000. [a]1-octene was used instead of cyclooctene. [b]Turnover number (TN, mols of product / mols of catalyst), E = epoxide, D = diol. D/E = (mols of D / mols of E). [c]Origin of the oxygen atom (%) in the diol: both oxygens from H$_2$O$_2$ / one oxygen from H$_2$O$_2$ and one from water / both oxygens from water. [d]Origin of the oxygen atom in the epoxide (%): from H$_2$O$_2$ / from water. [e]Retention of configuration for the diol. [f]Retention of configuration for the epoxide.

Table 3 shows that conversion of the oxidant in cylooctene oxidation can be as high as 84%, and diol:epoxide ratios range from 0.1 to 16.8. Diol product does not derive from the epoxide, as both products are formed at the same time, and the use of epoxide as a potential substrate under the same reaction conditions does not afford *cis*-diol. It is clear from the results that the ligand structure exerts a significant control on the diol:epoxide ratio. A general trend is that the presence of methyl groups in the α position of the pyridine ring results in an increase in the diol:epoxide ratio. In most cases, high retention of configuration is observed in the oxidation of *cis*-2-heptene. This observation together with the incorporation of oxygen from water into oxidation products clearly indicates that a metal-based oxidant is operating in these reactions.

Pentadentate ligands which only leave one labile coordination site have also been used but the catalytic results are poorer.[147,148] On the other hand, tetradentate ligands which adopt an equatorial coordination and leave two labile sites in a relative *trans* disposition have also been applied to these catalytic tranformations but no *cis*-diol is formed.[148,149] It seems clear from these results that the availability of two labile sites in a *cis* configuration is necessary to model the *cis*-dihydroxylation reaction catalyzed by Rieske dioxygenases in biological systems.

Remarkably, Jacobsen *et al.* used a mononuclear iron(II) complex based on the bpmen ligand (Scheme 29) which could perform the epoxidation of alkenes using a combination of H$_2$O$_2$ and acetic acid as the oxidant.[150] Aliphatic olefins were epoxidized in high yields (60 – 90%) in less than 5 min. Nowadays this methodology constitutes a synthetic useful strategy for the synthesis of epoxides.

The most selective catalyst for *cis*-dihydroxylation is 5Me$_3$-tpa, which can catalyze the oxidation of olefins to *cis*-diols under conditions of limiting substrate with high conversion and efficiency.[151] Moreover, chiral ligands have been used for the development of asymmetric systems capable of giving diols with some enantiomeric excess and with high selectivity.[144,146] Overall, these mononuclear non-heme iron(II) systems may constitute an attractive environmentally benign alternative to the traditional toxic and more expensive osmium reagents

used for *cis*-dihydroxylation, though significant improvement in reaction efficiencies is highly required to achieve this goal.

I3.2.2.4. A common mechanistic landscape

The mechanism implicated in the oxidation of alkanes and olefins in the previously described systems has been a matter of debate during the last decade. Labeling studies together with DFT calculations are key tools in order to draw a mechanistic landscape that can explain both alkane hydroxylation and olefin epoxidation and *cis*-dihydroxylation (Scheme 30).
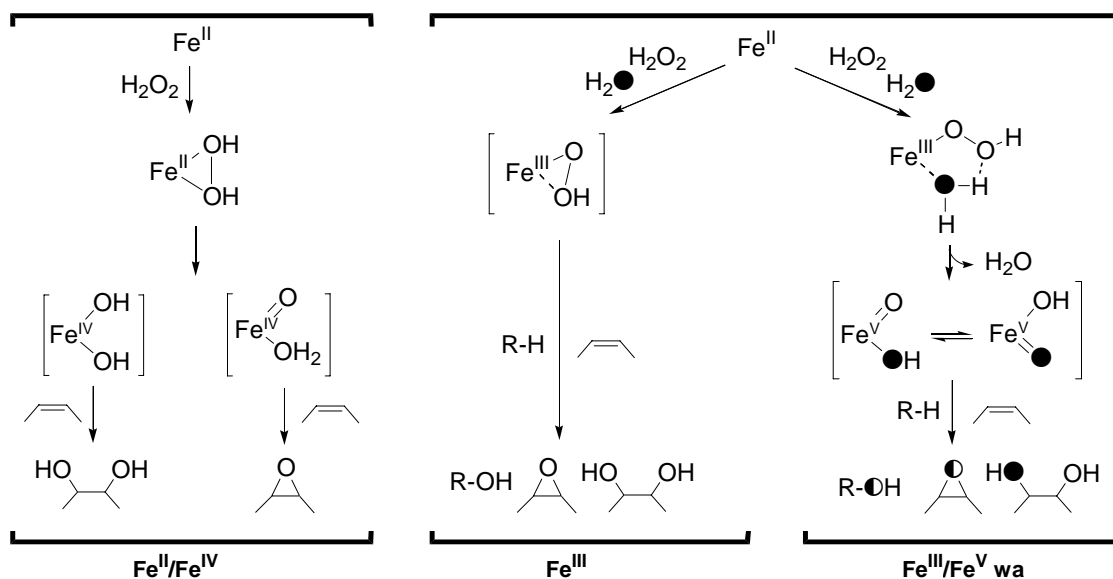
Scheme 30. A common mechanistic landscape for the oxidation of alkanes and alkenes by mononuclear iron(II) complexes.

The isotopic labeling results in the *cis*-dihydroxylation reaction is a valuable tool to address the active species responsible for the chemistry. Class A catalysts insert one atom of oxygen from water and one atom of oxygen from H_2O_2 (tpa, α-bpmcn, 5Me$_3$-tpa), while class B catalysts insert both oxygens from peroxide (6Me$_3$-tpa, bispidine) (see Table 3 for labeling results).

In class A catalysts the labeling results suggest the implication of a $Fe^V(O)(OH)$ species formed *via* water assisted O-O heterolysis of the Fe(III)-hydroperoxo species (Fe^{III}/Fe^V wa in Scheme 30). Thus, both oxygen atoms from the iron(V)-oxo-hydroxo intermediate end up into the diol. The product formed depends on the initial attack of the iron(V)-oxo-hdyroxo: the formation of the diol occurs when the attack over the olefin starts by the hydroxo group of HO-Fe^V=O, while epoxide formation is achieved by direct insertion of the oxo group into the double bond.[152] In class B catalysts two mechanistic scenarios can be depicted to account for the lack of water incorporation into oxidized products: the intervention of an iron(III)-hydroperoxo without the mediation of water (Fe^{III} in Scheme 30) or an alternative pathway in which the high valent species responsible for the oxidation is an Fe^{IV} compound formed by O-O homolysis of a $Fe^{II}(H_2O_2)$ intermediate (Fe^{II}/Fe^{IV} in Scheme 30). This mechanism has been studied using

bispidine type of ligands and by means of DFT calculations it has been established that two isomers are energetically favored: $Fe^{IV}(OH)_2$ and $H_2O\text{-}Fe^{IV}=O$.[145] Theoretical calculations indicate that the former is responsible for the *cis*-dihydroxylation and the latter affords the epoxide product.

In the oxidation of alkanes, the incorporation of oxygen from water into the alcohol product is taken as an indication for the involvement of a high-valent iron-oxo species (Fe^{III}/Fe^V wa in Scheme 30).[103] The oxo group of the $Fe^V(O)(OH)$ species abstracts the hydrogen atom from the substrate to form an alkyl radical which rapidly rebounds with the newly formed hydroxo group to give the corresponding alcohol (Scheme 31).
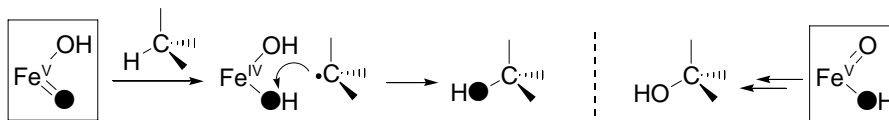
Scheme 31. Mechanism of alkane hydroxylation by HO-Fe^V=O. One tautomer allows the incorporation of oxygen from H_2O_2 and the other from H_2O into the oxidized products.

Through this mechanism the maximum amount of oxygen from water that can be incorporated into the alcohol should be 50%. In addition, because of the competition between oxo-hydroxo tautomerism and substrate oxidation, the extent of water incorporation into products is inversely related to the strength of the hydroxylated C-H bond, a phenomenon which has already been observed in oxidation reactions catalyzed by non-heme iron complexes.[103] The involvement of a non-water assisted pathway (Fe^{III} pathway in Scheme 30) has also been postulated in some cases to explain some labeling results for alkane oxidation.

I3.3. Future prospects

Despite all the advances done in the recent years in the study of mononuclear non-heme iron enzymes implicated in O_2 activation, there is still a long way to run in part because their great structural variety suggests that their reaction mechanisms are much richer than in heme systems, which open the door to develop new routes to introduce new reactivity. Moreover, mononuclear non-heme iron systems may have implications in medicine and biotechnology through the development of drugs based on activated bleomycin, a non-heme iron system implicated in the reactivity of a family of glycopeptides-derived antibiotics that has anti-tumor activity. In activated bleomycin a Fe^{III}-OOH type of intermediate is the last detectable species prior to DNA cleavage, and it may serve as the precursor of a formally Fe^V=O species.

Though several highly efficient bioinspired catalysts have been prepared, developing methodologies to perform the selective oxidation of C-H bonds at synthetic scale will represent a huge step to reach important technological applications. The ability of these complexes to perform *cis*-dihydroxylation reactions is especially interesting because they constitute an environmentally friendly alternative to OsO_4 and $KMnO_4$, the oxidants used nowadays. In fact, the toxicity of OsO_4 and the stoichiometric nature of the $KMnO_4$ dihydroxylation, which usually

provides only modest yields of diols, are strong incentives for the development of more efficient systems. Finally, preparation of high-valent metal species (Fe^{IV}, Fe^{V}) that reproduce the structural and electronic properties of biological systems may be of great importance to unravel the mechanistic pathways by which nature performs highly efficient and selective oxidative transformations.

I.4. References

1. Kovaleva, E. G.; Lipscomb, J. D., *Nature Chemical Biology* **2008,** *4*, 186-193.

2. Bertini, I.; Gray, H. B.; Stiefel, E. I.; Valentine, S. J., *Biological inorganic Chemistry: structure & reactivity.* University Science Books: Sausalito, California, 2007.

3. Holm, R. H.; Kennepohl, P.; Solomon, E. I., *Chem. Rev.* **1996,** *96*, 2239-2314.

4. Costas, M.; Mehn, M. P.; Jensen, M. P.; Que Jr., L., *Chem. Rev.* **2004,** *104*, 939-986.

5. Seigbahn, P. E. M.; Borowski, T., *Acc. Chem. Res.* **2006,** *39*, 729-738.

6. Nam, W., *Acc. Chem. Res.* **2007,** *40*, 465.

7. Mirica, L. M.; Ottenwaelder, X.; Stack, T. D. P., *Chem. Rev.* **2004,** *104*, 1013-1046.

8. Kraatz, H.-B.; Metzler-Nolte, N., *Concepts and Models in Bioinorganic Chemistry.* Wiley-VCH: Weinheim, 2006.

9. Lippard, S. J.; Berg, J. M., *Principles of Bioinorganic Chemistry*. University Science Books: Mill Valley, CA, 1994.

10. Bento, I.; Carrondo, M. A.; Lindley, P. F., *J. Biol. Inorg. Chem.* **2006,** *11*, 539-547.

11. Solomon, E. I.; Sundaram, U. M.; Machonkin, T. E., *Chem. Rev.* **1996,** *96*, 2563-2605.

12. Himmelwright, R. S.; Eickman, N. C.; LuBien, C. D.; Lerch, K.; Solomon, E. I., *J. Am. Chem. Soc.* **1980,** *102*, 7339-7344.

13. Cuff, M. E.; Miller, K. I.; van Holde, K. E.; Hendrickson, W. N., *J. Mol. Biol.* **1998,** *278*, 855-870.

14. Matoba, Y.; Kumagai, T.; Yamamoto, A.; Sugiyama, M. J., *J. Biol. Chem.* **2006,** *281*, 8981-8990.

15. van Holde, K. E.; Miller, K. I.; Decker, H., *J. Biol. Chem.* **2001,** *276*, 15563-15566.

16. Morioka, C.; Tachi, Y.; Suzuki, S.; Itoh, S., *J. Am. Chem. Soc.* **2006,** *128*, 6788-6789.

17. Decker, H.; Schweikardt, T.; Tuczek, F., *Angew. Chem. Int. Ed.* **2006,** *45*, 4546-4550.

18. Lewis, E. A.; Tolman, W. B., *Chem. Rev.* **2004,** *104*, 1047-1076.

19. Zhang, C. X.; Kaderli, S.; Costas, M.; Kim, E.; Neuhold, Y.; Karlin, K. D.; Zuberbühler, A. D., *Inorg. Chem.* **2003,** *42*, 1807-1824.

20. Fujisawa, K.; Tanaka, M.; Moro-oka, Y.; Kitajima, N., *J. Am. Chem. Soc.* **1994,** *116*, 12079-12080.

21. Spencer, D. J. E.; Aboelella, N. W.; Reynolds, A. M.; Holland, P. L.; Tolman, W. B., *J. Am. Chem. Soc.* **2002,** *124*, 2108-2109.

22. Reynolds, A. M.; Gherman, B. F.; Cramer, C. J.; Tolman, W. B., *Inorg. Chem.* **2005,** *44*, 6989-6997.

23. Würtele, C.; Gaoutchenova, E.; Harms, K.; Holthausen, M. C.; Sundermeyer, J.; Schindler, S., *Angew Chem. Int. Ed.* **2006,** 3867-3869.

24. Aboelella, N. W.; Lewis, E. A.; Reynolds, A. M.; Brennessel, W. W.; Cramer, C. J.; Tolman, W. B., *J. Am. Chem. Soc.* **2002,** *124*, 10660-10661.

25. Prigge, S. T.; Eipper, B. A.; Mains, R. E.; Amzel, L. M., *Science* **2004,** *304*, 864-867.

26. Juda, G. A.; Shepard, E. M.; Elmore, B. O.; Dooley, D. M., *Biochemistry* **2006,** *45*, 8788-8800.

27. Kamachi, T.; Kihara, N.; Shiota, Y.; Yoshizawa, K., *Inorg. Chem.* **2005,** *44*, 4226-4236.

28. Jacobson, R. R.; Tyeklár, Z.; Farooq, A.; Karlin, K. D.; Liu, S.; Zubieta, J., *J. Am. Chem. Soc.* **1988,** *110*, 3690-3692.

29. Tyeklár, Z.; Jacobson, R. R.; Wei, N.; Murthy, N. N.; Zubieta, J.; Karlin, K. D., *J. Am. Chem. Soc.* **1993,** *115*, 2677-2689.

30. Becker, M.; Heinemann, F. W.; Schindler, S., *Chem. Eur. J.* **1999,** *5*, 3124-3129.

31. Weitzer, M.; Schatz, M.; Hampel, F.; Heinemann, F. W.; Schindler, S., *J. Chem. Soc., Dalton Trans.* **2002,** *5*, 686-694.

32. Kitajima, N.; Fujisawa, K.; Moro-oka, Y., *J. Am. Chem. Soc.* **1989,** *111*, 8975-8976.

33. Kitajima, N.; Fujisawa, L.; Fujimoto, C.; Moro-oka, Y.; Hashimoto, S.; Kitagawa, T.; Toriumi, K.; Tatsumi, K.; Nakamura, A., *J. Am. Chem. Soc.* **1992,** *114*, 1277-1291.

34. Mahapatra, S.; Halfen, J. A.; Wilkinson, E. C.; Pan, G.; Wang, X.; Young, V. G., Jr.; Cramer, C. J.; Que, L., Jr.; Tolman, W. B., *J. Am. Chem. Soc.* **1996,** *118*, 11555-11574.

35. Halfen, J. A.; Mahapatra, S.; Wilkinson, E. C.; Kaderli, S.; Young, V. G., Jr.,; Que, L., Jr.; Zuberbühler, A. D.; Tolman, W. B., *Science* **1996,** *271*, 1397-1400.

36. Mahapatra, S.; Young, V. G. J.; Kaderli, S.; Zuberbühler, A. D.; Tolman, W. B., *Angew. Chem. Int. Ed.* **1997,** *26*, 130-133.

37. Mahadevan, V.; Hou, Z.; Cole, A. P.; Root, D. E.; Lal, T. K.; Solomon, E. I.; Stack, T. D. P., *J. Am. Chem. Soc.* **1997,** *119*, 11996-11997.

38. Cole, A. P.; Mahadevan, V.; Mirica, L. M.; Ottenwaelder, X.; Stack, T. D. P., *Inorg. Chem.* **2005,** *44*, 7345-7364.

39. Tolman, W. B., *Acc. Chem. Res.* **1997,** *30*, 227-237.

40. Mahadevan, V.; Henson, M. J.; Solomon, E. I.; Stack, T. D. P., *J. Am. Chem. Soc.* **2000,** *122*, 10249-10250.

41. Hatcher, L. Q.; Vance, M. A.; Sarjeant, A. A. N.; Solomon, E. I.; Karlin, K. D., *Inorg. Chem.* **2006,** *45*, 3004-3013.

42. Maiti, D.; Woertink, J. S.; Sarjeant, A. A. N.; Solomon, E. I.; Karlin, K. D., *Inorg. Chem.* **2008,** *47*, 3787-3800.

43. Cole, A. P.; Root, D. E.; Mukherjee, P.; Solomon, E. I.; Stack, T. D. P., *Science* **1996,** *273*, 1848-1850.

44. Taki, M.; Teramae, S.; Nagatomo, S.; Tachi, Y.; Kitagawa, T.; Itoh, S.; Fukuzumi, S., *J. Am. Chem. Soc.* **2002,** *124*, 6367-6377.

45. Mahapatra, S.; Young, V. G., Jr.; Kaderli, S.; Zuberbühler, A. D.; Tolman, W. B., *Angew. Chem. Int. Ed. Eng.* **1997,** *36*, 130-133.

46. Kodera, M.; Katayama, K.; Tachi, Y.; Kano, K.; Hirota, S.; Fujinami, S.; Suzuki, M., *J. Am. Chem. Soc.* **1999,** *121*, 11006-11007.

47. Karlin, K. D.; Nasir, M. S.; Cohen, B. I.; Cruse, R. W.; Kaderli, S.; Zuberbühler, A. D., *J. Am. Chem. Soc.* **1994,** *116*, 1324-1336.

48. Pidcock, E.; Obias, H. V.; Zhang, C. X.; Karlin, K. D.; Solomon, E. I., *J. Am Chem. Soc.* **1998,** *120*, 7841-7847.

49. Santagostini, L.; Gullotti, M.; Monzani, E.; Casella, L.; Dillinger, R.; Tuczek, F., *Chem. Eur. J.* **2000,** *6*, 519-522.

50. Menif, R.; Martell, A. E.; Squattrito, P. J.; Clearfield, A., *Inorg. Chem.* **1990,** *29*, 4723-4729.

51. Costas, M.; Xifra, R.; Llobet, A.; Solà, M.; Robles, J.; Parella, T.; Stoeckli-Evans, H.; Neuburger, M., *Inorg. Chem.* **2003,** *42*, 4456-4468.

52. Costas, M.; Ribas, X.; Poater, A.; López Valbuena, J. M.; Xifra, R.; Company, A.; Duran, M.; Solà, M.; Llobet, A.; Corbella, M.; Usón, M. A.; Mahía, J.; Solans, X.; Shan, X.; Benet-Buchholz, J., *Inorg. Chem.* **2006,** *45*, 3569-3581.

53. Mahapatra, S.; Halfen, J. A.; Tolman, W. B., *J. Am. Chem. Soc.* **1996,** *118*, 11575-11586.

54. Itoh, S.; Nakao, H.; Berreau, L. M.; Kondo, T.; Komatsu, M.; Fukuzumi, S., *J. Am. Chem . Soc.* **1998,** *120*, 2890-2899.

55. Holland, P. L.; Rodgers, K. R.; Tolman, W. B., *Angew. Chem. Int. Ed. Engl.* **1999,** *38*, 1139-1142.

56. Nasir, M. S.; Karlin, K. D.; McGowty, D.; Zubieta, J., *J. Am. Chem. Soc.* **1991,** *113*, 698-700.

57. Obias, H. V.; Lin, Y.; Murthy, N. N.; Pidcock, E.; Solomon, E. I.; Ralle, M.; Blackburn, N. J.; Neuhold, Y.-M.; Zuberbühler, A. D.; Karlin, K. D., *J. Am. Chem. Soc.* **1998,** *120*, 12960-12961.

58. Zhang, C. X.; Liang, H.-C.; Kim, E.-i.; Shearer, J.; Helton, M. E.; Kim, E.; Kaderli, S.; Incarvito, C. D.; Zuberbuhler, A. D.; Rheingold, A. L.; Karlin, K. D., *J. Am. Chem. Soc.* **2003,** *125*, 634-635.

59. Shearer, J.; Zhang, C. X.; Zakharov, L. N.; Rheingold, A. L.; Karlin, K. D., *J. Am. Chem . Soc.* **2005,** *127*, 5469-5483.

60. Mirica, L. M.; Rudd, D. J.; Vance, M. A.; Solomon, E. I.; Hodgson, K. O.; Hedman, B.; Stack, T. D. P., *J. Am. Chem. Soc.* **2006,** *128*, 2654-2665.

61. Mahadevan, V.; DuBois, J. L.; Hedman, B.; Hodgson, K. O.; Stack, T. D. P., *J. Am. Chem. Soc.* **1999,** *121*, 5583-5584.

62. Battaini, G.; Granata, A.; Monzani, E.; Gullotti, M.; Casella, L., *Adv. Inorg. Chem.* **2006,** *58*, 185-233.

63. Itoh, S.; Kumei, H.; Taki, M.; Nagatomo, S.; Kitagawa, T.; Fukuzumi, S., *J. Am. Chem. Soc.* **2001,** *123*, 6708-6709.

64. Palavicini, S.; Granata, A.; Monzani, E.; Casella, L., *J. Am. Chem. Soc.* **2005,** *127*, 18031-18036.

65. Itoh, S.; Fukuzumi, S., *Acc. Chem. Res.* **2007,** *40*, 592-600.

66. Mirica, L. M.; Vance, M.; Rudd, D. J.; Hedman, B.; Hodgson, K. O.; Solomon, E. I.; Stack, T. D. P., *Science* **2005,** *308*, 1890-1892.

67. Cotton, F. A.; Wilkinson, G.; Murillo, C. A.; Bochmann, M., *Advanced Inorganic Chemistry*. 6th ed.; John Wiley & Sons, INC.: 1999.

68. Wallar, B. J.; Lipscomb, J. D., *Chem. Rev.* **1996,** *96*, 2625-2657.

69. Montellano de Ortiz, P. R., *Cytochrome P-450. Structure, Mechanism and Biochemistry*. Plenum Press: New York, 1986.

70. Schlichting, I.; Berendzen, J.; Chu, K.; Stock, A. M.; Maves, S. A.; Benson, D. E.; Sweet, R. M.; Ringe, D.; Petsko, G. A.; Sligar, S. G., *Science* **2000,** *287*, 1615-1622.

71. Meunier, B.; de Visser, S. P.; Shaik, S., *Chem. Rev.* **2004,** *104*, 3947-3980.

72. Koehntop, K. D.; Emerson, J. P.; Que, J., L., *J. Biol. Inorg. Chem.* **2005,** *10*, 87-93.

73. Hegg, E. L.; Lawrence Que, J., *Eur. J. Biochem.* **1997,** *250*, 625-629.

74. Kauppi, B.; Lee, K.; Carredano, E.; Parales, R. E.; Gibson, D. T.; Eklund, H.; Ramaswamy, S., *Structure* **1998,** *6*, 571-586.

75. Gibson, D. T.; Resnick, S. M.; Lee, K.; Brand, J. M.; Torok, D. S.; Wackett, L. P.; Schocken, M. J.; Haigler, B. E., *J. Bacteriol.* **1995,** *177*, 2615-2621.

76. Wolfe, M. D.; Altier, D. J.; Stubna, A.; Popescu, C. V.; Münck, E.; Lipscomb, J. D., *Biochemistry* **2002,** *41*, 9611-9626.

77. Ziffer, H.; Jerina, D. M.; Gibson, D. T.; Kobal, V. M., *J. Am. Chem. Soc.* **1973,** *95*, 4048-4049.

78. Crutcher, S. E.; Geary, P. J., *Biochem. J.* **1979,** *177*, 393-400.

79. Pavel, E. G.; Martins, L. J.; Ellis, W. R., Jr.; Solomon, E. I., *Chem. Biol.* **1994,** *1*, 173-183.

80. Karlsson, A.; Parales, J. V.; Parales, R. E.; Gibson, D. T.; Eklund, H.; Ramaswamy, S., *Science* **2003,** *299*, 1039-1042.

81. Lee, D. G.; Chen, T., *J. Am. Chem . Soc.* **1989,** *111*, 7534 - 7538.

82. Schröder, M., *Chem. Rev.* **1980,** *80*, 187-213.

83. Wolfe, M. D.; Lipscomb, J. D., *J. Biol. Chem.* **2003,** *278*, 829-835.

84. Wackett, L. P.; Kwart, L. D.; Gibson, D. T., *Biochemistry* **1988,** *27*, 1360-1367.

85. Markis, T. M.; von Koenig, K.; Schlichting, I.; Sligar, S. G., *J. Inorg. Biochem.* **2006,** *100*, 507-518.

86. Bollinger, J. M., Jr.; Price, J. C.; Hoffart, L. M.; Barr, E. W.; Krebs, C., *Eur. J. Inorg. Chem.* **2005,** 4245-4254.

87. Krebs, C.; Price, J. C.; Baldwin, J.; Saleh, L.; Green, M. T.; Bollinger, J. M., Jr., *Inorg. Chem.* **2005,** *44*, 742-757.

88. Hoffart, L. M.; Barr, E. W.; Guyer, R. B.; Bollinger, J. M.; Krebs, C., *Proc. Natl. Acad. Sci. U. S. A.* **2006,** *103*, 14738-14743.

89. Eser, B. E.; Barr, E. W.; Frantom, P. A.; Saleh, L.; Bollinger, J. M. J.; Krebs, C.; Fitzpatrick, P. F., *J. Am. Chem. Soc.* **2007,** *129*, 11334-11335.

90. Galonic, D. P.; Barr, E. W.; Walsh, C. T.; Bollinger, J. M.; Krebs, C., *Nat. Chem. Biol.* **2007,** *3*, 113-116.

91. Sturgeon, B. E.; Burdi, D.; Chen, S.; Huynh, B.-H.; Edmondson, D. E.; Stubbe, J.; Hoffman, B. M., *J. Am. Chem. Soc.* **1996,** *118*, 7551-7557.

92. Riggs-Gelasco, P. J.; Shu, L.; Chen, S.; Burdi, D.; Huynh, B. H.; Que, L., Jr.; Stubbe, J., *J. Am. Chem. Soc.* **1998,** *120*, 849-860.

93. Shu, L.; Nesheim, J. C.; Kauffmann, K.; Münck, E.; Lipscomb, J. D.; Que, L., Jr., *Science* **1997,** *275*, 515-518.

94. Quiñonero, D.; Morokuma, K.; Musaev, D. G.; Mas-Ballesté, R.; Que, L., Jr., *J. Am. Chem. Soc.* **2005,** *127*, 6548-6549.

95. Park, M. J.; Lee, J.; Suh, Y.; Kim, J.; Nam, W., *J. Am. Chem. Soc.* **2006,** *128*, 2630-2634.

96. Groves, J. T.; Haushalter, R. C.; Nakamura, M.; Nemo, T. E.; Evans, B. J., *J. Am. Chem. Soc.* **1981,** *103*, 2884-2886.

97. Rohde, J.-U.; In, J.-H.; Lim, M.-H.; Brennessel, W. W.; Bukowski, M. R.; Stubna, A.; Münck, E.; Nam, W.; Que, J., L., *Science* **2003,** *229*, 1037-1039.

98. Jensen, M. P.; Lange, S. J.; Mehn, M. P.; Que, E. L.; Que Jr., L., *J. Am. Chem. Soc.* **2003,** *125*, 2113-2128.

99. Lange, S. J.; Miyake, H.; Que, L., Jr., *J. Am. Chem. Soc.* **1999,** *121*, 6330-6331.

100. Miyake, H.; Chen, K.; Lange, S. J.; Que, J., L., *Inorg. Chem.* **2001,** *40*, 3534-3538.

101. Klinker, E. J.; Brennessel, W. W.; Woodrum, N. L.; Cramer, C. J.; Que, L., Jr., *Angew. Chem. Int. Ed.* **2005,** *44*, 3690-3694.

102. de Oliveira, F. T.; Chanda, A.; Banerjee, D.; Shan, X.; Mondal, S.; Que, L., Jr.; Bominaar, E. L.; Münck, E.; Collins, T. J., *Science* **2007,** *315*, 835-838.

103. Chen, K.; Que, L., Jr., *J. Am. Chem. Soc.* **2001,** *123*, 6327-6337.

104. Penner-Hahn, J. E.; Eble, K. S.; McMurry, T. J.; Renner, M.; Balch, A. L.; Groves, J. T.; Dawson, J. H.; Hodgson, K. O., *J. Am. Chem. Soc.* **1986,** *108*, 7819-7825.

105. Wolter, T.; Meyer-Klaucke, W.; Müther, M.; Mandon, D.; Winkler, H.; Trautwein, A. X.; Weiss, R., *J. Inorg. Biochem.* **2000,** *78*, 117-122.

106. Lim, M. H.; Rohde, J.-H.; Stubna, A.; Bukowski, M. R.; Costas, M.; Ho, R. Y. N.; Münck, E.; Nam, W.; Que Jr., L., *Proc. Acad. Sci. USA* **2003,** *100*, 3665-3670.

107. Jensen, M. P.; Costas, M.; Ho, R. Y. N.; Kaizer, J.; Mairata i Payeras, A.; Münck, E.; Que, L., Jr.; Rohde, J.-H.; Stubna, A., *J. Am. Chem. Soc.* **2005,** *127*, 10512-10525.

108. Kaizer, J.; Klinker, E. J.; Oh, N. Y.; Rohde, J.-H.; Song, W. J.; Stubna, A.; Kim, J.; Münck, E.; Nam, W.; Que, L., Jr., *J. Am. Chem. Soc.* **2004,** *126*, 472-473.

109. Bautz, J.; Bukowski, M. R.; Kerscher, M.; Stubna, A.; Comba, P.; Lienke, A.; Münck, E.; Que, L., Jr., *Angew. Chem. Int. Ed.* **2006,** *45*, 5681-5684.

110. Kostka, K. L.; Fox, B. G.; Hendrich, M. P.; Collins, T. J.; Rickard, C. E. F.; Wright, L. J.; Münck, E., *J. Am. Chem. Soc.* **1993,** *115*, 6746-6757.

111. Sastri, C. V.; Seo, M. S.; Park, M. J.; Kim, K. M.; Nam, W., *Chem. Commun.* **2005,** *11*, 1405-1407.

112. Balland, V.; Charlot, M.-F.; Banse, F.; Girerd, J.-J.; Mattioli, T. A.; Bill, E.; Bartoli, J.-F.; Battioni, P.; Mansuy, D., *Eur. J. Inorg. Chem.* **2004,** 301-308.

113. Price, J. C.; Barr, E. W.; Glass, T. E.; Krebs, C.; J. Martin Bollinger, J., *J. Am. Chem . Soc.* **2003,** *125*, 13008 - 13009.

114. de Visser, S. P.; Oh, K.; Han, A.-R.; Nam, W., *Inorg. Chem.* **2007,** *46*, 4632-4641.

115. Oh, N. Y.; Suh, Y.; Park, M. J.; Seo, M. S.; Kim, J.; Nam, W., *Angew. Chem. Int. Ed.* **2005,** *44*, 4235-4239.

116. Nehru, K.; Seo, M. S.; Kim, J.; Nam, W., *Inorg. Chem.* **2007,** *46*, 293-298.

117. Seo, M. S.; In, J.-H.; Kim, S. O.; Oh, N. Y.; Hong, J.; Kim, J.; Que, L., Jr.; Nam, W., *Angew. Chem. Int. Ed.* **2004,** *43*, 2417 - 2420.

118. Chen, K.; Que, L., Jr., *Chem. Commun.* **1999,** 1375-1376.

119. Aliaga-Alcalde, N.; DeBeer George, S.; Mienert, B.; Bill, E.; Wieghardt, K.; Neese, F., *Angew. Chem. Int. Ed.* **2005,** *44*, 2908-2912.

120. Chanda, A.; Popescu, D.-L.; de Oliveira, F. T.; Bominaar, E. L.; Ryabov, A. D.; Münck, E.; Collins, J. T., *J. Inorg. Biochem.* **2006,** *100*, 606-619.

121. Bäckvall, J.-E., *Modern Oxidation Methods*. Wiley-VCH: Weinheim, 2004.

122. Walling, C., *Acc. Chem. Res.* **1998,** *31*, 155-157.

123. Sawyer, D. T.; Sobkowiak, A.; Matsushita, T., *Acc. Chem. Res.* **1996,** *29*, 409-416.

124. MacFaul, P. A.; Wayner, D. D. M.; Ingold, K. U., *Acc. Chem. Res.* **1998,** *31*, 159-162.

125. Costas, M.; Chen, K.; Que, L., Jr., *Coord. Chem. Rev.* **2000,** *200-202*, 517-544.

126. Buxton, G. V.; Greenstock, C. L.; Helman, W. P.; Ross, A. B., *J. Phys. Chem. Ref. Data* **1988,** *17*, 513-886.

127. Melander, L.; Saunders, W. H., Jr., *Reaction rates of isotopic molecules*. Wiley-Interscience: New York, 1980.

128. Sono, M.; Roach, M. P.; Coulter, E. D.; Dawson, J. H., *Chem. Rev.* **1996,** *96*, 2841-2887.

129. Nesheim, J. C.; Lipscomb, J. D., *Biochemistry* **1996,** *35*, 10240-10247.

130. Barton, D. H. R.; Beck, A. H.; Taylor, D. K., *Tetrahedron* **1995,** *51*, 5245-5254.

131. Groves, J. T.; Nemo, T. E., *J. Am. Chem. Soc.* **1983,** *105*, 6243-6248.

132. Russell, G. A., *J. Am. Chem. Soc.* **1957,** *79*, 3871-3877.

133. Khenkin, A. M.; Shilov, A. E., *New J. Chem.* **1989,** *13*, 659-667.

134. Krusic, P. J.; Meakin, P.; Jesson, J. P., *J. Phys. Chem.* **1971,** *75*, 3438-3453.

135. Bernadou, J.; Meunier, B., *Chem. Commun.* **1998,** 2167-2173.

136. Lee, K. A.; Nam, W., *J. Am. Chem. Soc.* **1997,** *119*, 1916-1922.

137. Britovsek, G. J. P.; England, J.; Spitzmesser, S. K.; White, A. J. P.; Williams, D. J., *Dalton Trans.* **2005,** 945-955.

138. Britovsek, G. J. P.; England, J.; White, A. J. P., *Inorg. Chem.* **2005,** *44*, 8125-8134.

139. Tang, J.; Gamez, P.; Reedijk, J., *Dalton Trans.* **2007,** *41*, 4644-4646.

140. Chen, M. S.; White, M. C., *Science* **2007,** *318*, 783-787.

141. Oldenburg, P. D.; Que, L., Jr., *Catal. Today* **2006,** *117*, 15-21.

142. Chen, K.; Costas, M.; Kim, J.; Tipton, A. K.; Que, L., Jr., *J. Am. Chem. Soc.* **2002,** *124*, 3026-3035.

143. Costas, M.; Que, J., L., *Angew Chem. Int. Ed. Engl.* **2002,** *12*, 2179-2181.

144. Suzuki, K.; Oldenburg, P. D.; Que, L., Jr., *Angew. Chem. Int. Ed.* **2008,** *47*, 1887-1889.

145. Bautz, J.; Comba, P.; Lopez de Laorden, C.; Menzel, M.; Rajaraman, G., *Angew. Chem. Int. Ed.* **2007,** *46*, 8067-8070.

146. Costas, M.; Tipton, A. K.; Chen, K.; Jo, D.-H.; Que, L., Jr., *J. Am. Chem. Soc.* **2001,** *123*, 6722-6723.

147. Bukowski, M. R.; Comba, P.; Lienke, A.; Limberg, C.; Lopez de Laorden, C.; Mas-Ballesté, R.; Merz, M.; Que, L., Jr., *Angew. Chem. Int. Ed.* **2006,** *45*, 3446-3449.

148. Chen, K.; Que, L., Jr., *Angew. Chem. Int. Ed.* **1999,** *38*, 2227-2229.

149. Mas-Ballesté, R.; Costas, M.; van den Berg, T.; Que, L., Jr., *Chem. Eur. J.* **2006,** *12*, 7489-7500.

150. White, M. C.; Doyle, A. G.; Jacobsen, E. N., *J. Am. Chem. Soc.* **2001,** *123*, 7194-7195.

151. Ryu, J. Y.; Kim, J.; Costas, M.; Chen, K.; Nam, W.; Que, J., L., *Chem. Commun.* **2002,** *12*, 1288-1289.

152. Bassan, A.; Blomerg, M. R. A.; Siegbahn, P. E. M.; Que, L., Jr., *Angew. Chem. Int. Ed.* **2005,** *44,* 2939-2941.

Chapter II

General objectives

II. General objectives

Understanding the mechanisms by which nature activates molecular O_2 is of great interest not only because of the fundamental importance of these reactions in biological systems but also due to the technological applications of this type of processes. The use of model systems that structurally and/or functionally mimic a particular enzyme constitutes a successful approach towards the better knowledge on how nature works. Iron and copper are the most common metals present in the active site of proteins involved in O_2 activation. Their abundance in the geosphere, inherent electronic properties and accessible redox potentials make them convenient for such a purpose.

In this thesis we take advantage of the model chemistry approach to prepare bioinspired systems that can mimic the activity of enzymes involved in O_2 activation.

In the first part of this dissertation (Chapter III) we aim to design bioinspired models of the copper proteins that possess a coupled dinuclear active center (hemocyanin, tyrosinase). In these biological systems the two metal centers interact together to activate a single O_2 molecule. In this sense, we envision that a suitable model system should fulfill the following requirements: presence of a dinucleating ligand (two metal centers held in a single complex molecule), available coordination sites for interaction with O_2 (low coordination numbers), a nitrogen-based ligand to mimic the histidine-rich natural active site, and enough flexibility to ensure the proper interaction of the metals with molecular oxygen. Aliphatic amines as coordinating atoms and *meta*-xylyl spacers to connect the two binding sites are the main features for the targeted model systems.
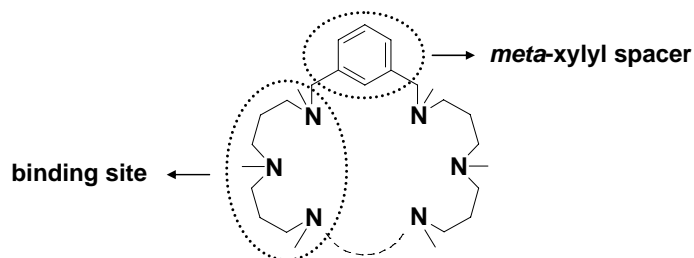
The reactivity of the resulting dinuclear copper(I) complexes towards O_2 will be examined in detail in order to detect and characterize metaestable reaction intermediates generated from the interaction of the metal site with activated forms of oxygen. The mechanism of O_2 activation by these complexes will be also examined taking special attention into the synergistic effects between the metal sites of a given complex. In order to do so, we will compare the O_2 activation process of the dinuclear complexes prepared in this work and we will contrast it with related mononuclear analogues. Moreover, the properties and reactivity of the newly formed copper-oxygen adducts will be analyzed. In particular, their ability to perform bioinspired oxidations, for example the *ortho*-hydroxylation of phenols, will be tested.

In the second part of this dissertation (Chapter IV) we will focus on the development of mononuclear non-heme iron complexes with the aim of reproducing the activity of non-heme iron enzymes of the Rieske dioxygenases family, and creating effective and selective catalysts for the oxidation of substrates under mild conditions. The ligands of choice for these systems should satisfy some essential characteristics: a tripodal tetradentate architecture, so that free coordination sites in a *cis* configuration are available for interaction with exogenous ligands (the oxidant or the substrate), and an oxidatively robust structure. A triazacyclonane ring derivatized with a methylpyridine group will afford ligands with these required features. The introduction of substituents in the pyridine ring and modifications in the N-alkyl groups of the triazacyclononane ring will be done to fine tuning the properties of the resulting complexes.
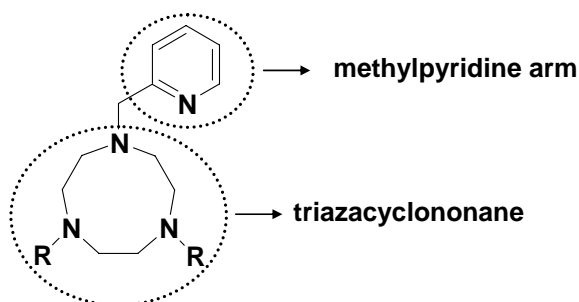
The corresponding mononuclear iron(II) compounds will be synthesized and used as catalysts in several oxidative transformations using H_2O_2 as the oxidant. Under the appropriate conditions we aim to oxidize non-activated C-H bonds such as alkanes, olefins and sulfides. Mechanistic information about these transformations will be gained by isotopic labeling studies using $H_2^{18}O$ or $H_2^{18}O_2$. By means of these studies we will establish the origin of the oxygen atoms that end up into the oxidized products, thus providing relevant information about the active species involved in these oxidations.

Finally, the direct preparation of high valent iron-oxo species using the same ligand platform will be studied. These species are postulated as the active species in many biological systems and studying their reactivity is of fundamental interest.

Chapter III

O$_2$ activation by dinuclear copper complexes

Chapter III.1

O_2 chemistry of dicopper complexes with alkyltriamine ligands. Comparing synergistic effects on O_2 binding

---

Departament de Química, Institut de Química Computacional, Universitat de Girona, 17071, Girona, Spain

Abstract

Two dicopper(I) complexes containing tertiary N-methylated hexaaza ligands which impose different steric constraints to the Cu ions have been synthesized, and their reactivity toward O_2 has been compared with a mononuclear related system, highlighting the importance of cooperative effects between the metal centers in O_2 activation.

Chapter III.2

Tyrosinase-like reactivity in a $Cu^{III}_2(\mu\text{-}O)_2$ species

Departament de Química, Institut de Química Computacional, Universitat de Girona, 17071, Girona, Spain

Abstract

IR spectra were taken in a Mattson-Galaxy Satellite FT-IR spectrophotometer using a MKII Golden Gate single reflection ATR system. UV-vis spectroscopy was performed on a Cary 50 Scan (Varian) UV-vis spectrophotometer with 1 cm quartz cells or with an immersion probe of 5 mm path length. The low temperature control was performed with a cryostat from Unisoku Scientific Instruments, Japan. Elemental analyses were performed using a CHNS-O EA-1108 elemental analyzer from Fisons. Resonance Raman spectra were collected on an Acton AM-506 spectrometer (1200 groove grating) using a Kaiser Optical holographic super-notch filters with a Princeton Instruments liquid-N2-cooled (LN-1100PB) CCD detector with a 4 cm-1 spectral resolution. The 568 and 407 cm-1 laser excitation lines were obtained with a Spectra Physics BeamLok 2060-KR-V krypton ion laser. The Raman frequencies were referenced to indene. Solutions of 1SbF6 in acetone (1 mM) were prepared in a glovebox, and after exposition to pure O2 at –90oC, 1.5 equivalents of sodium p-chlorophenolate (p-Cl-C6H4ONa) were added. The resulting dark solution was frozen 20-30 seconds after addition of p-Cl-C6H4ONa at 77 K using a gold-plated copper cold finger in thermal contact with a Dewar containing liquid N2. No photobleaching was observed upon repeated scans. Baseline corrections (polynomial fits) were carried out using Grams/32 Spectral Notebase Version 4.04 (Galactic). HPLC analysis was performed using a Supelco LC18 semipreparative column (250x10 mm). Elution was carried out using 0.1% TFA in distilled water (solvent A) and 0.1% TFA in acetonitrile (solvent B), with a flow rate of 5.0 mL/min. Elution started with 80% solvent A for 5 min, during additional 50 min the eluting solvent decreased to 0 % A, remained stable for 5 min, and finally returned to 80% A over 5 min. Spectrophotometric detection of the HPLC elution profile in the range 200-650 nm was performed with a Jasco MD-1510 diode array instrument. Quantification of the catechol in the reaction mixtures was performed using p-cyano-phenol as internal standard. All HPLC-MS spectra were obtained on a Micromass ZQ mass spectrometer in electrospray positive ionization (ES+) mode in-line with a Waters® 2795 HPLC system (separation module, AllianceTM) and a Waters® Dual Absorbance Detector. Stopped-flow kinetic measurements were performed using a Hi-Tech Scientific (presently, TgK Scientific, Salisbury, Wiltshire, U.K.) SF-43 cryogenic double-mixing stopped-flow instrument equipped with stainless steel plumbing, a 1.00 cm stainless steel mixing cell with sapphire windows, and an anaerobic gas-flushing kit. The instrument was connected to an IBM computer with IS-2

Rapid Kinetics Software by Hi-Tech Scientific (presently TgK Scientific). The mixing cell was maintained to ±0.1 K, and the mixing time was 2-3 ms. The source of light was either a visible lamp combined with a monochromator (low intensity light irradiation of the sample) or a xenon lamp combined with a diode array rapid scanning unit (strong UV-vis irradiation of the sample).

Chapter III.3

Fast O$_2$ binding at dicopper complexes containing Schiff-base dinucleating ligands

Departament de Química, Institut de Química Computacional, Universitat de Girona, 17071, Girona, Spain

Abstract:

A new family of dicopper(I) complexes $[Cu^I_2{}^R L](X)_2$ (R = H, 1X, R = ^{t}Bu, 2X and R = NO$_2$, 3X, X = CF$_3$SO$_3$, ClO$_4$, SbF$_6$, or BArF, BArF = $[B\{3,5\text{-}(CF_3)_2C_6H_3\}_4]^-$), where ^{R}L is a Schiff-base ligand containing two tridentate binding sites linked by a xylyl spacer, has been prepared and characterized, and its reaction with O$_2$ has been studied. The complexes were designed with the aim of reproducing structural aspects of the active site of type 3 dicopper proteins; they contain two three-coordinate copper sites and a rather flexible podand ligand backbone. The solid-state structures of 1ClO$_4$, 2CF$_3$SO$_3$, 2ClO$_4$, and 3BArF·CH$_3$CN have been established by single-crystal X-ray diffraction analysis. 1ClO$_4$ adopts a polymeric structure in the solid state while 2CF$_3$SO$_3$, 2ClO$_4$, and 3BArF·CH$_3$CN are monomeric. The complexes have been studied in solution by means of ^{1}H and ^{19}F NMR spectroscopy, which put forward the presence of dynamic processes. 1−3BArF and 1−3CF$_3$SO$_3$ in acetone react rapidly with O$_2$ to generate metaestable $[Cu^{III}_2(\mu\text{-}O)_2(^R L)]^{2+}$ 1−3(O$_2$) and $[Cu^{III}_2(\mu\text{-}O)_2(CF_3SO_3)(^R L)]^+$ 1−3(O$_2$)(CF$_3$SO$_3$) species, respectively, that have been characterized by UV−vis spectroscopy and resonance Raman analysis. Instead, reaction of 1−3BArF with O$_2$ in CH$_2$Cl$_2$ results in intermolecular O$_2$ binding. DFT methods have been used to study the chemical identities and structural parameters of the O$_2$ adducts, and the relative stability of the Cu$^{III}_2(\mu\text{-}O)_2$ form with respect to the Cu$^{II}_2(\mu\text{-}\eta^2{:}\eta^2\text{-}O_2)$ isomer. The reaction of 1X, X = CF$_3$SO$_3$ and BArF, with O$_2$ in acetone has been studied by stopped-flow UV-vis exhibiting an unexpected very fast reaction rate ($k = 3.82(4) \times 10^3$ M^{-1} s^{-1}, $\Delta H = 4.9 \pm 0.5$ kJ·mol^{-1}, $\Delta S = -148 \pm 5$ J·K^{-1}·mol^{-1}), nearly 3 orders of magnitude faster than in the parent $[Cu^I_2(m\text{-}XYL^{MeAN})]^{2+}$. Thermal decomposition of 1−3(O$_2$) does not result in aromatic hydroxylation. The mechanism and kinetics of O$_2$ binding to 1X (X = CF$_3$SO$_3$ and BArF) are discussed and compared with those associated with selected examples of reported models of O$_2$-processing copper proteins. A synergistic role of the copper ions in O$_2$ binding and activation is clearly established from this analysis.

Chapter IV

O$_2$ activation by mononuclear non-heme iron systems

Chapter IV.1

A novel platform for modeling oxidative catalysis in non-heme iron oxygenases with unprecedented efficiency

Departament de Química, Institut de Química Computacional, Universitat de Girona, 17071, Girona, Spain

Abstract:

Non-heme monoiron dependent oxygenases are emerging as a very diverse and versatile group of enzymes involved in a number of oxidative transformations, which also hold potential technological implications.[1] These biological catalysts constitute a source of inspiration for the development of environmentally benign oxidation technologies.[2] On the other hand, bioinspired synthetic catalysts constitute a valuable tool to explore the reaction mechanisms by which non-heme enzymes perform their chemistry.[3] Iron complexes derived from tripodal TPA (TPA=tris(2-methylpyridyl)amine) and linear BMPEN (BPMEN = N,N'-bis(2-methylpyridyl)-N,N'-dimethyldiaminoethane) type of ligands are particularly exceptional compounds because of their ability to perform stereoselective enzyme-like transformations such as alkane hydroxylation and alkene epoxidation and *cis*-dihydroxylation, with remarkable efficiency.[3] Such tetradentate backbones wrap around an iron(II) center giving rise to complexes with two *cis* available coordination sites which can be occupied by labile ligands like CH_3CN or CF_3SO_3. Parallel to the development of these two families of complexes, several other examples including tri-,[4] tetra-[5] and pentadentate[6] ligands have been explored, yet none of them can compare with TPA and BPMEN families in terms of selectivity, versatility and efficiency.

Keywords:
bioinorganic chemistry • enzyme catalysis • model compounds • non-heme oxygenases • oxidation

Chapter IV.2

Alkane hydroxylation by a nonheme iron catalyst that challenges the heme paradigm for oxygenase action

Departament de Química, Institut de Química Computacional, Universitat de Girona, 17071, Girona, Spain

Abstract

A nonheme iron catalyst catalyzed stereoselective oxidation of alkanes with H_2O_2 with remarkable efficiency and exhibiting an unprecedented high incorporation of water into the oxidized products. The present results challenge the canonical description of oxygenases, the standard oxo-hydroxo tautomerism that applies to heme systems and serves as a precedent for alternative pathways for the oxidation of hydrocarbons at nonheme iron oxygenases.

Chapter IV.3

Setereoselective C-H hydroxylation at bioinspired non-heme iron complexes containing *cis*-labile sites. Rethinking the rebound mechanism

Company, A., Güell, M., Fontrodona, X., et al. "Stereoselective C-H Hydroxylation at Bioinspired Non-heme Iron Complexes Containing cis-Labile Sites. Rethinking the Rebound Mechanism".

Abstract

A novel family of non-heme complexes [Fe(XPyTACN)(L')], XPyTACN = (1,4-dimethyl-7-(2-pyridylmethyl)-1,4,7-triazacyclononane) where X denotes different pyridine derivates, and L' = Cl, H_2O, CH_3CN, and CF_3SO_3, have been prepared and structurally and spectroscopically characterized. Substitution of the pyridine ring by methyl, fluorine or pinene groups allows fine tuning of the electronic properties of the resulting iron(II) complexes as ascertained by the measurement of the redox potential of the FeIII/FeII pair of the corresponding chlorocomplexes [FeCl2(XPyTACN)] (1Cl-6Cl). Magnetic susceptibility experiments (Evans' method) indicate that depending on the specific substituent in the α position of the pyridine ring, different spin state of the bis-acetonitrile iron(II) complexes ([1CH3CN]-[6CH3CN]) is obtained: low spin configuration when no substituent is present ([1CH3CN], [4CH3CN] and [5CH3CN]), high spin state when there is a methyl group ([2CH3CN] and [6CH3CN]) and a complex undergoing a spin transition process in the presence of a fluorine atom ([3CH3CN]). X-ray diffraction analysis of [2CH3CN]ClO4 shows that the ferrous ion is in the high spin state at 210K, but it undergoes a spin transition upon lowering the temperature and adopts a low spin configuration at 100K. 1CF3SO3-6CF3SO3 act as efficient catalysts in the stereospecific hydroxylation of non-activated C-H bonds of alkanes and they can be considered as functional models of non-heme iron oxygenases with two labile sites in a cis configuration. Information about the mechanisms operating in catalysts 1-6 was obtained by isotope labeling studies and mechanistic probes. These studies evidence that C-H hydroxylation catalyzed by these complexes is a metal centered reaction in which oxygen atoms from water are incorporated into products and free diffusing radicals are not significantly involved. Isotopic labeling studies show important differences between the six catalysts, especially in the level of water incorporation into oxidized products. These mechanistic experiments combined with computational work have allowed us to determine the mechanism by which the oxidative transformations take place. A rebound-type of mechanism by a FeV(O)(OH) species operates but, most remarkably, after hydrogen atom abstraction, rebound of the incipient carbon centered radical can take place with any of the two hydroxide ligands of the newly formed FeIV(OH)2 which dictates the origin of the oxygen atom that ends up into the final product. These results provide a novel understanding of the mechanism of C-H bond hydroxylation at non-heme iron centers containing cis-labile sites, with relevance in biology.

Chapter IV.4

Olefin-dependent discrimination between two non-heme HO-Fe^V=O tautomeric species in catalytic H$_2$O$_2$ epoxidations

Company, A., Feng, Y., Güell, M., et al. "Olefin-Dependent Discrimination Between Two Nonheme HO-FeV=O Tautomeric Species in Catalytic H2O2 Epoxidations"

Abstract

Nonheme iron oxygenases are emerging as versatile biological catalysts involved in a number of oxidative processes with biomedical, environmental and technologic implications.[1] Their heme counterparts are commonly taken as precedents for their chemistry.[2] In the heme paradigm, O-O heterolytic cleavage of an FeIII-OOH intermediate affords a high valent metal-oxo species that acts as the oxidant for the reaction (Scheme 1). Although nonheme iron oxygenases are less well understood, evidence has accumulated in the last few years that high valent iron-oxo species are also involved in some of their catalytic pathways..[3] Furthermore, a number of synthetic model complexes have been described.[4]

Chapter IV.5

A second oxidant in H_2O_2 oxidation reactions catalyzed by a functional model of Rieske dioxygenases

Company, A., Ribas, X. and Costas, M., "A Second Oxidant in H2O2 Oxidation Reactions Catalyzed by a Functional Model of Rieske Dioxygenases".

Abstract:

Mononuclear non-heme iron dependent oxygenases are emerging as a versatile group of enzymes exhibiting a wide range of structural motifs and diverse reactivity.[1,2] Among them, Rieske dioxygenases are bacterial enzymes involved in the cis-dihydroxylation of arenes and the stereoselective hydroxylation of alkanes.[3,4] Crystallographic analyses have shown that O_2 activation occurs via formation of a ferric (hydro)peroxide FeIII-OO(H) species (P in Scheme 1),[5] which constitutes the last detectable intermediate before substrate oxidation occurs. Mechanistic[6-8] and computational[9] studies on this enzyme have established close similarities with the catalytic cycle of cytochrome P450.[10,11] Analogous to cytochrome P450, it has been proposed that O-O cleavage leads to a high valent FeV(O)(OH) (O) species that is the actual executor of the substrate oxidation.[6-8] Studies with selected non-heme synthetic compounds have built on this proposal by firmly establishing that a high valent FeV(O)(OH) intermediate, formed via water assisted lysis of a low-spin FeIII-OOH can elicit enzyme-like reactivity such as stereoselective alkane hydroxylation and alkene cis-dihydroxylation.[12-15] As earlier considered in cytochrome P450, the ability of the FeIII-OOH species to perform direct attack to the substrate before O-O bond breakage has also been proposed, but the proposal was recently challenged by the observation that well-defined model species such as [FeIII(OOR)(TPA)] (TPA = tris-(2-pyridilmethyl)amine, R = H or tBu) fail to elicit oxygen atom transfer reactions to olefins and sulfides.[16,]

Chapter IV.6

Spectroscopic and chemical characterization of a novel non-heme iron(IV)-oxo compound bearing a nitrogen-based tetradentate ligand

Company, A., Güell, M, Mas-Ballesté, R., et al. "Spectroscopic and chemical characterization of a novel non-heme iron(IV)-oxo compound bearing a nitrogen-based tetradentate ligand".

Abstract:

The synthesis, spectroscopic and chemical characterization of $[Fe^{IV}(O)(L)(Me2Pytacn)]^{n+}$ (Me2Pytacn = 1,4-dimethyl-7-(2-pyridylmethyl)-1,4,7-triazacyclononane, L = CH_3CN or H_2O) is described in this work. $[Fe^{IV}(O)(CH_3CN)(Me2Pytacn)]^{2+}$ (2) was prepared by reaction of $[Fe^{II}(CF_3SO_3)_2(Me2Pytacn)]$ (1) with peracetic acid. 2 bears a N4 tetradentate ligand that enforces two cis-labile sites, and it shows remarkable stability at room temperature. Its ability to exchange the oxygen atom with water has been analyzed in detail by means of kinetic studies, and a mechanism has been proposed on the basis of DFT calculations. The ability of 2 to perform hydrogen-atom abstraction of C-H bonds and oxygen atom transfer to sulfides has also been tested. 2 exchanges its bound CH_3CN ligand with anionic ligands X by reaction with NBu4X (X = Cl, Br or CF_3CO_2) to generate oxoiron(IV) complexes $[Fe^{IV}(O)(X)(Me2Pytacn)]^+$ (2-X). 2 and 2-X (X = Cl, Br) are synthetic models for the active species operating in α-ketoglutarate dependent oxygenases and halogenases, respectively.

Chapter V

Results and discussion

V. Results and discussion

The use of O_2 as the oxidant in chemical transformations has become of great industrial interest in part because it constitutes an environmentally friendly alternative to the highly toxic oxidants used nowadays in several chemical transformations, and also because of its relatively low cost. However, using molecular oxygen is not straightforward. The main problem has to do with the inherent poor reactivity of O_2 with most closed-shield organic molecules due to its triplet electronic configuration. Biological systems have developed strategies to overcome this problem. One of the most extended methods is based on the use of transition metals that reductively activate molecular oxygen to oxidatively active forms (superoxo, peroxo or high valent metal-oxo species). This process is done in a controlled fashion to achieve highly selective transformations.[1] In biological systems there are several transition metals in the active center of proteins which are implicated in the activation of molecular oxygen but, among them, the most prominent are undoubtedly copper and iron. These proteins act either as O_2-carriers or as catalysts to selectively oxidize a specific substrate.

Chemists have long sought to unravel the mechanisms of such biological oxidations, with the ultimate objectives of inventing new reagents for organic synthesis and industrial catalysis, exerting control over reactivity and selectivity, and getting fundamental information about enzymatic reactions. A key issue concerns the nature of the oxidizing species that is directly responsible for effecting the reaction. In particular, the characterization of metal–based intermediates that act as the active species is critical for obtaining detailed mechanistic insight. However, due to their nature as reactive oxidizing molecules, most commonly they are difficult to isolate or even to observe directly.

Model chemistry constitutes a useful tool to achieve this goal.[2] It gains inspiration from biological systems to develop low-molecular weight complexes which reproduce structural characteristics of an enzyme and hopefully its activity. These complexes are useful to understand how nature works and in selected cases they constitute excellent catalysts that can elicit unprecedented and highly specific chemical transformations analogously to enzymes.[3] In this thesis we take advantage of the model chemistry approach and we prepare model complexes that mimic dinuclear copper proteins and mononuclear non-heme iron systems implicated in O_2 activation.

Chapter III. O_2 activation by dinuclear copper systems

One of the most relevant families of copper proteins is constituted by enzymes that possess a dinuclear coupled center in which two copper ions act cooperatively to activate one oxygen molecule.[4] Within this class hemocyanin (O_2-carrier), tyrosinase (conversion of phenols to quinones) and catechol oxidase (oxidation of catechol to quinones) are included. The X-ray structure of the three enzymes has been solved and it has been observed that their active sites are almost identical despite their different activity. In all cases, a side-on μ-η^2:η^2-peroxo species forms upon reaction of the reduced form of the enzyme with O_2. The two copper centers in the active site act cooperatively to transfer 2e$^-$ to a single O_2 molecule. Thus, a key issue to achieve the coupled interaction between the two copper centers has to do with the ability of the two metals to act in a synergistic manner.

The use of dinucleating ligands constitutes an especially interesting approach to model copper proteins with a coupled dinuclear center. In this line, dinucleating hexaaza macrocyclic ligands have been widely used for O_2 activation because they can preorganize two copper centers in a particular Cu···Cu distance.[5] Despite the fact that in selected cases aromatic hydroxylation of the supporting ligand occurs,[6,7] metal-dioxygen adducts derived from the interaction between the metal sites and activated forms of dioxygen have never been detected in these systems, and thus fundamental knowledge of these reactions is difficult to obtain. One of the reasons for the lack of intermediates accumulation most likely arises from the rigidity of the macrocyclic systems, that poses kinetic barriers to changes in the distance and relative orientation of the two metal centers. These changes are necessary in order that the two metal sites can interact simultaneously with a single O_2 molecule. In the works presented in Chapter III, we address this issue and we prepare dinuclear copper complexes based on flexible versions of previously reported hexaaza macrocyclic ligands.

Chapter III.1. O_2 chemistry of dicopper complexes with alkyltriamine ligands. Comparing synergistic effects on O_2 binding

In Chapter III.1[8] dinucleating nitrogen-based ligands are prepared, so that two copper centers are hold by a single ligand molecule. In Me3m ligand the two binding sites are connected by two *meta*-xylyl linkers giving a hexaaza macrocycle, while *m*-XYL^{MeAN} is constituted by two triamine ligands connected by a single *meta*-xylyl group (Scheme 1). Reaction of one equivalent of each ligand with two equivalents of a copper salt into the glove box gave the corresponding dinuclear copper(I) complexes [Cu$^I_2$(Me3m)]$^{2+}$ (**1**) and [Cu$^I_2$(*m*-XYL^{MeAN})]$^{2+}$ (**2**) (Scheme 1).
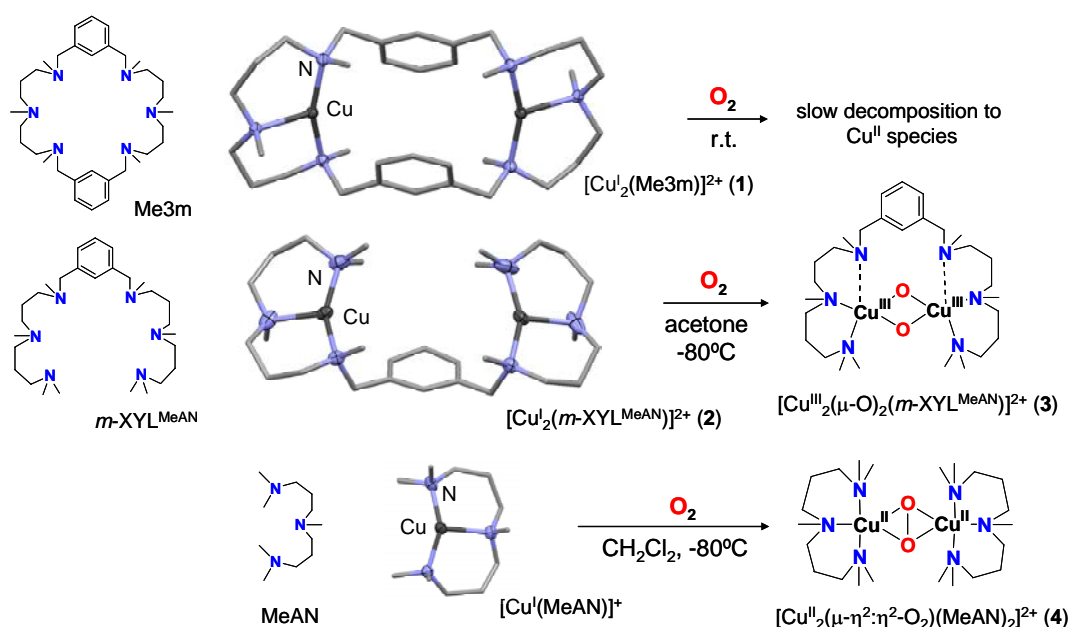
Scheme 1. Representation of the copper(I) complexes used in Chapter III.1 along with their reaction with molecular O_2.

Complexes **1** and **2** present important similarities: in both cases the copper sites are coordinated to three aliphatic nitrogen atoms (the average Cu-N distance is 2.066 Å for **1** and 2.032 Å for **2**) and they possess a distorted trigonal planar geometry. The coordination sphere of the copper centers exhibited by these complexes is structurally related to the one found in tyrosinase, in which each copper ion is coordinated to three histidine residues in the reduced form.[9] Apart from this structural similarity, copper sites in **1** and **2** are also electronically equivalent as ascertained by FT-IR analysis of their Cu-CO adducts (ν(CO) = 2084±1 cm^{-1}). Therefore copper(I) ions in **1** and **2** possess electronically and structurally analogous properties. On the other hand, $[Cu^I(MeAN)]^+$ (Scheme 1) constitutes a mononuclear analogue of the dinuclear complexes **1** and **2**. Its X-ray structure has already been reported[10] and it shows a copper(I) center with a distorted trigonal planar geometry (average Cu-N distance is 2.036 Å) structurally equivalent to the one found in **1** and **2**.

Despite the almost identical structure in the copper(I) centers of **1**, **2** and $[Cu^I(MeAN)]^+$, their reactivity towards O_2 is completely dependent on the specific ligand. Compound **1** reacts slowly with O_2 even at room temperature and no metal-oxygen adduct is accumulated or detected in the course of the reaction. In contrast, reaction of **2** in acetone at -80ºC is much faster and a bis(μ-oxo) species (**3**) has been trapped and spectroscopically characterized by UV-vis (λ_{max} = 308 nm, ε = 20000 M$^{-1}\cdot$cm^{-1}; λ_{max} = 413 nm, ε = 28000 M$^{-1}\cdot$cm^{-1}) and resonance Raman (ν = 600 cm^{-1}, $\Delta[^{18}O_2]$ = -23 cm^{-1}) spectroscopy. Although it is well established that $Cu^{III}_2(\mu$-O$)_2$ species are usually close in energy to their $Cu^{II}_2(\mu$-η^2:η^2-$O_2)$ isomers,[3,15] the structure of **3** is unperturbed by either the counterion (CF$_3$SO$_3$, BArF) or the solvent (THF, acetone, CH$_2$Cl$_2$). Finally, the mononuclear analogue $[Cu^I(MeAN)]^+$ exhibits the exclusive formation of a side-on μ-η^2:η^2-peroxo species (**4**) formed upon reaction of two complex molecules with a single O_2.[10]

The nature of **3** was determined by means of diffusion experiments by NMR spectroscopy (pulse gradient spin-echo, PGSE). The diffusion rate for **3** measured in d_6-acetone at -80ºC was 1.25±0.14·10^{-10} m$^2\cdot$s^{-1}, which compares well with the values obtained for **1** (0.98±0.12·10^{-11} m$^2\cdot$s^{-1}) and **2** (0.89±0.11·10^{-10} m$^2\cdot$s^{-1}). This indicates that the three species have similar hydrodynamic radii, which, in turn, strongly supports the intramolecular nature of O_2 binding. Although several bis(μ-oxo) species have been reported in the literature,[11] most of them are prepared by interaction of two mononuclear molecules. **3** constitutes the second example of an intramolecular bis(μ-oxo) core.[12] By means of DFT calculations at the B3LYP level it was confirmed the experimental observation that the bis(μ-oxo) isomer is exclusively formed, as the corresponding μ-η^2:η^2-peroxo isomer was found to be much higher in energy (35.5 kJ·mol^{-1}) (Figure 1). It is also interesting to notice that the computed structure for **3** shows the elongation of one of the Cu-N distances, thus providing an almost square planar geometry for the Cu^{III} center (d^8 electronic configuration).

Cu$^{III}_2$(μ-oxo)$_2$ isomer is 35.5 kJ·mol^{-1} more stable than Cu$^{II}_2$(μ-η^2:η^2-peroxo)

Cu$^{III}_2$(μ-oxo)$_2$ (**3**)   **DFT calculated structures**   Cu$^{II}_2$(μ-η^2:η^2-peroxo)
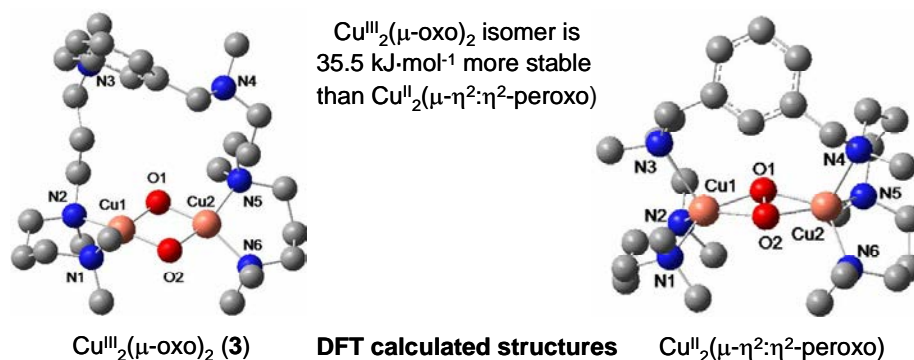
Figure 1. Structure of the Cu$_2$O$_2$ adducts obtained by DFT calculations. Left: calculated structure of the bis(μ-oxo) compound **3**. Right: calculated structure of its (μ-η^2:η^2-peroxo) isomer.

Stopped-flow kinetic analysis of the oxygenation reactions indicates that **2** reacts reversibly with O$_2$ to generate **3** (Scheme 2).[17] At low temperatures (from -80 to -50 ºC), the equilibrium is shifted to the right, and the formation of **3** is essentially quantitative. Under these conditions, the reaction is first order in O$_2$ and **2** concentration.

$$LCu^I_2 + O_2 \underset{k_{-1}}{\overset{k_1}{\rightleftharpoons}} LCu^ICu^{II}O_2 \xrightarrow{k_2} LCu^{III}_2O_2 \qquad v = k_{ox}[\mathbf{2}][O_2]$$

2   **3**

$k_{ox} = k_1k_2/k_{-1}$
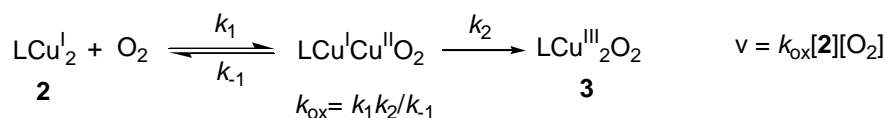
Scheme 2.

Activation parameters for the oxygenation reactions are characterized by a rather low $\Delta H^{\neq} = 9.5 \pm 2$ kJ·mol^{-1} and a large negative $\Delta S^{\neq} = -175 \pm 10$ J·K^{-1}·mol^{-1}. The simple second-order rate law observed at low temperature is consistent with a stepwise reaction scheme (Scheme 2) similar to the oxygenation mechanisms of other dicopper(I) complexes.[13] This mechanistic picture involves reversible reaction of O$_2$ with **2** to generate a putative superoxo Cu^{I}Cu^{II}O$_2^-$ species in a left-lying preequilibrium process, followed by intramolecular collapse into the final dinuclear [Cu$^{III}_2$(μ-O)$_2$(*m*-XYL^{MeAN})]$^{2+}$ structure (**3**).

It is also interesting to point out that the oxygenation of the related mononuclear [Cu(MeAN)]$^+$ complex exhibits a second order rate law in copper complex.[10] Comparison between the kinetic parameters associated to the formation of **3** and [Cu$^{II}_2$(μ-η^2:η^2-O$_2$)(MeAN)$_2$]$^+$ (**4**) indicates a higher $\Delta H^{\neq}$ and a lower $\Delta S^{\neq}$ for the former, probably associated with its more organized dinuclear structure. Direct interpretation of these parameters is hampered by the different rate law and the multistep nature of the oxygenation reaction in both complexes. Also unexpected is the dramatic difference in the O$_2$ reactivity of **1** and **2**. Given the comparable coordination sphere and electronic properties of the Cu^I ions in both complexes, it is rather unlikely that the initial O$_2$ binding to a single Cu^I ($k_1 \cdot k_{-1}^{-1}$, Scheme 2) depends on the particular complex, and therefore the different O$_2$ reactivity highlights the important role played by the second metal ion. The reaction in complex **1** is slower than in **2** presumably because there is an enthalpic barrier to surmount to bring the two Cu ions together, due to some strain from the ligand. In complex **2**, the ligand is flexible, allowing copper sites to approach close enough to promote their synergistic actuation in O$_2$ binding/reduction. Instead, the rather rigid nature of the macrocyclic ligand (Me3m) imposes a higher barrier to this process, shutting down the reaction. The stability of **3**, which

allows its spectroscopic characterization, in comparison with the lack of stability of any reaction intermediate formed along the **1** + O_2 pathway may also be explained on the basis of the different structural strains imposed by the ligands.

Thus, in chapter III.1 the importance of synergistic effects between two copper centers to activate O_2 has been demonstrated by a rather simple model. Further support for this concept comes from the recent observation that the active site of the natural enzyme tyrosinase accommodates remarkable changes occurring along its catalytic cycle which requires the presence of a rather flexible active center.[9]

Chapter III.2. Tyrosinase-like reactivity in a Cu$^{III}_2$(μ-O)$_2$ species

As stated above, one of the final goals of model chemistry is the development of model systems capable of reproducing the activity of a specific enzyme. In particular, in Chapter III.2 we test the ability of bis(μ-oxo) species **3** to perform the *ortho*-hydroxylation of phenolates analogously to the reactivity exhibited by tyrosinase.[14]

Reaction of **3** with 10 equiv sodium *para*-chlorophenolate affords the corresponding 4-chlorocatechol in 67% yield with respect to the initial dicopper complex. Moreover, an immediate color change is observed when **3** reacts with *para*-chlorophenolate (p-Cl-C_6H_4ONa) and a new brown species (**5^{Cl}**) is formed. Its UV-vis spectrum shows two bands at 390 and 563 nm (Figure 2, left). Resonance Raman experiments (Figure 2, right) of frozen solutions of **5^{Cl}** with laser excitation at 407 nm show a resonance enhanced feature at 597 cm^{-1} that experiences a -26 cm^{-1} shift when $^{18}O_2$ is used in the generation of **3**. This feature is not enhanced when 568 nm laser excitation is used in the experiment. Moreover, no isotope-sensitive features that could be assigned to a (μ-η^2:η^2-peroxo)dicopper(II) species are observed in the 700-770 cm^{-1} region.[11] On the other hand, laser excitation at 568 nm shows intense peaks at 1264, 1409, and 1642 cm^{-1}, characteristic of phenolate vibration modes. These vibrational features are not affected by the use of $^{18}O_2$, and they are not enhanced with laser excitation at 407 nm. Thus, rRaman data provide direct evidence for phenolate binding to the Cu_2O_2 core in **5^{Cl}**.
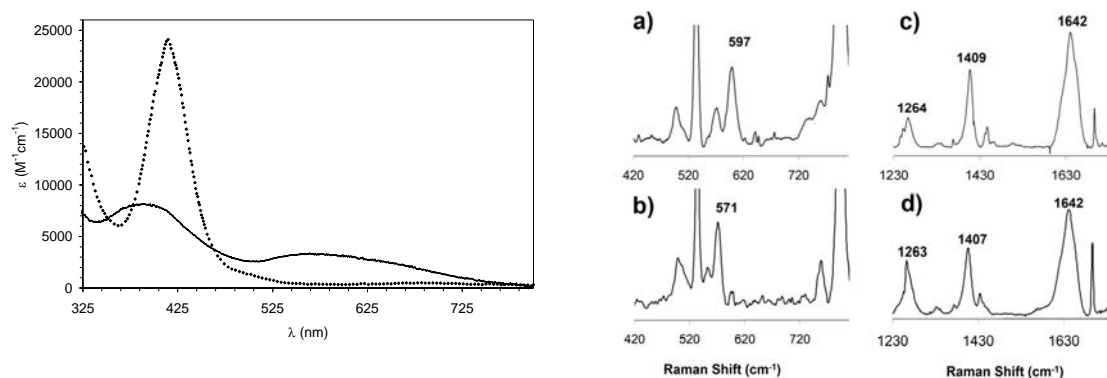
Figure 2. Left: UV-vis spectra of **3** (dashed line) and **5^{Cl}** (solid line) in acetone at -90ºC. Right: Resonance Raman spectra of **5^{Cl}** generated with $^{16}O_2$ (a) and $^{18}O_2$ (b) using laser excitation at 407 nm. Spectra of **5^{Cl}** generated with $^{16}O_2$ (c) and $^{18}O_2$ (d) using laser excitation at 568 nm.

The accumulated data can be interpreted with two different scenarios. The first is that 5^{Cl} is actually a mixture of residual bis(μ-oxo)dicopper(III) (**3**) and some type of copper-phenolate species. Alternatively, 5^{Cl} may be formulated as $[Cu^{III}_2(\mu\text{-O})_2(p\text{-Cl-C}_6H_4O)(m\text{-XYL}^{MeAN})]^+$, where bis($\mu$-oxo) and phenolate vibrations are uncoupled. We favor the latter hypothesis on the basis of the following observations. Kinetic analysis indicates that reaction of p-Cl-C$_6$H$_4$ONa is fast even for stopped-flow methodology and no residual **3** should be present under the experimental conditions used to prepare the resonance Raman sample. Furthermore, the UV-vis spectrum of 5^{Cl} does not change upon varying the concentration of phenolate and the UV-vis features associated with the bis(μ-oxo) core (390 nm), and with the phenolate (563 nm) decay with the same kinetic behavior (as followed by UV-vis spectroscopy). In addition, we have observed negligible perturbations in the energy of the Cu_2O_2 breathing mode in the resonance Raman spectra of the bis(μ-oxo) core in a related system upon coordination to a $CF_3SO_3^-$ group in acetone (Chapter III.3).[15] This observation can explain the similarity between the rRaman enhanced vibrations of the bis(μ-oxo) core in **3** and 5^{Cl}. Finally, the spectral features associated to 5^{Cl} are reminiscent of those reported for the $[Cu^{III}_2(\mu\text{-O})_2(\text{phenolate})(\text{DBED})]^+$ species recently described by Stack and co-workers.[16] Therefore, we conclude that 5^{Cl} is best described as the phenolate adduct of the bis(μ-oxo) species **3** (Scheme 3).

UV-vis: λ_{max} = 390, 563 nm
rRaman: ν = 597 cm^{-1} ($\Delta[^{18}O]$ = -26 cm^{-1})

UV-vis: λ_{max} = 418, 630 nm
rRaman: ν = 590 cm^{-1} ($\Delta[^{18}O]$ = -20 cm^{-1})
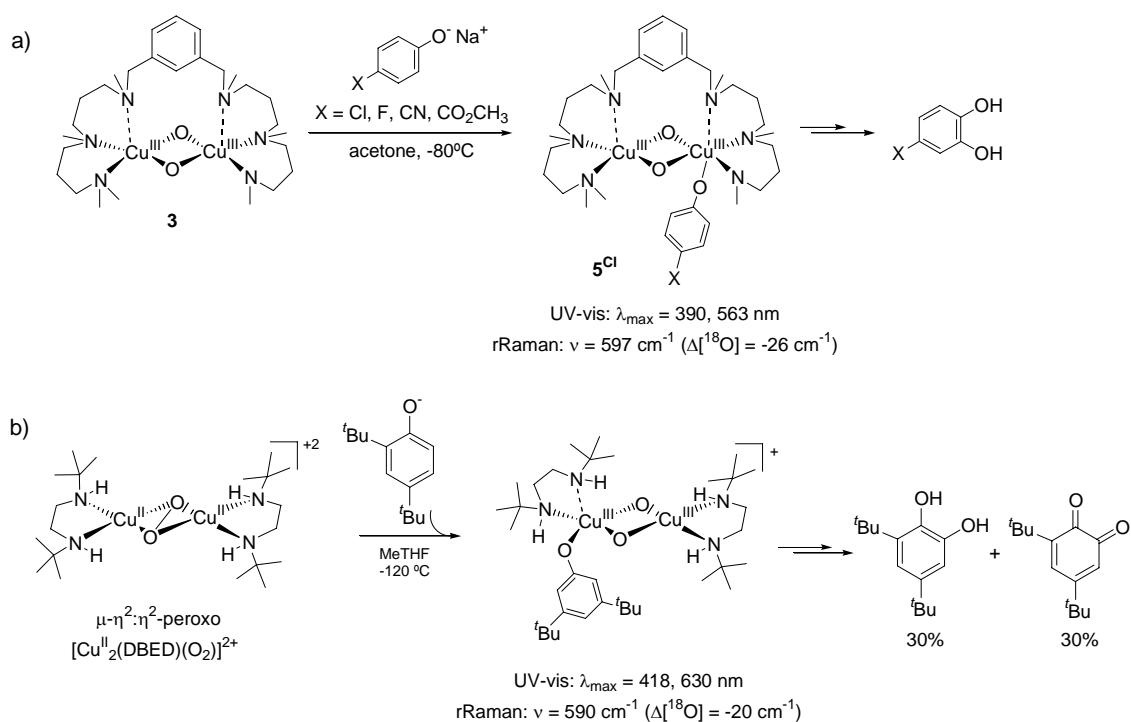
Scheme 3. (a) Representation of the reactions described in Chapter III.2. (b) Phenolate hydroxylation mechanism by $[Cu^{II}_2(O_2)(DBED)]^{2+}$.[16]

Formation and decay of 5^{Cl} were studied by UV-vis stopped-flow methods. The reaction between **3** and the phenolate to form 5^{Cl} is too fast ($k > 10^6$ M^{-1}·s^{-1}) even for stopped-flow techniques at very low temperatures (-88ºC), and neither precise reaction rates nor activation parameters could be obtained for this process. However, some mechanistic information could be gained by following the decay of 5^{Cl} which showed first-order kinetics. A series of analogous species (5^X) were generated by reaction of **3** with 1.5 equiv of sodium *para*-substituted-phenolates (X = F, CO$_2$CH$_3$, Cl, CN). Plot of the

decay rates of 5^X against the Hammett parameter (σ^+) afforded a linear correlation with a negative slope indicative of an electrophilic oxidizing species that attacks the aromatic ring. Moreover activation parameters for the decomposition reaction were determined by stopped-flow techniques ($\Delta H^{\neq} = 37.1$ kJ·mol^{-1} and $\Delta S^{\neq} = -55$ J·K^{-1}·mol^{-1}) and the values compared with the ones reported for tyrosinase[17] and for other model systems capable of performing phenolate hydroxylation by means of a Cu$^{II}_2$(μ-η^2:η^2-peroxo) core[18] (see Chapter III.2 for details).

Compound **3** and [Cu$^{II}_2$(O$_2$)(DBED)]$^{2+}$ (Scheme 3) constitute the only reported examples of a bis(μ-oxo) core capable of performing the *ortho*-hydroxylation of exogenous phenolates. However, a significant difference can be found between these two systems: while in **3** the O-O bond breakage occurs prior to coordination to the phenolate, in [Cu$^{II}_2$(DBED)(O$_2$)]$^{2+}$ the O-O breakage is concomitant with phenolate binding (Scheme 3) giving the corresponding bis(μ-oxo) isomer with a bound phenolic substrate.

In the literature there are two other model systems capable of performing the *ortho*-hydroxylation of exogenous phenolates to give catechols (Scheme 4).[19,20] Both of them bear a side-on μ-η^2:η^2-peroxo type of species and an electrophilic oxidizing species is implied by means of Hammett analyses. Reaction of peroxo complexes [Cu$^{II}_2$(O$_2$)(L^{Py2Bz})]$^{2+}$ and [Cu$^{II}_2$(O$_2$)(MeL66)]$^{2+}$ with phenolate did not afford the formation of any adduct derived from the interaction between copper and phenolate. Instead, direct bleaching of the spectroscopic characteristics of the peroxo species was observed concomitant with direct formation of the catechol product.

[Cu$^{II}_2$(O$_2$)(L^{Py2Bz})]$^{2+}$ [Cu$^{II}_2$(O$_2$)(MeL66)]$^{2+}$
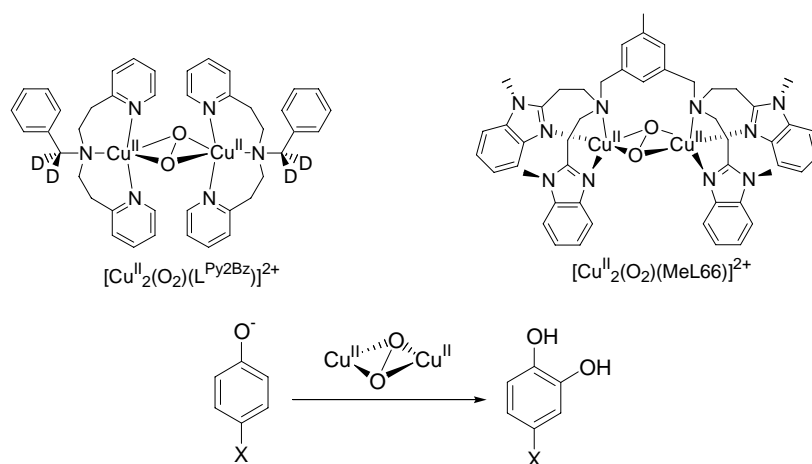
Scheme 4. Reported model systems capable of performing the *ortho*-hydroxylation of exogenous phenolates to give catechols.

As far as the catalytic cycle of tyrosinase is concerned, a side-on μ-η^2:η^2-peroxo species is formed upon transfer of 2e$^-$ from the two reduced copper centers to a single oxygen molecule. It is considered that this species performs an electrophilic attack over the aromatic ring of the phenolic substrate giving rise to the formation of the corresponding catechols and further oxidation to quinones (Scheme 5).[4]
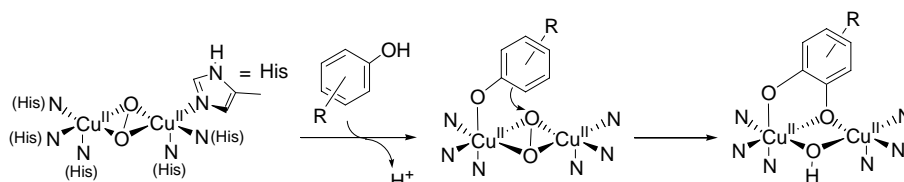
Scheme 5. Mechanism of action of tyrosinase towards the hydroxylation of a monophenolic substrate.

Through the use of model systems, Tolman and co-workers demonstrated the existence of a reversible O-O bond breakage so that bis(μ-oxo) and μ-η^2:η^2-peroxo isomers can be in equilibrium (Scheme 6).[21] This observation calls into question which of the two isomers is the actual executor of the hydroxylation in tyrosinase. As stated above, up to now model systems have demonstrated that the bis(μ-oxo) core, despite not being detected in biological systems, is also competent for performing the *ortho*-hydroxylation of exogenous phenolates to give catechols. Thus, the actual isomer responsible for the *ortho*-hydroxylation of phenols remains unclear.

$$LCu^{III} \overset{O}{\underset{O}{<}} Cu^{III}L \quad \rightleftharpoons \quad LCu^{II} \overset{O}{\underset{O}{|>}} Cu^{II}L$$

bis(μ-oxo) (O) μ-η^2:η^2-peroxo (^{S}P)
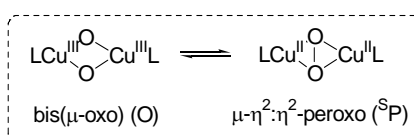
Scheme 6. Equilibrium between bis(μ-oxo) and μ-η^2:η^2-peroxo complexes.

Chapter III.3. Fast O$_2$ binding at dicopper complexes containing Schiff-base dinucleating ligands

In Chapter III.3 we report on the development of a new family of dicopper(I) complexes structurally related to *m*-XYL^{MeAN} but replacing one of N-methyl units of each binding site by a Schiff-base group (^{H}L, Scheme 7).[15] With the aim of tuning the electronic properties of the complexes, *t*Bu and NO$_2$ groups were introduced in the aromatic ring (^{tBu}L and ^{NO2}L). The corresponding dicopper(I) complexes $[Cu^I_2(^XL)]^{2+}$ (**6^X**) are highly sensitive to O$_2$ oxidation. By X-ray analysis it was ascertained that in the solid state the copper(I) centers are coordinated to a tertiary aliphatic amine, a secondary one and a Schiff-base group. In the solid state, a polymeric structure is found for complex **6^H**, while **6^{tBu}** and **6^{NO2}** present a monomeric configuration (Figure 3). Moreover, coordination of one of the two copper sites with CF$_3$SO$_3$ anion or solvent acetonitrile is detected in **6^{tBu}** and **6^{NO2}** respectively. Despite the different solid state structures ascertained by crystallography, complexes **6^X** exhibit similar ^{1}H-NMR spectra, suggesting that analogous species are present in solution and that the different solid state structures arise from solid state packing effects. The measured diffusion coefficient of **6^H** is 8.57·10^{-10} m^2·s^{-1}, a value closely resembling the values obtained for **1** and **2**. This is a clear indication that its polymeric structure determined by X-ray crystallography is not retained in solution. Overall indicates that the dicopper(I) complexes **6^H**, **6^{tBu}** and **6^{NO2}** present analogous monomeric species in solution.
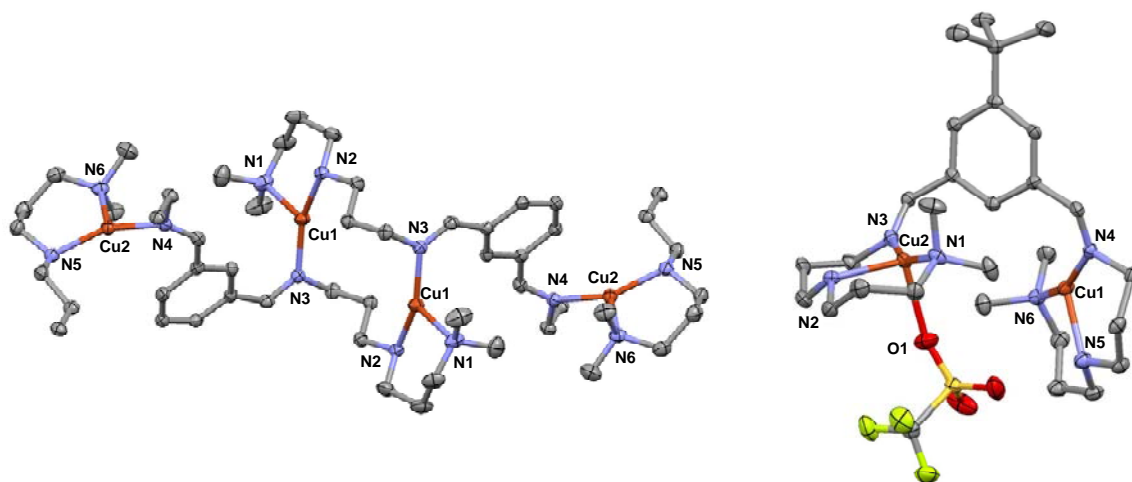
Figure 3. Left: X-Ray structure of **6^H**. Right: X-Ray structure of **6^{tBu}**. Hydrogen atoms and non-coordinated anions have been omitted for clarity.

The electronic properties of the metal sites were analyzed by FT-IR of the respective carbon monoxide adducts. Despite the distinctive richness of the *meta*-xylyl linker due to the substitution in the aromatic ring, the electronic properties are only slightly modulated as ascertained by the similar vibration frequency of the coordinated CO (ν(CO) = 2085 cm^{-1} for **6^H** and **6^{tBu}** and 2089 cm^{-1} for **6^{NO2}**).

Complexes **6^X** react with O$_2$ at low temperatures to give a yellow metaestable species (**7^X**) with common features in their UV-vis spectra: two intense bands near 300 and 400 nm. Moreover, resonance Raman spectra of **7^X** in acetone show a single O$_2$-isotope sensitive peak at ν = 601 ± 1 cm^{-1}, indicative of the formation of a bis(μ-oxo) core upon reaction with O$_2$ (Scheme 7).
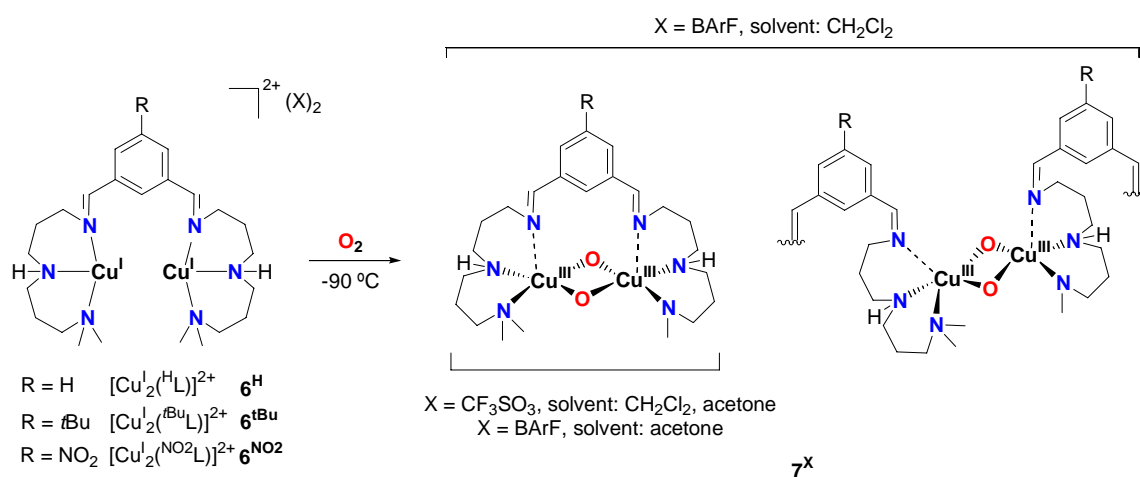
Scheme 7. Schematic representation of the complexes used in Chapter III.3.

Kinetic analyses by low temperature stopped-flow UV-vis spectroscopy of the oxygenation reaction indicate that complex **6^H** reacts much faster with O$_2$ than its analogue [Cu$^I_2$(*m*-XYL^{MeAN})]$^{2+}$ (**2**) described in Chapter III.1 (Table 1). This difference originates both from a smaller $\Delta H^{\neq}$ and a less negative $\Delta S^{\neq}$. Indeed, O$_2$ binding to **6^H** is the fastest reported in the literature for a *meta*-xylyl bridged system (Table 1). We rationalize this fast reactivity by three reasons: (a) higher preorganization conferred by the more rigid imine N group in comparison with tertiary amines, (b) a possible

hemilability of the imine group that may lower the coordination number of the copper ion, enhancing its reactivity, and (c) the presence of a NH group which may stabilize O_2 binding to the first copper ion *via* hydrogen-bonding or *via* a better stabilization of the copper(II) or copper(III) oxidation state.

Table 1. Rate constants for the oxygenation of 6^H and related complexes.

complex	k_{ox} ($M^{-1} \cdot s^{-1}$)	Temperature
$[Cu^I_2(^HL)]^{2+}$ (6^H)	3.84×10^3 $M^{-1} \cdot s^{-1}$	193 K
$[Cu^I_2(m\text{-}XYL^{MeAN})]^{2+}$ (2)	3.2 $M^{-1} \cdot s^{-1}$	193 K
$[Cu^I(MeAN)]^+$	690 $M^{-2} \cdot s^{-1}$	183 K
$[Cu^I_2(MeL66)]^{2+}$	7.72×10^{-2} $M^{-1} \cdot s^{-1}$	183 K
$[Cu^I_2(XYL\text{-}H)]^{2+}$	1.58×10^3 $M^{-1} \cdot s^{-1}$	253 K

$[Cu^I_2(XYL\text{-}H)]^{2+}$
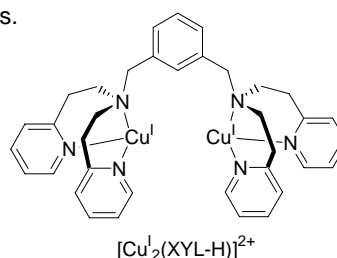
Resonance Raman spectroscopy unravels some interesting observations. A single vibration peak of the bis(μ-oxo) core is observed when spectra are recorded in CH_2Cl_2 using CF_3SO_3 as the counterion. On the other hand, when spectra are registered using a non-coordinating solvent (CH_2Cl_2) and a non-coordinating anion (BArF), two different peaks corresponding to the breathing mode of the bis(μ-oxo) core are present (ν = 607±1 and 623±2 cm^{-1}) and their relative intensity is highly dependent on the concentration of the sample (from 0.2 to 20 mM). Overall, it suggests that when non-coordinating ligands are used (BArF as counterion and CH_2Cl_2 as the solvent) two different bis(μ-oxo) species exist. On the basis of the concentration dependence, we suggest that a competition between intra and intermolecular O_2 binding takes place, so that intermolecular bis(μ-oxo) forms are favored at higher complex concentrations. In contrast, the presence of coordinating ligands (CF_3SO_3 as counterion or acetone as solvent) directs the reaction towards the exclusive formation of the intramolecular core (Scheme 7).

All these experimental observations were confirmed by DFT calculations. Firstly, theoretical studies demonstrate that the bis(μ-oxo) core is much more favored than the corresponding μ-η^2:η^2-peroxo isomer. The viability of the intermolecular nature of the O_2-adducts was also computed and computational results indicate that there is an increase of 7 cm^{-1} of the breathing mode of the bis(μ-oxo) core with respect to the intramolecular species, thus reinforcing the hypothesis that the observed higher frequency vibration corresponds to the species where O_2 binding occurs intermolecularly.

Chapter IV. O_2 activation by mononuclear non-heme iron systems

Mononuclear non-heme iron enzymes that activate oxygen are widely spread in nature. Despite they are less known than their heme counterparts, they are capable of performing a wide range of chemical transformations.[22-24] The preparation of functional biomimetic systems constitutes a good tool to shed light on how iron centers in such active sites carry out the activation of dioxygen to affect a diverse range of oxidative transformations.

Rieske dioxygenases have emerged as the non-heme analogues of cytochrome P450s. These enzymes bear the widely-spread 2-His-1-carboxylate facial triad coordinating the center and they can

catalyze interesting transformations from a technological point of view, such as alkane hydroxylation, olefin epoxidation and *cis*-dihydroxylation of double bonds to give *cis*-diols. So far, the latter chemical transformation has been exclusively detected at these non-heme iron sites. By analogy to heme systems, in Rieske dioxygenases it is proposed that a high valent $Fe^V(O)(OH)$ intermediate, formed *via* water assisted heterolysis of a low-spin Fe^{III}-OOH, is the actual executor of substrate oxidation (Scheme 8).
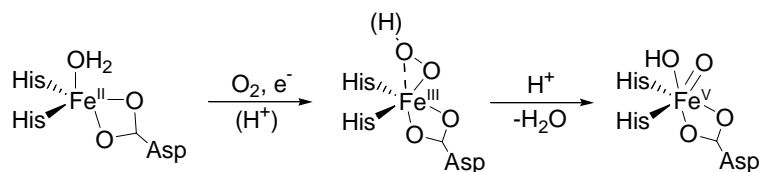
Scheme 8. Proposed mechanism of action of Rieske dioxygenases.

In Chapter IV we show the preparation of a new family of mononuclear iron complexes bearing a tripodal N_4 tetradentate triazacyclononane ligand derivatized with a methylpyridine arm, Pytacn (Scheme 9). We have applied these compounds as catalysts in several oxidative transformations including alkane hydroxylation, olefin epoxidation and *cis*-dihydroxylation, and sulfide oxidation (Scheme 9). The oxidant used in these reactions is H_2O_2 which may be considered as a "green" reagent due to its good atom efficiency and its relatively low cost. Thus, these oxidative processes can be envisioned as environmentally friendly technologies. Moreover, we also get insight into the mechanisms operating in these transformations by means of isotope labeling experiments using labeled reagents ($H_2^{18}O_2$ or $H_2^{18}O$). The mechanism involved in these bioinspired transformations may be helpful to better understand the mechanisms by which non-heme iron enzymes work. Finally, in Chapter IV.6 we have used the Pytacn platform to synthesize a new high-valent iron(IV)-oxo species and some of its reactivity has been studied in detail. The importance of such species in biological systems is beyond question as such compounds have been directly detected in selected non-heme biological enzymes.[25]
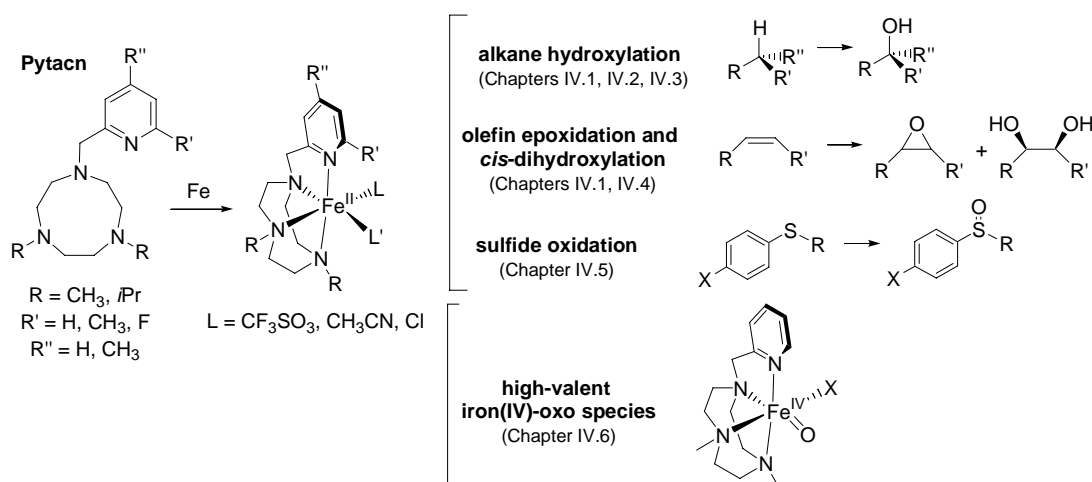
Scheme 9. Schematic representation of the works presented in Chapter IV.

Chapter IV.1. A novel platform for modeling oxidative catalysis in non-heme iron oxygenases with unprecedented efficiency

In Chapter IV.1 the preparation of four iron(II) complexes of the Pytacn family is reported and their ability to act as catalysts for alkane and olefin oxidation is studied.[26] The ligands and complexes described in this work are depicted in Scheme 10.

[Fe(CF$_3$SO$_3$)$_2$(Py(iPr)$_2$tacn)]	**1**CF$_3$SO$_3$:	R = iPr R' = H
[Fe(CF$_3$SO$_3$)$_2$(6Me-Py(iPr)$_2$tacn)]	**2**CF$_3$SO$_3$:	R = iPr R' = CH$_3$
[Fe(CF$_3$SO$_3$)$_2$(PyMe$_2$tacn)]	**3**CF$_3$SO$_3$:	R = CH$_3$ R' = H
[Fe(CF$_3$SO$_3$)$_2$(6Me-PyMe$_2$tacn)]	**4**CF$_3$SO$_3$:	R = CH$_3$ R' = CH$_3$

1CH$_3$CN
2CH$_3$CN
3CH$_3$CN
4CH$_3$CN
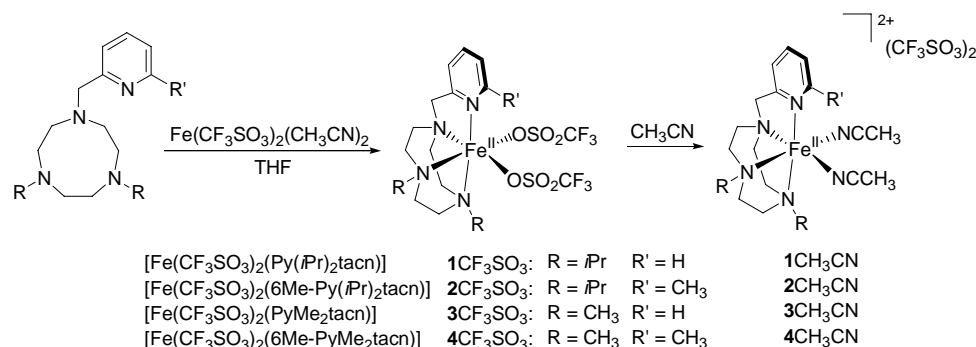
Scheme 10. Ligands and complexes used in Chapter IV.1.

Complexes **1**CF$_3$SO$_3$-**4**CF$_3$SO$_3$ (Scheme 10) were prepared by reaction of the corresponding ligands with 1 equiv of Fe(CF$_3$SO$_3$)$_2$(CH$_3$CN)$_2$ in THF into the glovebox to avoid oxidation by direct reaction with molecular O$_2$. The complexes precipitated directly from the reaction solution and they could be obtained as crystalline solids upon recrystallization with CH$_2$Cl$_2$:Et$_2$O. They contain a high spin iron(II) center as evidenced by their ^{1}H-NMR spectra which expand from -20 to 120 ppm (in CD$_2$Cl$_2$) and X-ray analysis that shows average Fe-N distances of 2.2 Å (Figure 4. left). Upon dissolution in CH$_3$CN, displacement of the bound triflate groups occurs so that the corresponding bis-acetonitrile solvato cationic complexes **1**CH$_3$CN-**4**CH$_3$CN are formed (Scheme 10). While complexes **1**CH$_3$CN, **2**CH$_3$CN and **4**CH$_3$CN posses a high-spin configuration (evidenced by ^{1}H-NMR spectroscopy), compound **3**CH$_3$CN presents a low spin iron(II) center as ascertained by its compact ^{1}H-NMR spectrum that expands from 0 to 12 ppm. This assignation was further confirmed by X-Ray analysis of [**3**CH$_3$CN]PF$_6$ which shows an average Fe-N distance of 2.0 Å, typical of a low spin iron(II) center (Figure 4, right)
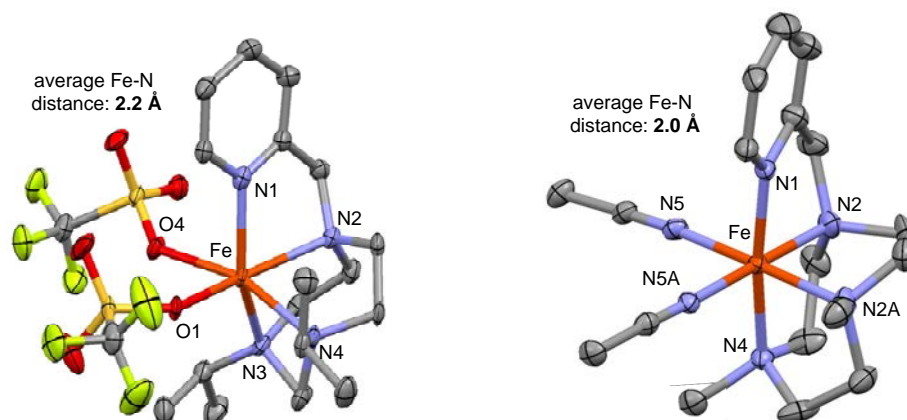
Figure 4. Thermal ellipsoid plot (50% probability) of **1**CF$_3$SO$_2$ (left) and [**3**CH$_3$CN]PF$_6$ (right). Hydrogen atoms and non-coordinated anions have been omitted for clarity.

The complexes prepared in this work were applied as catalysts in the oxidation of alkanes and olefins using H_2O_2 as the oxidant. Although compounds $1CF_3SO_3$-$4CF_3SO_3$ were used as the starting form of the catalyst, the acetonitrile media where the reactions took place transformed them into the corresponding bis-acetonitrile cationic complexes $1CH_3CN$-$4CH_3CN$. H_2O_2 was slowly added to the reaction mixture (catalyst and substrate dissolved in acetonitrile) by syringe pump addition (normally over 30 min) in order to avoid disproportionation reactions. Normally, for the evaluation of mechanistic aspects (isotope labeling experiments and mechanistic probes) conditions of large excess of substrate (1 equiv cat: 10 equiv H_2O_2: 1000 equiv substrate) were used.

In the first place, the ability of the new catalysts to perform the hydroxylation of cyclohexane was tested (Table 2). The results indicate that the most efficient ones are those bearing methyl groups in the triazacyclononane (tacn) backbone (complexes **3** and **4**), while catalysts with isopropyl groups (**1** and **2**) show remarkably lower yields, which may be attributed to the weak tertiary C-H bond of the *i*Pr group that renders the complexes susceptible to self-oxidation. In complexes **3** and **4**, large alcohol:ketone ratios (A/K), large kinetic isotope effects (KIE) in the oxidation of cyclohexane and high percentages of retention of configuration in the oxidation of *cis*-1,2-dimethylcyclohexane (DMCH) suggest that a metal-based oxidant is responsible for the chemistry. However, some degree of loss of stereoretention in the oxidation of DMCH in **1** and **2** indicates the involvement of longer lived carbon centered radicals for these two catalysts.

Complexes **1**-**4** also act as efficient catalysts in the oxidation of cyclooctene to give the corresponding *cis*-diol (D) and epoxide (E) products. As shown in Table 2, the diol:epoxide ratio (D/E) is increased when *i*Pr groups are present in the tacn ring. The oxidation of alkenes also points towards a metal-based character of the active species in **3** and **4** as ascertained by the high level of retention of configuration in the oxidation of *cis*-2-heptene. Interestingly, increasing the amount of peroxide up to 300 equiv did not cause significant loss of activity for complexes **3** and **4**, and 252 TN (D/E = 0.8) and 170 TN (D/E = 4.9) of products were obtained respectively. These values are higher than in any previously described iron complex suggesting that upon optimization of reaction conditions these complexes could be used as efficient catalysts from a synthetic point of view.

Table 2. Alkane and olefin oxidation reactions catalyzed by complexes **1**-**4**.[a]

| cat | equiv H_2O_2 | cyclohexane | | | DMCH | clooctene | | | *cis*-2-heptene |
		TN_{A+K}[b]	A/K[c]	KIE[d]	RC (%)[e]	TN_D[b]	TN_E[b]	D/E[f]	RC (%)[g] epoxide:diol
1	10	2.4	3.6	4.8	86	6.2	1.9	3.3	88:99
	100	-	-			73	12	6.0	
2	10	0.8	2.7	-	78	4.5	0.5	9.0	64:97
	100	-	-			10	4.0	2.5	
3	10	6.5	12.3	4.3	93	4.1	4.0	1.0	93:90
	100	39	2.6			50	49	1.0	
	300	-	-			123	129	0.8	
4	10	7.6	10.2	3.4	94	6.0	1.1	5.5	91:90
	100	64	4.3			74	12	6.2	
	300	-	-			141	29	4.9	

[a]1000 equiv substrate. [b]Turnover number (mols of product/mols of catalyst). A = cyclohexanol, K = cyclohexanone, D = *cis*-diol, E = epoxide. [c]A/K = mols alcohol/mols ketone. [d]Kinetic isotope effect for cyclohexanol formation. [e]Percentage of retention of configuration in the oxidation of the tertiary C-H bonds of *cis*-1,2-dimethylcyclohexane (DMCH) = (*cis-trans*)/(*cis+trans*)x100. [f]D/E = mols *cis*-diol/mols epoxide. [g]Percentage of retention of configuration in the oxidation of the C=C bond of *cis*-2-heptene for epoxide and *cis*-diol products = (*cis-trans*)/(*cis+trans*)x100.

In order to get information about the mechanisms operating in the oxidative transformations catalyzed by complexes **1**-**4**, isotope labeling studies were performed using $H_2^{18}O_2$ or $H_2^{18}O$ (see chapter IV.1 for experimental details) (Figure 5).
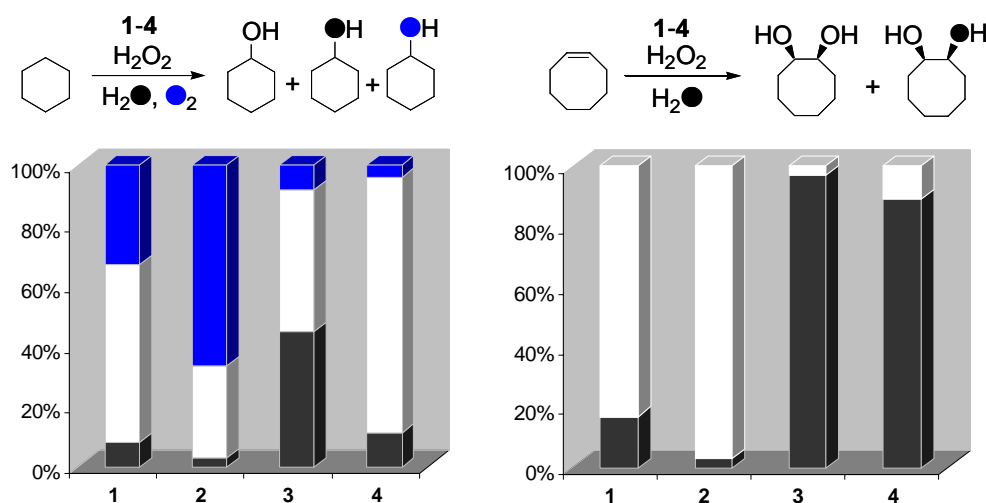
Figure 5. Left: Origin of the oxygen atoms incorporated into cyclohexanol in the oxidation of cyclohexane catalyzed by complexes **1**-**4**. Percentage of cyclohexanol with the oxygen atom originating from H_2O_2 (white), H_2O (black) or O_2 (blue). Right: Origin of the oxygen atoms incorporated into the *cis*-diol product in the oxidation of cyclooctene catalyzed by complexes **1**-**4**. White: percentage of *cis*-diol with the two oxygen atoms originating from H_2O_2. Black: percentage of *cis*-diol with one oxygen from H_2O_2 and the other from H_2O.

In the oxidation of alkanes the level of water incorporation into the cyclohexanol product is highly dependent on the specific catalyst (Figure 5). Complexes **1** and **2** show low levels of oxygen incorporation from water (8% and 3% respectively) and high percentages of O_2 incorporation. This observation further supports the notion that carbon centered radicals with long lifetimes may be involved in the reactions catalyzed by **1** and **2** because molecular O_2 from air can be trapped into products. On the other hand, in catalysts **3** and **4** O_2-incorporation is minimal (8 and 4% respectively) and most of the oxygen atoms come from H_2O_2 or H_2O. Especially remarkable is the high level of water incorporation in **3** (45 %) which is the highest ever reported for a non-heme iron catalyst. The incorporation of oxygen from water into oxidized products and the mechanistic probes clearly suggest the implication of high-valent metal-centered oxidants in the oxidative transformations catalyzed by **3** and **4**.

Isotope labeling experiments for alkene oxidation indicate the presence of two clear tendencies. While for catalysts **3** and **4** the *cis*-diol product contains one oxygen coming from water and the other from H_2O_2 (class A catalysts), in **1** and **2** both oxygen atoms that end up into the *cis*-diol product come from H_2O_2 (class B catalysts) (Figure 5). These labeling results can be explained on the basis of different mechanisms of action for class A and class B catalysts (Scheme 11).
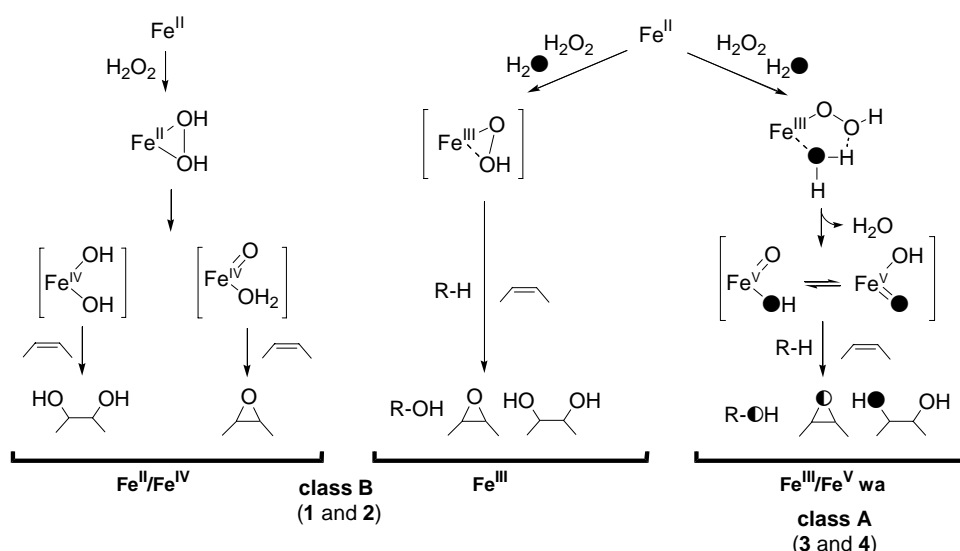
Scheme 11. Proposed mechanisms for alkane and alkene oxidation performed by catalysts **1**-**4**.

Class A catalysts insert one atom of oxygen from water and one atom of oxygen from H_2O_2 into the *cis*-diol which is reminiscent to the *cis*-diol labeling patterns observed for previously reported $[Fe(tpa)(CH_3CN)_2]^{2+}$ and $[Fe(bpmen)(CH_3CN)_2]^{2+}$ systems (Scheme 12).[27] These labeling results are a clear indication of the implication of a $Fe^V(O)(OH)$ species formed *via* water assisted O-O heterolysis of a H_2O-Fe^{III}-OOH species, presumably favored by the low-spin state of the iron center, which weakens the hydroperoxide O-O bond (Fe^{III}/Fe^V wa pathway, Scheme 11). Olefin interaction with the oxo group leads to epoxide, while *cis*-diol originates from initial attack of the hydroxide ligand of the $Fe^V(O)(OH)$ species.[28] For class B catalysts, the absence of water incorporation into *cis*-diol products can be explained through two mechanistic scenarios: (a) oxidation by direct interaction with a side-on Fe^{III}-OOH species (Fe^{III} pathway, Scheme 11); (b) O-O homolysis of a $Fe^{II}(H_2O_2)$ compound (Fe^{II}/Fe^{IV} pathway, Scheme 11) which leads to two tautomeric species: $Fe^{IV}(OH)_2$ responsible for *cis*-dihydroxylation and $Fe^{IV}(O)(OH_2)$ which performs epoxidation.[29] Both mechanisms give oxidation products with no incorporation of oxygen from water.
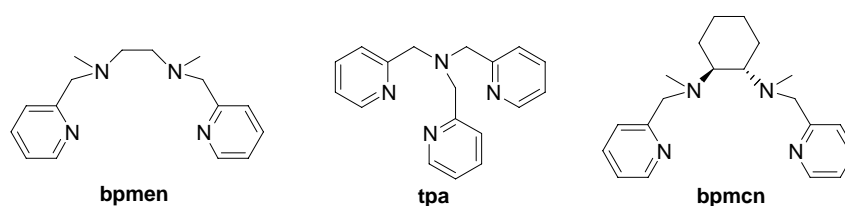
Scheme 12. Schematic representation of bpmen, tpa and bpmcn ligands.

In conclusion we have developed a new family of mononuclear non-heme iron complexes capable of performing the hydroxylation of alkanes and the epoxidation and *cis*-dihydroxylation of olefins. While the presence of *i*Pr groups in the tacn ring (catalysts **1** and **2**) decreases the robustness of the catalysts, the presence of methyl groups (catalysts **3** and **4**) gives highly active catalysts even when large amounts of oxidant (H_2O_2) are used. For complexes **3** and **4** the high selectivity of the

reactions and the large degree of stereoretention suggests the implication of a $Fe^V(O)(OH)$ intermediate with relevance to the active species involved in non-heme iron enzymes.

Due to the remarkable efficiency of complexes bearing methyl groups in the tacn ring (**3** and **4**), in Chapters IV.2, IV.3, IV.4 and IV.5 we study in more details the mechanism of action of these complexes in the oxidation of alkanes, olefins and sulfides.

Chapters IV.2 and IV3. Alkane hydroxylation by non-heme iron catalysts that challenges the heme paradigm for oxygenase action. Rethinking the rebound mechanism

A family of non-heme monoiron complexes of general formula $[Fe(L)_2(X-PyMe_2tacn)]$ (L = Cl, CF_3SO_3 or CH_3CN) was prepared (Scheme 13).

[Fe(CF_3SO_3)_2(PyMe_2tacn)] **3**CF_3SO_3: R' = H   R" = H   **3**CH_3CN
[Fe(CF_3SO_3)_2(6Me-PyMe_2tacn)] **4**CF_3SO_3: R' = CH_3   R" = H   **4**CH_3CN
[Fe(CF_3SO_3)_2(6F-PyMe_2tacn)] **5**CF_3SO_3: R' = F   R" = H   **5**CH_3CN
[Fe(CF_3SO_3)_2(4Me-PyMe_2tacn)] **7**CF_3SO_3: R' = H   R" = CH_3   **7**CH_3CN
[Fe(CF_3SO_3)_2(4,6Me_2-PyMe_2tacn)] **8**CF_3SO_3: R' = CH_3   R" = CH_3   **8**CH_3CN

[Fe(CF_3SO_3)_2(pinene-PyMe_2tacn)] **6**CF_3SO_3   **6**CH_3CN
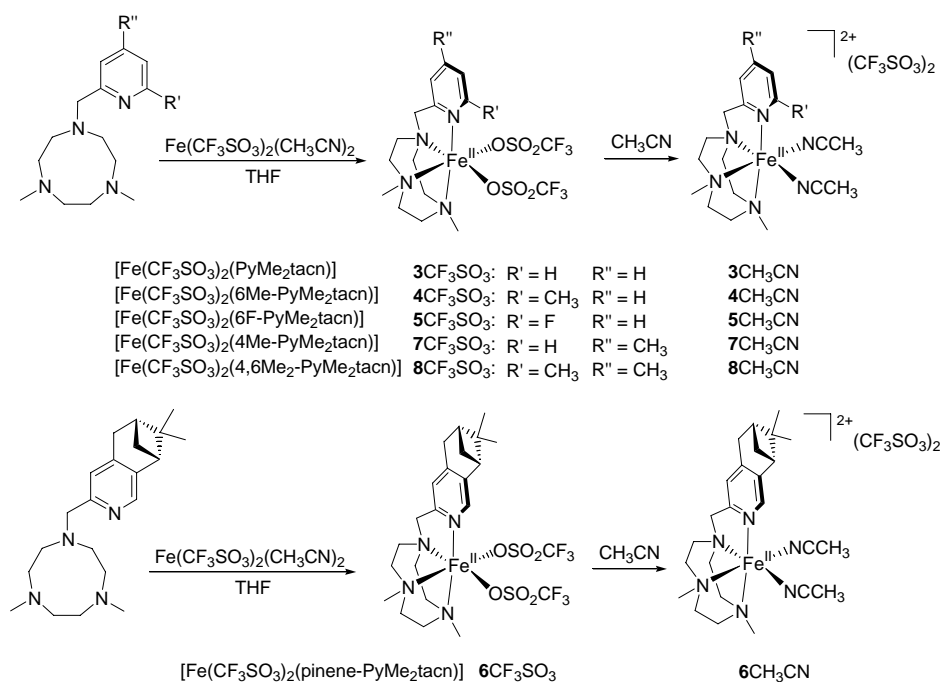
Scheme 13. Ligands and complexes used in Chapters IV.2 and IV.3.

Apart from the previously described PyMe_2tacn and 6Me-PyMe_2tacn ligands (Chapter IV.1) we synthesized additional ligands incorporating systematic modifications in the 4th, 5th and 6th positions of the pyridine ring (6F-PyMe_2tacn, pinene-PyMe_2tacn, 4Me-PyMe_2tacn and 4,6Me_2-PyMe_2tacn) (Scheme 13).

The basicity of this family of ligands is modulated by rather simple structural variations. This is clearly evidenced in the Fe^{III}/Fe^{II} redox potential of the corresponding chlorocomplexes $[Fe(Cl)_2(X-PyMe_2tacn)]$ (**3**Cl-**8**Cl) which expands from 138 to 238 mV *vs* SSCE (Table 3). In general terms, the presence of a methyl group in the 6th position of the pyridine ring (**4**Cl and **8**Cl) causes an increase in the redox potential with respect to a hydrogen atom (**3**Cl and **7**Cl) as previously reported for tpa

systems (see Scheme 12 for ligand's structure).[30] On the other hand, an unexpected increase in the redox potential is observed upon introduction of a methyl group in the 4th position of the pyridine (**7**Cl and **8**Cl), while the presence of a pinene ring fused in the 4th and 5th positions of the aromatic moiety (**6**Cl) has almost no effect in the redox potential. These observations are totally counterintuitive as the electron donating abilities of alkyl groups were initially expected to facilitate the access to higher oxidation states. The proper measurement of the electrochemical potential of **5**Cl was not possible due to the presence of multiple waves related with the decoordination of the 6-fluoro-pyridine arm.[31] Finally, complexes bearing *i*Pr groups in the tacn ring (**1**Cl and **2**Cl, Chapter IV.1) exhibit a redox couple 150 mV higher than the corresponding complexes with methyl groups (**3**Cl and **4**Cl). It is also interesting to notice that complex **3**Cl exhibits a Fe^{III}/Fe^{II} redox pair ($E_{1/2}$ = 138 mV *vs* SSCE) at lower potentials than analogous [FeCl$_2$(tpa)] ($E_{1/2}$ = 200 mV vs SSCE),[30] and [FeCl$_2$(bpmcn)] ($E_{1/2}$ = 170 mV *vs* SSCE)[32] thus indicating that the PyMe$_2$tacn backbone is more basic than tripodal tpa and linear bpmcn (see Scheme 12 for ligands' structures). High-valent species have been established as key elements on tpa[30] and bpmcn[33] catalytic oxidation of alkanes and alkenes with H$_2$O$_2$, and consequently the major basicity of the X-PyMe$_2$tacn derived ligands strongly suggests that high oxidation states are also accessible for these systems under analogous reaction conditions.

Table 3. Spin state of complexes **1**CH$_3$CN-**8**CH$_3$CN in the solid state and in CD$_3$CN solution and Fe^{III}/Fe^{II} redox potential of **1**Cl-**8**Cl.

complex	R	R'	Spin State (in CD$_3$CN)	Spin state (X-ray)	complex	$E_{1/2}$ (mV)[a] in CH$_3$CN
1CH$_3$CN	*i*Pr	H	High	-	**1**Cl	289
2CH$_3$CN	*i*Pr	CH$_3$	High	-	**2**Cl	360
3CH$_3$CN	CH$_3$	H	Low	Low	**3**Cl	138
4CH$_3$CN	CH$_3$	CH$_3$	High	Spin transition	**4**Cl	211
5CH$_3$CN	CH$_3$	F	Spin transition	-	**5**Cl	-
6CH$_3$CN	CH$_3$	H	Low	-	**6**Cl	143
7CH$_3$CN	CH$_3$	H	Low	-	**7**Cl	176
8CH$_3$CN	CH$_3$	CH$_3$	High	-	**8**Cl	238

[a]$E_{1/2}$ values referred to SSCE.
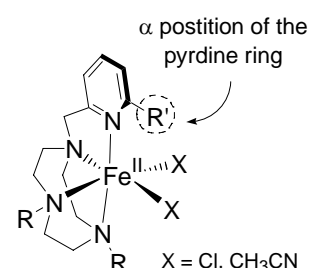
Iron(II) triflate complexes (**3**CF$_3$SO$_3$-**8**CF$_3$SO$_3$) were synthesized by reaction of each ligand with one equivalent of Fe(CF$_3$SO$_3$)$_2$(CH$_3$CN)$_2$ and they were fully characterized. Upon dissolution in acetonitrile, the corresponding bis-acetonitrile complexes [Fe(X-PyMe$_2$tacn)(CH$_3$CN)$_2$]$^{2+}$ (**3**CH$_3$CN-**8**CH$_3$CN) (Scheme 13) were obtained as proven by ^{1}H-NMR spectroscopy and measurement of μ_{eff} values. In all cases, the tripodal X-PyMe$_2$tacn ligand wraps around the metal center so that two *cis* positions are available for interaction with other ligands such as CF$_3$SO$_3$, CH$_3$CN, the oxidant or the substrate. The structure of the ligands also allows for the regulation of the spin state of the Fe^{II} site in **3**CH$_3$CN-**8**CH$_3$CN as ascertained by UV-vis spectroscopy and measurement of the μ_{eff} values by the Evans' method. Indeed, the substituent in the α position of the pyridine ring entails strong differences in the spin state of the corresponding complexes: a methyl group favors high spin configurations (**4**CH$_3$CN and **8**CH$_3$CN), no substituent affords low spin compounds (**3**CH$_3$CN, **6**CH$_3$CN and **7**CH$_3$CN) and a fluorine atom gives a spin transition phenomenon (**5**CH$_3$CN) (Table 3). In the latter case, the

spin transition was evidenced by a decrease in the μ_{eff} values upon lowering the temperature (from 4.77 MB at 320K to 0.92 MB at 235K) and an enhancement in the intensity of the UV-vis absorption band at λ_{max} = 385 nm (characteristic of low spin iron(II) centers) at low temperatures (Figure 6). On the other hand, complex **4**CH$_3$CN exhibits a spin crossover phenomenon in the solid state evidenced by a clear color change from colorless to dark blue upon lowering the temperature accompanied by a shortening of the Fe-N distances from 2.2 Å at 210K to 2.0 Å at 100K.
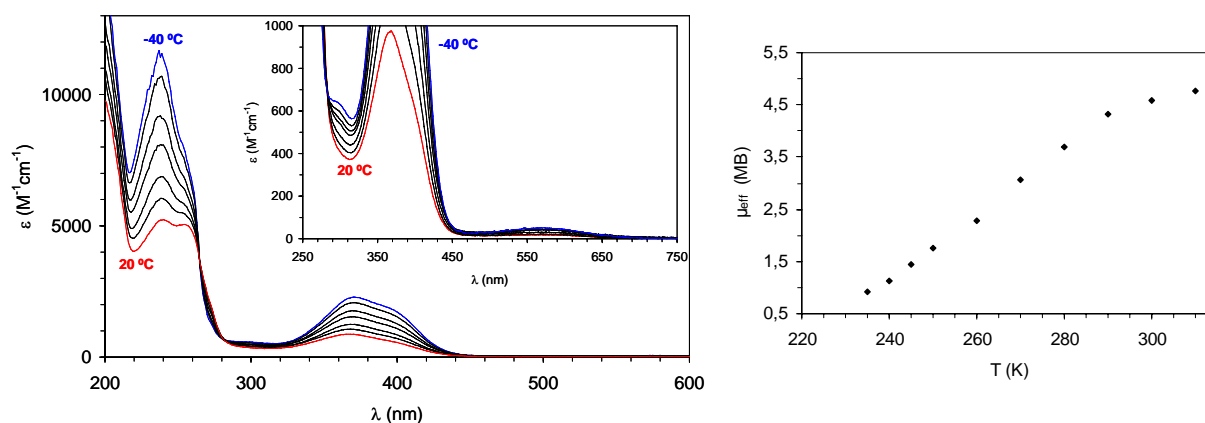
Figure 6. Left: UV-vis spectra of **5**CF$_3$SO$_3$ in CH$_3$CN at different temperatures (from 20 to -40 ºC). Right: Representation of μ_{eff} of **5**CF$_3$SO$_3$ at different temperatures (measured in CD$_3$CN solution by Evans' method).

From all these observations, it seems clear that substitution in the α position of the pyridine ring disfavors the low spin configuration, but also allows fine tuning of the spin state of the corresponding iron(II) complexes: when the bulkiness of the α-substituent increases (CH$_3$ > F > H), the high spin is favored. This can be explained if it is taken into account that bulky substituents favor metal centers with larger ionic radii, so high spin (average Fe-N distance ~ 2.2 Å) is favored over low spin (average Fe-N distance ~ 2.0 Å). Despite these differences, several experimental evidences indicate that low spin configurations are accessible for complexes **3**CH$_3$CN-**8**CH$_3$CN.

The α substituent also has a marked effect on the accessibility to the two *cis* positions not occupied by the X-PyMe$_2$tacn ligand (A and B positions in Figure 7): the bulkiness of the substituent in the α position of the pyridine ring strongly influences the accessibility to position A (an increase in the bulkiness of the α substituent causes an important increase in the steric constrictions) while the accessibility to B position is independent on the pyridine substitution. These steric interactions are important to explain some of the catalytic results described below.
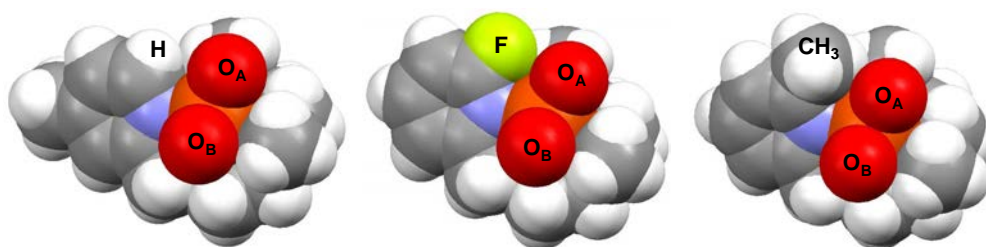
Figure 7. Space filling diagrams for complexes **7**CF$_3$SO$_3$ (left), **5**CF$_3$SO$_3$ (middle), and cationic part of [**4**H$_2$O]CF$_3$SO$_3$ (right). Triflate groups and water molecules have been omitted for clarity, but the oxygen atoms directly bound to the iron center are represented.

Complexes **3**CH$_3$CN-**8**CH$_3$CN (**3-8**) are excellent catalysts in the hydroxylation of cyclohexane to the corresponding alcohol and ketone products with variable efficiencies that range from 40 to 76% (Table 4). These reactions show large selectivity towards the formation of the alcohol product using H$_2$O$_2$ as the oxidant, and they can compare to the well-known [Fe(tpa)(CH$_3$CN)$_2$]$^{2+}$ and [Fe(bpmen)(CH$_3$CN)$_2$]$^{2+}$ catalysts (Scheme 12 for ligands' structures).[30] Moreover, on the basis of mechanistic probes it is clear that the active species responsible for the chemistry is a metal-based oxidant, as high A/K ratios in the oxidation of cyclohexane (from 9.3 to 15.6), high stereoselectivity in DMCH oxidation (86 – 96%), large KIE values on the oxidation of cyclohexane (3.4 – 5.0) and high normalized 3º/2º adamantane selectivities (15 – 30) are observed for the six catalysts (Table 4).

Table 4. Alkane hydroxylation reactions catalyzed by **3-8**, [Fe(tpa)(CH$_3$CN)$_2$]$^{2+}$ and [Fe(bpmen)(CH$_3$CN)$_2$]$^{2+}$.[a]

catalyst	A+K[b] (A/K) cyclohexane	KIE[c]	3º/2º adamantane[d]	RC (%) DMCH[e]
3	6.5 (12.3)	4.3	30	93
4	7.6 (10.2)	3.4	20	94
5	4.1 (9.8)	4.5	19	86
6	4.0 (15.6)	5.5	21	96
7	5.5 (14.5)	5.0	30	88
8	6.1 (9.3)	4.0	15	95
[Fe(tpa)(CH$_3$CN)$_2$]$^{2+}$	3.2 (5)	3.5	17	99
[Fe(bpmen)(CH$_3$CN)$_2$]$^{2+}$	6.3 (8)	3.2	15	96

[a]10 equiv H$_2$O$_2$. 1000 equiv substrate for cyclohexane and DMCH. 10 equiv for adamantane. [b]Turnover number (mols of product/mols of catalyst), A = cyclohexanol, K = cyclohexanone. [c]Kinetic Isotope Effect of cyclohexanol formation. [d]3º/2º ratio in adamantane oxidation = 3 x (1-adamantanol)/(2-adamantanol + 2-adamantanone). [e]Percentage of retention of configuration in the oxidation of the tertirary C-H bonds of *cis*-1,2-dimethylcyclohexane (DMCH) = (*cis-trans*)/(*cis*+trans)x100.

Catalytic experiments using 10 equiv H$_2$O$_2$ and 1000 equiv H$_2$^{18}O showed that the level of water incorporation into products is highly dependent on the specific structure of the catalyst and the substrate (Figure 8).
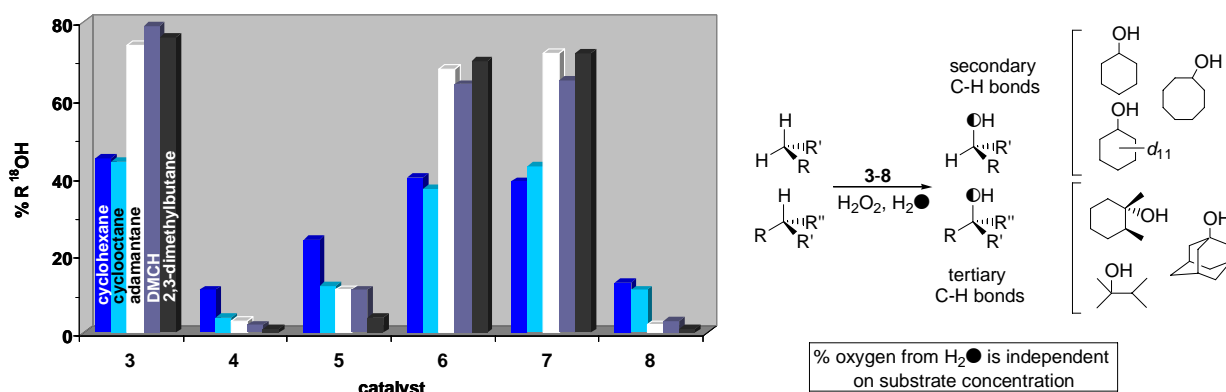
Figure 8. Percentage of ^{18}O-incorporation into alcohol products obtained in the oxidation of alkanes catalyzed by complexes **3-8** in the presence of H$_2$^{18}O.

As shown in Figure 8, all complexes are capable of incorporating oxygen from water into oxidized alcohol products formed in the stereoselective oxidation of C-H bonds. Complementary experiments using H$_2$^{18}O$_2$ showed that peroxide is the source of oxygen in the remaining oxidized products, so O$_2$ incorporation is minimal. On the other hand, the level of water incorporation does not depend on substrate concentration. However, there is a strong dependence of the labeling results with the particular substitution in the α position of the aromatic ring. Those complexes bearing no

substitution in this position (**3**, **6** and **7**) afford high levels of water incorporation especially for tertiary C-H bonds (72±8%). When a methyl group is present (**4** and **8**) the level of water incorporation decreases dramatically and it is higher for secondary C-H bonds (12±1%) than for tertiary ones. Finally, the presence of a fluorine atom (**5**) gives higher levels of water incorporation than a methyl group but still secondary C-H bonds incorporate larger amounts of water than tertiary ones.

Pioneer studies by Que and co-workers established a close analogy between the catalytic cycle of cytochrome P450s and the reactivity of non-heme model compounds of the tpa and bpmen families (Scheme 14).[30] These studies proposed that alkane oxidation occurs through the Fe^{III}/Fe^V wa pathway (Scheme 11) in which the active species is a $Fe^V(O)(OH)$ intermediate formed by water-assisted O-O bond cleavage of a H_2O-Fe^{III}-OOH species. Through this mechanism, alkane hydroxylation takes place by the so-called "oxygen rebound" mechanism, which involves initial hydrogen-atom abstraction by the oxo group and posterior rebound of the nascent alkyl radical with the newly formed $Fe^{IV}(OH)$ moiety so that the same oxygen atom that abstracts the hydrogen atom ends up into the oxidized compound (Scheme 14). Analogous to heme systems,[34] it is proposed that oxo-hydroxo tautomerism also occurs in non-heme $Fe^V(O)(OH)$ species. This phenomenon involves the conversion of the hydroxo ligand into an electrophilic oxo entity through the rapid shift of two electrons and one proton between the hydroxo ligand and the oxo group (Scheme 14). Thus, if complete oxo-hydroxo tautomerism occurs, the maximum amount of water that can be incorporated into products is 50%. Moreover, if oxo-hydroxo tautomerism competes with hydrogen-atom abstraction, a decrease in the oxygen incorporation from water is observed in the oxidation of weaker C-H bonds (such as tertiary C-H bonds) and upon increase of substrate concentration.[30] Complexes **3**-**8** share characteristics with $[Fe(tpa)(CH_3CN)_2]^{2+}$ and $[Fe(bpmen)(CH_3CN)_2]^{2+}$ systems. These analogies include similar structural and electronic properties as well as catalytic reactivity patterns. This suggests that common mechanistic considerations may apply.
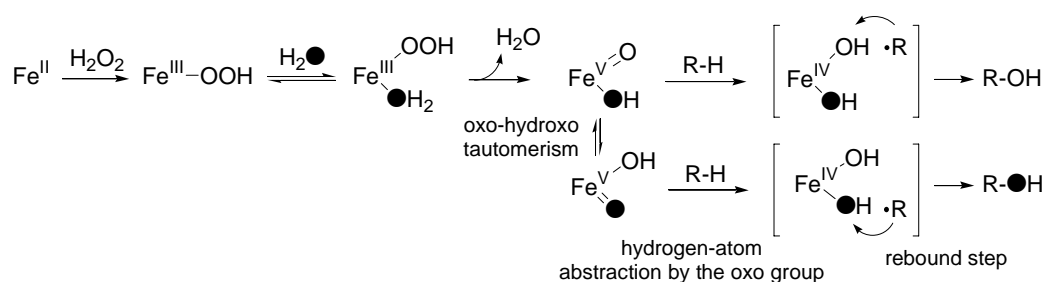
Scheme 14. Mechanism of action proposed for the hydroxylation of alkanes by non-heme iron catalysts such as $[Fe(tpa)(CH_3CN)_2]^{2+}$ and $[Fe(bpmen)(CH_3CN)_2]^{2+}$.

However, for complexes **3**, **6** and **7** there are some experimental results that do not fit with the canonical "oxygen rebound" mechanism depicted in Scheme 14: (a) the percentage of water incorporation in the oxidation of tertiary C-H bonds (72±8%) is larger than in secondary ones (42±3%) and surpasses the theoretical maximum of 50%; (b) the level of water incorporation into products does not depend on substrate concentration. Thus, for these catalysts it is necessary to reconsider some aspects of the proposed Fe^{III}/Fe^V wa pathway. We suggest that the inequivalence between the two *cis*

positions (A and B positions in Figure 7) in complexes **3-8** and their different steric constraints depending on the specific α substituent may be at the origin of the labeling results.

The lack of dependence between the level of water incorporation and substrate concentration gives some important mechanistic information: (a) Peroxide intermediates are not directly involved in alkane oxidation reactions. Should the Fe^{III}-OOH species be capable of oxidizing the substrate, a competition between substrate concentration and O-O bond breakage to give high valent iron(V)-oxo species would occur. Therefore, high substrate concentrations would cause a significant quenching of the O-O bond breakage path, and a decrease of the level of water incorporation into products. (b) There is no competition between oxo-hydroxo tautomerism and substrate oxidation. These conclusions suggest the sole implication of the Fe^{V}(O)(OH) species as the oxidant.

Deeper insight into the mechanism of action of these complexes was gained by means of DFT calculations performed on complex **3**. Due to the presence of non-equivalent *cis* positions, two isomeric forms for the Fe^{III}-OOH species (**3P**) are accessible: they are designated as **3P$_A$** and **3P$_B$** (Figure 9) depending on the position where the hydroperoxide group binds. However, isomer **3P$_A$** is energetically favored over **3P$_B$** by 2 kcal·mol^{-1} and subsequent heterolytic O-O cleavage of **3P$_A$** to form **3O$_A$** is further favored with respect to **3P$_B$** lysis by 4 kcal·mol^{-1}. Thus high-valent isomer **3O$_A$** is preferentially formed.
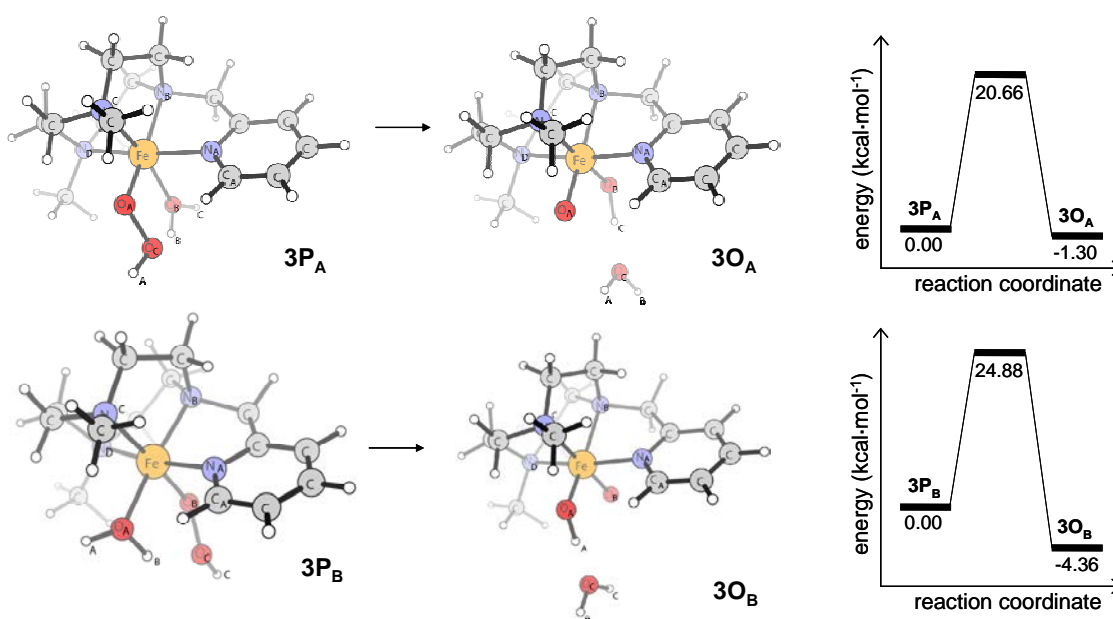
Figure 9. Left: Calculated structure of the **3P$_A$**, **3P$_B$**, **3O$_A$** and **3O$_B$** at the B3LYP level of theory. Right: Reaction paths for the heterolytic O-O bond cleavage of **3P$_A$** and **3P$_B$** to form **3O$_A$** and **3O$_B$** respectively.

Oxo-hydroxo tautomerism affords the formation of the corresponding isomer **3O$_B$** (Scheme 15). However, no matter which isomer (**3O$_A$** or **3O$_B$**) is responsible for abstracting the hydrogen atom from the substrate, a common Fe^{IV}(OH)$_2$ species is formed (Scheme 15). On the basis of DFT calculations, we propose that the rebound of the nascent alkyl radical can occur with any of the two hydroxo groups of the incipient Fe^{IV}(OH)$_2$ (the computed energy difference between the two

trajectores is < 2 kcal·mol⁻¹, Figure 10). Thus, the alkyl radical "chooses" with which hydroxo group takes place the rebound.
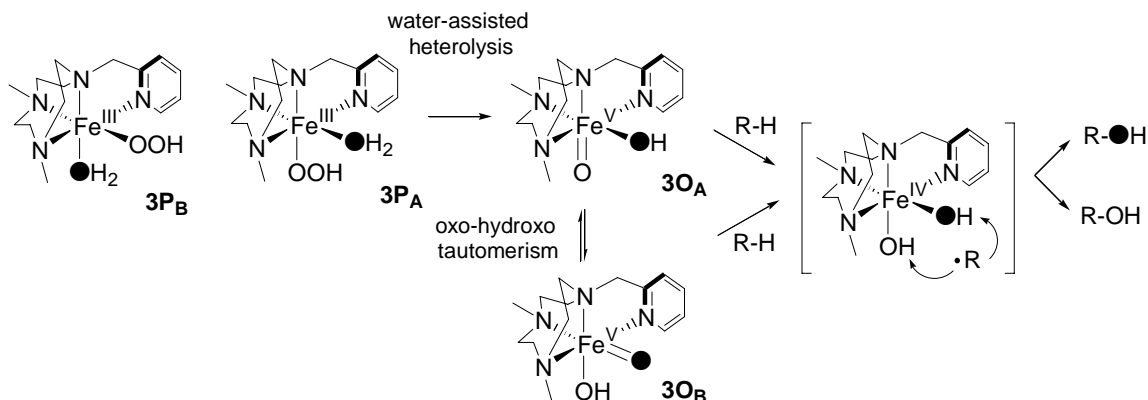
Scheme 15. Proposed mechanism of alkane hydroxylation by complex **3** (Chapter IV.2).
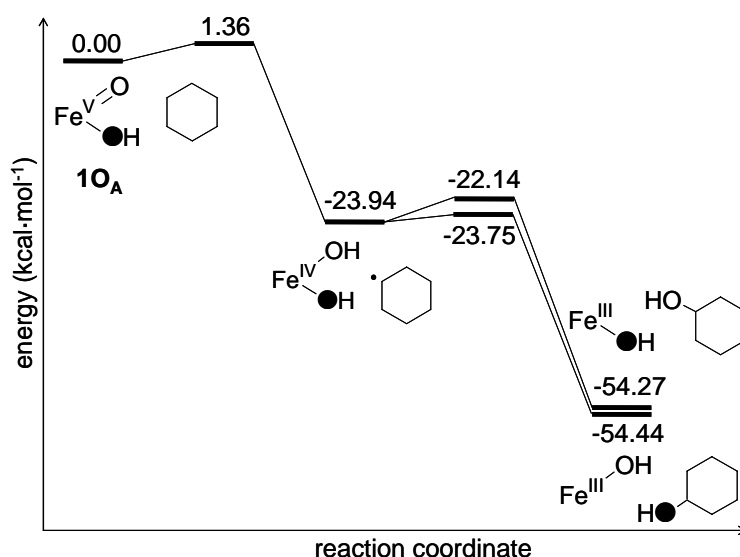
Figure 10. Calculated reaction paths for the reaction of Fe^V(O)(OH) (**3O$_A$**) with cyclohexane at the B3LYP level of theory.

A similar situation may apply to the other complexes that do not have a substituent in the α position of the pyridine ring (**6** and **7**). Thus, isomers **6O$_A$** and **7O$_A$** are preferentially formed (Scheme 16). Following substrate hydrogen-atom abstraction by **3O$_A$**, **6O$_A$** and **7O$_A$** substrate radical rebound in Fe^{IV}(OH^A)(OH^B) species can occur with both the oxidant derived hydroxyl ligand (OH^A), or with the water derived hydroxyl ligand (OH^B, Scheme 16). Sterically non-demanding radicals derived from secondary C-H bonds have no significant preference for any of the two positions and thus nearly equimolar mixtures of C-(OH^A) and C-(OH^B) alcohol products are obtained as indicated by the almost 50% water incorporation into cyclohexane (Figure 8). Instead, more sterically demanding radicals derived from tertiary C-H bonds rebound preferentially with the sterically less congested water derived OH^B ligand which explains the large percentages of oxygen from water (72±8%) in the corresponding alcohol products.

We propose that the situation is altered in catalysts that contain methyl (**4** and **8**) or fluorine (**5**) substitutents in the α position of the pyridine ring (X in Scheme 16). In these cases, because of steric interactions between the OOH ligand and the α-pyridine substituent, isomeric forms **4P$_B$**, **5P$_B$** and **8P$_B$** are preferentially formed (DFT calculations for these specific complexes are currently being performed to further substantiate this hypothesis). These species decay to generate Fe^V(O)(OH) isomers **4O$_B$**, **5O$_B$** and **8O$_B$**. In these isomers, the water derived hydroxyl ligand is highly sterically crowded (OH^A) due to interaction with the substituent present in the α position of the pyridine, thus limiting its accessibility. Accordingly, the level of water incorporation into products obtained with catalysts **4**, **5** and **8** are diminished with respect to those obtained with **3**, **6** and **7**. This phenomenon becomes especially evident for sterically congested tertiary C-H bonds which show minimum levels of water incorporation into alcohol products (1-11%, Figure 8).
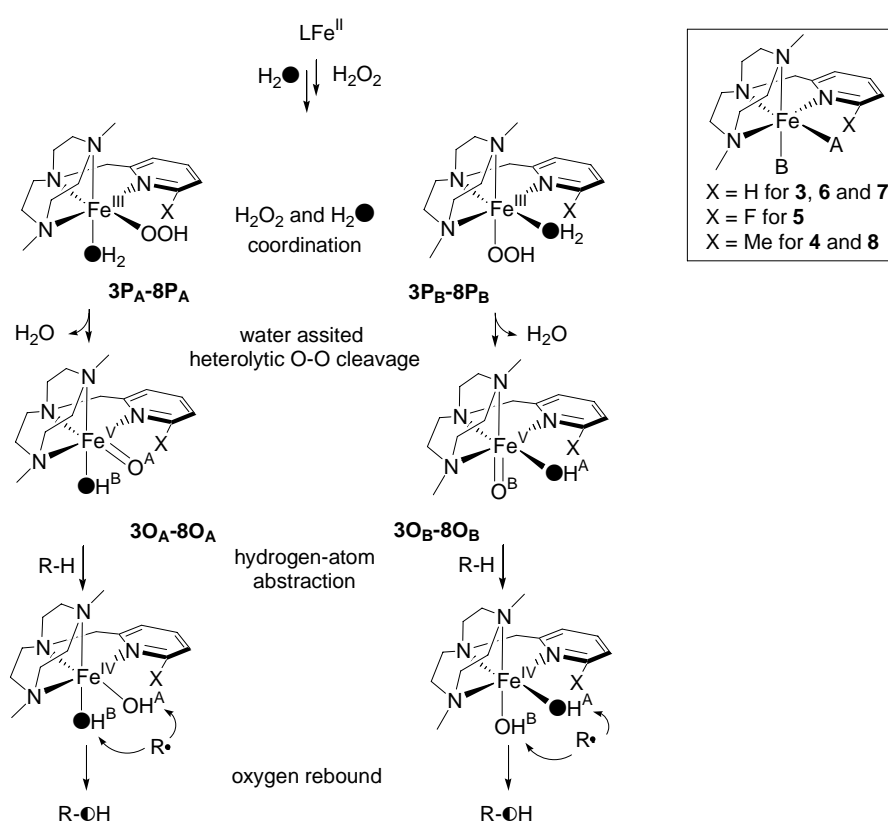
Scheme 16. Proposed mechanism of action of complexes **3**-**8** in alkane oxidation reactions.

In conclusion, we propose that in the reactions catalyzed by **3**-**8** water incorporation into the alcohol product is dictated at the rebound step on the basis of two energetically accessible trajectories, depending on the preference of the nascent alkyl radical to interact favorably with one of the two hydroxyl positions present in Fe^{IV}(OH)$_2$. This mechanistic scenario offers novel alternatives to the proposed mechanism of action of heme enzymes and it supports the idea that a rich mechanistic complexity underlines O$_2$ activation at non-heme systems and it calls into question the canonical description of oxygenase action.

Chapter IV.4. Olefin-dependent discrimination between two non-heme HO-Fe^V=O tautomeric species in catalytic H$_2$O$_2$ epoxidations

Mechanistic aspects of the catalytic ability of complex **3** in the oxidation of olefins were studied in detail. In a typical experiment 10 equiv of H$_2$O$_2$ were delivered by syringe pump together with 1000 equiv of H$_2$O over a period of 30 min into an acetonitrile solution containing 1 equiv of the iron catalyst **3** and the specific alkene (0.05-1 M). In all olefin oxidation reactions explored, mixtures of *cis*-diol and epoxide are obtained with modest to excellent efficiency in the conversion of H$_2$O$_2$ into products (3.9 to 8.9 TN, maximum TN = 9.5). However, the diol:epoxide ratio is highly dependent on the specific substrate and ranges from 3:2 for cyclooctene to 8:1 for 1-octene (Table 5).

Table 5. Olefin oxidation reactions catalyzed by **3** in the presence of H$_2$^{18}O.[a]

substrate	D/E (TN)[b]	diol % ^{16}O^{18}O[c]	epoxide % ^{18}O[d]
1-octene	8.1/0.8	80	60
trans-2-octene	2.6/1.3	73	33
trans-3-octene	3.7/1.6	75	33
trans-4-octene	3.7/2.1	71	33
cis-2-heptene	3.0/1.2	83	64
cyclooctene	4.7/3.1	84	61
cyclohexene	4.2/1.7	67	57
2-methyl-2-heptene	2.0/1.8	81	71

[a]10 equiv H$_2$O$_2$, 1000 equiv substrate and 1000 equiv H$_2$^{18}O. Reactions performed under N$_2$. [b]Turnover number (mols of product/mols of catalyst), D = diol, E = epoxide. [c]Percentage of diol with a singly ^{18}O labeled oxygen. [d]Percentage of ^{18}O labeled epoxide.

Analogously to alkane hydroxylation reactions, isotope labeling studies using H$_2$^{18}O (1000 equiv) gave important mechanistic information (Scheme 17, Table 5).
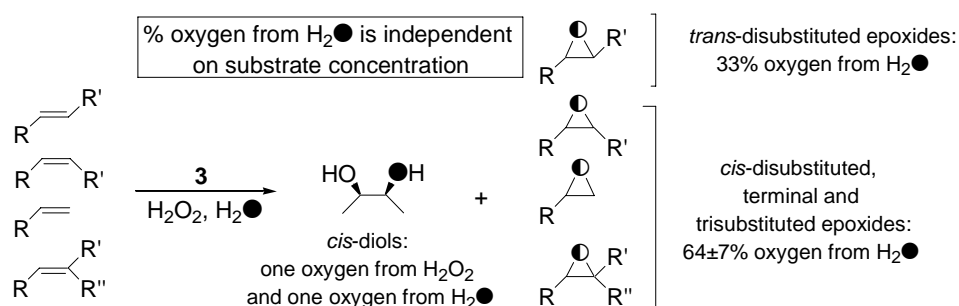
Scheme 17. Labeling results obtained in the epoxidation and *cis*-dihydroxylation of olefins by complex **3**.

As explained in Chapter IV.1, it is especially remarkable that a major fraction of the *cis*-diol products obtained in the oxidation of all substrates tested contain one oxygen atom from water and the other from H$_2$O$_2$, which strongly supports the implication of a Fe^V(O)(OH) species (**3O$_A$** and **3O$_B$**). Epoxides are formed by direct transfer of the oxo group to the olefin, while *cis*-diols are generated by transfer of both oxo and hydroxo groups to the double bond.[28] Much more surprising are the labeling results for the epoxidations. The activity of **3** is unprecedented as water is the main source of oxygen

in the epoxidation of *cis*-disubstituted, trisubstituted and terminal olefins (64±7%), while the level of water incorporation into epoxide products derived from *trans*-disubstituted olefins decreases down to 33%. A complementary experiment using $H_2^{18}O_2$ (10 equiv) and H_2O (1000 equiv) in the oxidation of cyclooctene gives epoxide 25% labeled, thus affording a good oxygen mass balance. Importantly, isotope labeling results are independent on substrate concentration, so that oxo-hydroxo tautomerism is not competing with substrate oxidation. Analogously to alkane hydroxylation, it seems clear that the structure of the specific olefin determines the origin of the oxygen that ends up into the epoxide product. Taking into account the proposed mechanism for alkane hydroxylation, we suggest that due to the inequivalence of the oxo group in isomers $3O_A$ and $3O_B$, the specific olefin "chooses" with which $Fe^V(O)(OH)$ isomer prefers to interact (Scheme 18).
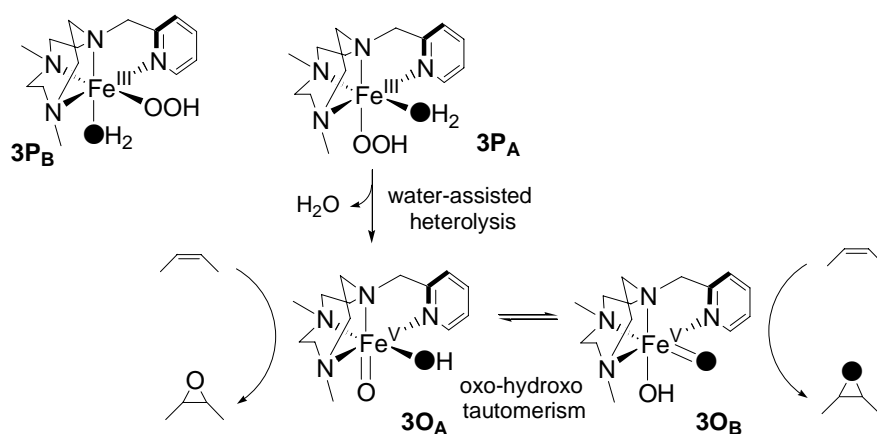
Scheme 18. Proposed mechanism for olefin epoxidation catalyzed by complex **3** (Chapter IV.4).

Thus, *trans*-disubstituted olefins react preferably with isomer $3O_A$ (incorporation of oxygen from H_2O_2), while terminal, *cis*-disubstituted and trisubstituted olefins interact mainly with the oxo group of isomer $3O_B$ according to the labeling results obtained for epoxide products.

The accumulated labeling results for the alkane hydroxylation and olefin epoxidation reactions catalyzed by **3** present a new twist in the reactivity of the high valent species ($3O_A$ and $3O_B$). Despite the large differences in the percentage of water incorporation into the oxidized products, these values translate into only small differences in energy, comparable to those associated with chiral discrimination. Catalyst **3** may give rise to the novel labeling results we observe because the two oxidants, though inequivalent, are quite close to each other in energy. Olefin epoxidation by HO-Fe^V=O ($3O_A$ and $3O_B$) and hydroxyl ligand transfer from a $Fe^{IV}(OH)_2$ species to an alkyl radical are inherently different reactions, but they may share a common energetic asymmetry in the approach of the olefin, or the alkyl radical, respectively towards two non-equivalent reactive sites. Differences in the reactivity of the two high valent isomers $3O_A$ and $3O_B$ may arise from a combination of electronic and steric factors. From a steric point of view, comparative analysis of their respective molecular structures shows that $3O_A$ likely contains a slightly more congested oxo group than $3O_B$. On the other hand, a recent electrochemical and reactivity study on Fe^{IV}=O complexes has revealed that pyridine rings parallel to the oxo group give rise to more electrophilic iron centers than analogous complexes

where the pyridine is perpendicular to the oxo group. Because of that, it is tempting to propose that **3O$_A$** is a more electrophilic oxidant than **3O$_B$**.

The mechanistic scenario arising from the study described in Chapters IV.2, IV.3 and IV.4 may be related to aspects of the catalytic cycle of the α-ketoglutarate-dependent Cyt-C3 halogenase,[35] in which two high-spin Fe^{IV}O(X) (X = Cl or Br) intermediates have been characterized by rapid-freeze-quench Mössbauer experiments and found to be directly responsible for the C-H activation event. The relative proportion of these two high-valent isomers remains constant along the reaction coordinate, suggesting that fast interconversion between them precedes hydrogen-atom abstraction from substrate. Indeed, the presence of non-equivalent *cis*-binding sites is a common structural characteristic of a number of non-heme iron oxygenases,[22] and therefore the interplay between two isomerically related high-valent species may be a rather common yet unexpected feature of their oxygen activation chemistry, substantially different from heme systems. The current study serves as a synthetic precedent for this novel mechanistic feature and it calls into question the canonical description of oxygenase action.

Chapter IV.5. A second oxidant in H$_2$O$_2$ oxidation reactions catalyzed by a functional model of Rieske dioxygenases

In Chapters IV.2 and IV.4 we have described the mechanism of action of catalyst **3** in the oxidation of alkanes and olefins. As stated above, high levels of water incorporation into products suggest that a high-valent Fe^V(O)(OH) (**3O$_A$/3O$_B$**) species is responsible for the chemistry. In addition, the lack of dependence between the level of water incorporation and substrate concentration demonstrates that no preceding intermediate to **3O$_A$/3O$_B$** is competent for performing these reactions, and that the oxo-hydroxo tautomerism is not kinetically competing with substrate oxidation.

However, in chapter IV.5 we examined the reactivity of **3** against sulfides, considered as very reactive substrates. Mechanistic studies in the oxidation of sulfides by complex **3** are described, providing compelling evidence for a second oxidant that precedes the formation of the Fe^V(O)(OH) species (**3O$_A$/3O$_B$**). We conclude that this second oxidant is not competent for alkane and olefin oxidation but it can elicit oxygen atom transfer to sulfides.

The first evidence for the existence of a second oxidant came from isotope labeling studies using ^{18}O-labeled water in the oxidation of sulfides (Scheme 19). In a typical experiment 10 equiv of H$_2$O$_2$ were delivered by syringe pump together with 1000 equiv of H$_2$O over a period of 30 min into an acetonitrile solution containing 1 equiv of the iron catalyst (**3**) and a specific amount of sulfide (0.10 mM - 1 M). In contrast to olefin and alkane oxidation, the percentage of oxygen atoms originating from water incorporated into the sulfoxide products is highly dependent on substrate concentration and it ranges from 10% when using 1000 equiv thioanisole to 39% when 10 equiv are used. Complementary experiments using H$_2$^{18}O$_2$ in the presence of H$_2$O demonstrate that the rest of oxygen atoms

incorporated into the sulfoxide product is derived from H_2O_2, so that no O_2 incorporation from air is involved.

X = H, CN, Cl, CH_3, OCH_3

% oxygen from $H_2\bullet$ is dependent on substrate concentration

↑ [sulfide]   ↓ % oxygen from $H_2\bullet$
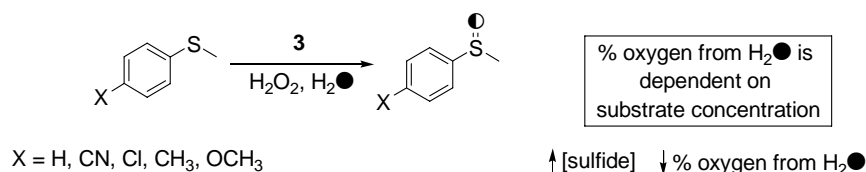
Scheme 19. Oxidation of sulfides by complex **3** (Chapter IV.5).

From a mechanistic point of view, the dependence of water incorporation with substrate concentration is consistent with two scenarios (Scheme 20): (a) competition between sulfide oxidation and water incorporation may occur at the HO-Fe^V=O level, thus indicating substrate quenching of the oxo-hydroxo tautomerism before it reaches equilibrium (**3O_A** to **3O_B**). In this case competition arises from the values of k_{AB} *vs* $k'_{OS}\cdot$[sulfide]; (b) substrate oxidation may occur not only *via* the HO-Fe^V=O species (with water incorporation), but also *via* a preceding intermediate to the high-valent (no water incorporation). In this scenario, the competition is expressed as k_{O-O} *vs* $k_{PS}\cdot$[sulfide].

Scenario A

Scenario B
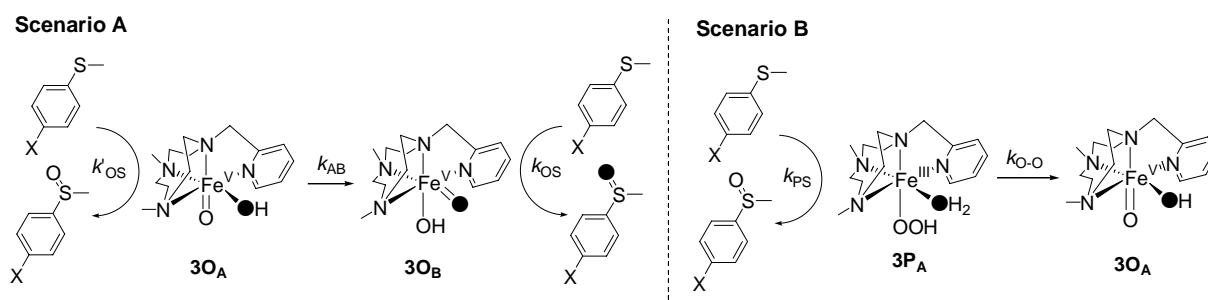
Scheme 20. Two possible mechanisms of action of complex **3** in the oxidation of sulfides.

Competitive oxidation of thioanisole and *cis*-2-heptene reveals that the sulfide is nearly 3 orders of magnitude more reactive than the olefin. In addition, the labeling value obtained for the epoxide and *cis*-diol was the same as the one measured in reactions where *cis*-2-heptene was the only substrate (63±3 % and 79±5 % respectively). This experiment definitively rules out the quenching of the oxo-hydroxo tautomerism (scenario A). If this was the case, the faster reacting substrate (sulfide) would prevent the tautomerism (Scheme 2, **3O_A** to **3O_B**, k_{AB}) and the extent of label incorporation would be diminished in epoxide product. These labeling results clearly point towards the implication of a preceding species to Fe^V(O)(OH) that is also competent for oxygen atom transfer to sulfides (scenario B). In addition, oxo-hydroxo tautomerism between **3O_A** and **3O_B** must be much faster than sulfide oxidation.

The lack of substrate oxidation upon reaction of **3** (Fe^{II}) with 0.5 equiv H_2O_2 in the presence of sulfide and the absence of direct interaction between the ferric center (Fe^{III}-OH) and sulfide (Scheme 21), clearly suggest that a Fe^{III}-OOH compound (**3P**) is the active species preceding Fe^V(O)(OH).
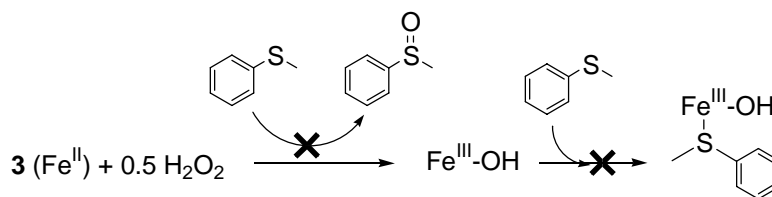
Scheme 21.

Reactions with *para*-X-substituted methyl phenyl sulfides (*p*-X-thioanisole, X = CN, Cl, CH$_3$, OCH$_3$) showed that electron-richer substrates incorporated less oxygen from water, so that they are more easily oxidized by **3P** species causing a decrease in the extent of water incorporation. Hammett analyses at different substrate concentration further confirmed the coexistence of two different oxidants. A Hammett parameter of -1.29 was obtained when using 500 equiv of substrate, and a value of -0.86 was obtained with 100 equiv of substrate (Figure 11). This significant difference is consistent with the different relative predominance of the two oxidants (**3P** or **3O$_A$**/**3O$_B$**) depending on substrate concentration.
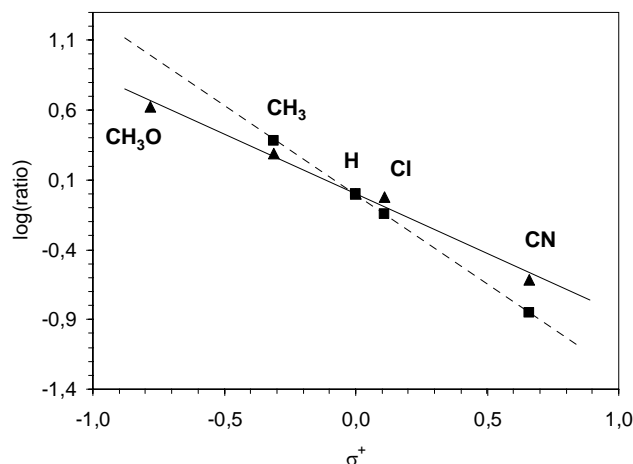
Figure 11. Hammett plots for the oxidation of *p*-X-thioanisoles by catalyst **3**. Dotted line: 500 equiv of substrate. Solid line: 50 equiv of substrate.

Plots of the logarithm of relative sulfide oxidation rates (with respect to thioanisole) against the oxidation potential of the substrates afforded linear correlations and the corresponding slopes were - 3.3 (500 equiv of substrate) and -2.6 (100 equiv. substrate). Such small values indicate a rather small dependence between oxidation rate constants and oxidation potential of the substrates and they strongly suggest that sulfide oxidation involves direct oxygen atom transfer rather than electron transfer.[36]

In conclusion, **3P** is capable of performing sulfide oxidation *via* an oxygen-atom transfer reaction, but it is not competent for olefin and alkane oxidation. In cytochrome P450 the possibility that a hydroperoxide type of species can act as the oxidant has been questioned on the basis of computational work.[37] For non-heme iron enzymes a different situation may apply, and in fact, computational studies indicate that water-assisted O-O bond cleavage in [Fe^{III}(OOH)(bpmen)(CH$_3$CN)]$^{2+}$ species has an activation barrier similar to direct oxygen atom transfer

to substrates (~ 20 kcal·mol^{-1}).[38] The neutral nature of the PyMe$_2$tacn ligand suggests that common energetic considerations may apply to **3**, and this may be a key issue on the promotion of the Lewis acidity of the ferric site, and in the increase of the barrier for O-O bond breakage. The work presented in Chapter IV.5 experimentally substantiates this hypothesis and suggests that non-heme iron sites exhibit a diverse and fascinating mechanistic landscape that surpasses the heme paradigm for oxygen activation (Scheme 22).
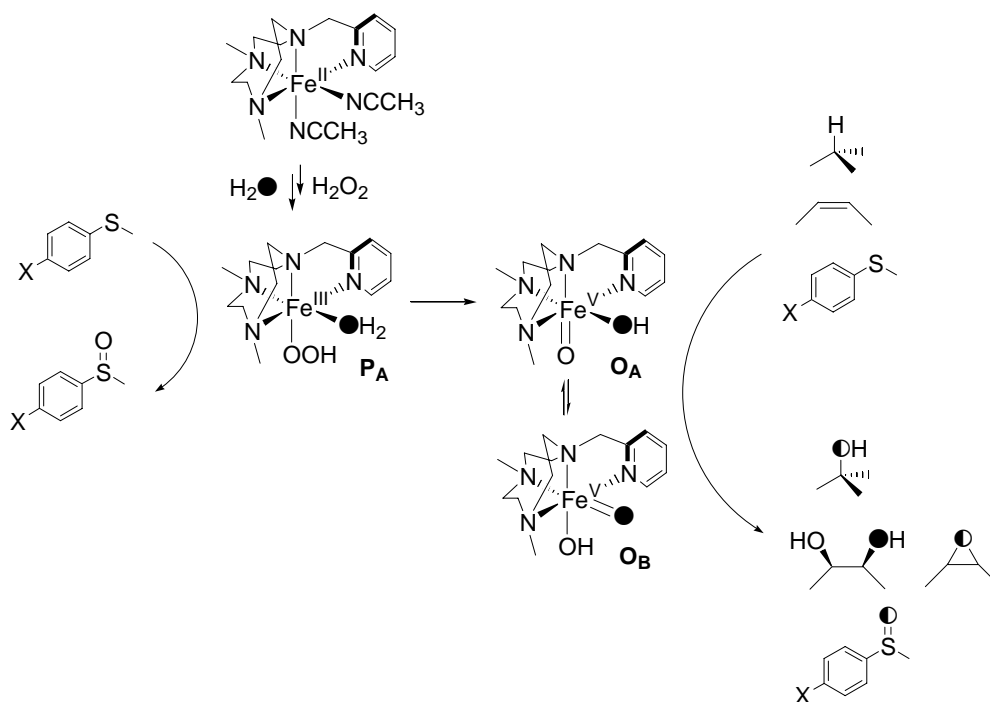
Scheme 22. General mechanism of action proposed for catalyst **3** in the oxidation of alkanes, alkenes and sulfides.

Chapter IV.6. Spectroscopic and chemical characterization of a novel non-heme iron(IV)-oxo compound bearing a nitrogen-based tetradentate ligand

Iron(IV)-oxo compounds are proposed as the active species in the catalytic cycle of several O$_2$-activating non-heme iron enzymes.[22] Quite recently, high spin iron(IV)-oxo intermediates have been trapped and spectroscopically characterized in different non-heme iron enzymes thus confirming their implication.[25] Concomitant with these findings, synthetic chemists have succeeded in the preparation of low spin iron(IV)-oxo compounds that can act as oxidants in several oxidative transformations analogous to the reactions occurring in biological systems. In Chapter IV.6 we take advantage of the basic PyMe$_2$tacn ligand backbone and we use it for the synthesis and characterization of a new iron(IV)-oxo compound.

Reaction of complex [Fe^{II}(CF$_3$SO$_3$)$_2$(PyMe$_2$tacn)] (**3**) with 2 equiv of CH$_3$CO$_3$H at 15ºC afforded a new species, that we assigned as a low spin **Fe^{IV}=O** species (S = 1) on the basis of ^{1}H-NMR and Mössbauer spectroscopy and by ESI-MS spectroscopy (Scheme 23). This compound showed

remarkable stability at room temperature ($t_{1/2}$ = 2.4 h at 15⁰C) which contrasts with other structurally related iron(IV)-oxo compounds which are only stable at low temperatures.[39] This stability has allowed us to study in detail some of the reactivity exhibited by **Fe^{IV}=O**.
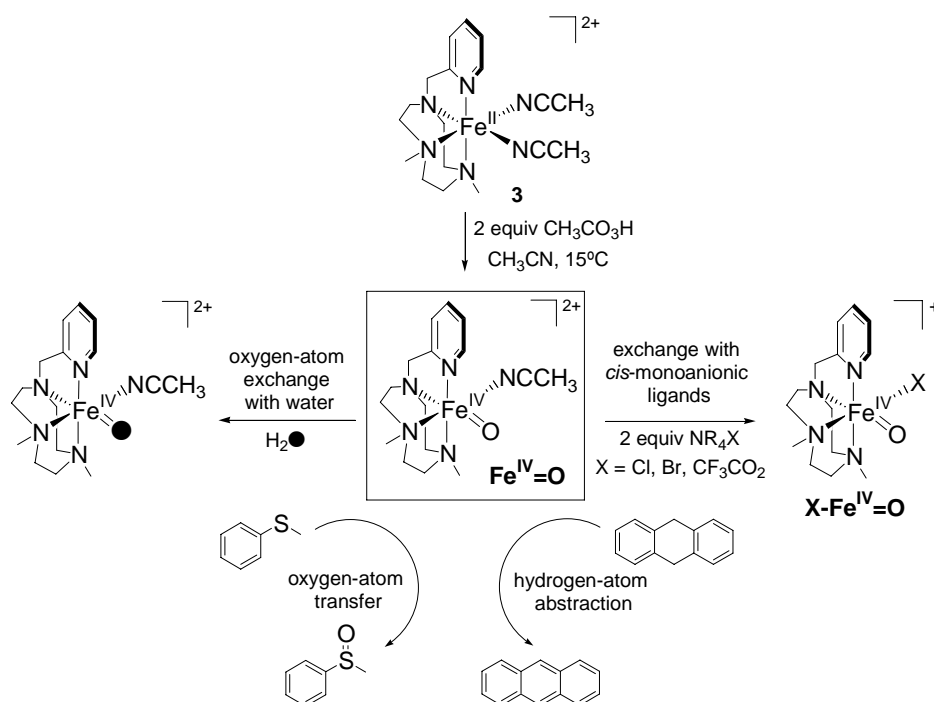
Scheme 23. Synthesis of **Fe^{IV}=O** along with the reactivity studied in Chapter IV.6.

Several aspects of the reactivity of the newly prepared **Fe^{IV}=O** species were analyzed in detail (Scheme 23):

- *Oxygen-atom exchange with water*: by means of MS analyses we could study the ability of **Fe^{IV}=O** to exchange its oxygen atom using ^{18}O-labeled water. Rate law and activation parameters could be obtained for this reaction ($\Delta H^{\neq}$ = 10.2±0.8 kcal·mol^{-1} and $\Delta S^{\neq}$ = -32±3 cal·K^{-1}·mol^{-1}) and detailed study of the mechanism implicated in this process was performed by means of DFT calculations. Theoretical studies indicate the participation of an exogenous water molecule that assists the hydrogen transfer from the bound water molecule to the oxo group.

- *Hydrogen-atom abstraction of activated C-H bonds*: hydrogen-atom abstraction of 9,10-dihydroanthracene afforded anthracene as the single product. Reactions with several substrates with well-known C-H bond dissociation energies (BDE) were performed. A direct correlation between the logarithm of the reaction rate and the BDE values was obtained. This observation together with a very large kinetic isotope effect value (KIE ~ 40) measured for the oxidation of dihydroanthracene indicates that reactions occur *via* a hydrogen-atom abstraction mechanism.

- *Oxygen-atom transfer to sulfides*: oxygen-atom transfer from **Fe^{IV}=O** to thioanisole was achieved, and the corresponding sulfoxide was obtained. Hammett analyses using *para*-substituted thioanisoles afford a linear correlation with a negative slope (ρ = -1.5) indicative of the electrophilic character of the **Fe^{IV}=O** species. Plot of the logarithm of k_{obs} *vs* sulfide redox potentials shows a small slope (-3.0)

which is inconsistent with an electron transfer initiated reaction, but instead it indicates that reactions occur *via* an oxygen-atom transfer process.[36]

- *Exchange with cis-monoanionic ligands*: in order to better mimicking the anionic coordination environment present in non-heme iron enzymes, the bound acetonitrile ligand in **Fe^{IV}=O** was replaced by biologically relevant anionic groups (X) such as halides (Cl, Br) or carboxylates (CF$_3$CO$_2$) to generate [Fe^{IV}(O)(X)(PyMe$_2$tacn)]$^+$ species (**X-Fe^{IV}=O**). This transformation was followed by UV-vis spectroscopy and confirmed by comparison with the spectroscopic properties of [Fe^{IV}(O)(X)(tpa)]$^+$.[40] This ligand exchange phenomenon enables the presence of a monoanionic group in a *cis* configuration with respect to the oxo group, and thus **X-Fe^{IV}=O** species constitute structural models for the active site in α-ketoglutarate dependent oxygenases.[22,24]

References

1. Bertini, I.; Gray, H. B.; Stiefel, E. I.; Valentine, S. J., *Biological inorganic Chemistry: structure & reactivity*. University Science Books: Sausalito, California, 2007.

2. Kraatz, H.-B.; Metzler-Nolte, N., *Concepts and Models in Bioinorganic Chemistry*. Wiley-VCH: Weinheim, 2006.

3. Que, L., Jr.; Tolman, W. B., *Nature* **2008,** *455*, 333-340.

4. Bento, I.; Carrondo, M. A.; Lindley, P. F., *J. Biol. Inorg. Chem.* **2006,** *11*, 539-547.

5. Costas, M.; Xifra, R.; Llobet, A.; Solà, M.; Robles, J.; Parella, T.; Stoeckli-Evans, H.; Neuburger, M., *Inorg. Chem.* **2003,** *42*, 4456-4468.

6. Menif, R.; Martell, A. E.; Squattrito, P. J.; Clearfield, A., *Inorg. Chem.* **1990,** *29*, 4723-4729.

7. Costas, M.; Ribas, X.; Poater, A.; López Valbuena, J. M.; Xifra, R.; Company, A.; Duran, M.; Solà, M.; Llobet, A.; Corbella, M.; Usón, M. A.; Mahía, J.; Solans, X.; Shan, X.; Benet-Buchholz, J., *Inorg. Chem.* **2006,** *45*, 3569-3581.

8. Company, A.; Lamata, D.; Poater, A.; Solà, M.; Rybak-Akimova, E. V.; Que Jr., L.; Fontrodona, X.; Parella, T.; Llobet, A.; Costas, M., *Inorg. Chem.* **2006,** *45*, 5239-5241.

9. Matoba, Y.; Kumagai, T.; Yamamoto, A.; Sugiyama, M. J., *J. Biol. Chem.* **2006,** *281*, 8981-8990.

10. Liang, H.-C.; Zhang, C. X.; Henson, M. J.; Sommer, R. D.; Hatwell, K. R.; Kaderli, S.; Zuberblühler, A. D.; Rheingold, A. L.; Solomon, E. I.; Karlin, K. D., *J. Am. Chem . Soc.* **2002,** *124*, 4170-4171.

11. Mirica, L. M.; Ottenwaelder, X.; Stack, T. D. P., *Chem. Rev.* **2004,** *104*, 1013-1046.

12. Mahapatra, S.; Young, V. G. J.; Kaderli, S.; Zuberbühler, A. D.; Tolman, W. B., *Angew. Chem. Int. Ed.* **1997,** *26*, 130-133.

13. Lewis, E. A.; Tolman, W. B., *Chem. Rev.* **2004,** *104*, 1047-1076.

14. Company, A.; Palavicini, S.; Garcia-Bosch, I.; Mas-Ballesté, R.; Que, J. L.; Rybak-Akimova, E. V.; Casella, L.; Ribas, X.; Costas, M., *Chem. Eur. J.* **2008,** *14*, 5335-5338.

15. Company, A.; Gómez, L.; Mas-Ballesté, R.; Korendovych, I. V.; Ribas, X.; Poater, A.; Parella, T.; Fontrodona, X.; Benet-Buchholz, J.; Solà, M.; Que, L., Jr.; Rybak-Akimova, E. V.; Costas, M., *Inorg. Chem.* **2007,** *46*, 4997-5012.

16. Mirica, L. M.; Vance, M.; Rudd, D. J.; Hedman, B.; Hodgson, K. O.; Solomon, E. I.; Stack, T. D. P., *Science* **2005,** *308*, 1890-1892.

17. Yamazaki, S.; Itoh, S., *J. Am. Chem. Soc.* **2003,** *125*, 13034-13035.

18. Palavicini, S.; Granata, A.; Monzani, E.; Casella, L., *J. Am. Chem. Soc.* **2005,** *127*, 18031-18036.

19. Santagostini, L.; Gullotti, M.; Monzani, E.; Casella, L.; Dillinger, R.; Tuczek, F., *Chem. Eur. J.* **2000,** *6*, 519-522.

20. Itoh, S.; Kumei, H.; Taki, M.; Nagatomo, S.; Kitagawa, T.; Fukuzumi, S., *J. Am. Chem. Soc.* **2001,** *123*, 6708-6709.

21. Tolman, W. B., *Acc. Chem. Res.* **1997,** *30*, 227-237.

22. Costas, M.; Mehn, M. P.; Jensen, M. P.; Que Jr., L., *Chem. Rev.* **2004,** *104*, 939-986.

23. Abu-Omar, M. M.; Loaiza, A.; Hontzeas, N., *Chem. Rev.* **2005,** *105*, 2227-2252.

24. Solomon, E. I.; Brunold, T. C.; Davis, M. I.; Kemsley, J. N.; Lee, S.-K.; Lehnert, N.; Neese, F.; Skulan, A. J.; Yang, Y.-S.; Zhou, J., *Chem. Rev.* **2000,** *100*, 235-349.

25. Krebs, C.; Fujimori, D. G.; Walsh, C. T.; Bollinger, J. M., Jr., *Acc. Chem. Res.* **2007,** *40*, 484-492.

26. Company, A.; Gómez, L.; Fontrodona, X.; Ribas, X.; Costas, M., *Chem. Eur. J.* **2008,** *14*, 5727-5731.

27. Chen, K.; Costas, M.; Kim, J.; Tipton, A. K.; Que, L., Jr., *J. Am. Chem. Soc.* **2002,** *124*, 3026-3035.

28. Bassan, A.; Blomerg, M. R. A.; Siegbahn, P. E. M.; Que, L., Jr., *Angew. Chem. Int. Ed.* **2005,** *44*, 2939-2941.

29. Bautz, J.; Comba, P.; Lopez de Laorden, C.; Menzel, M.; Rajaraman, G., *Angew. Chem. Int. Ed.* **2007,** *46*, 8067-8070.

30. Chen, K.; Que, L., Jr., *J. Am. Chem. Soc.* **2001,** *123*, 6327-6337.

31. Thallaj, N. K.; Rotthaus, O.; Benhamou, L.; Humbert, N.; Elhabiri, M.; Lachkar, M.; Welter, R.; Albrecht-Gary, A.-M.; Mandon, D., *Chem. Eur. J.* **2008,** *14*, 6742-6753.

32. Gómez, L. Master thesis: Stereoselective hydrocarbon oxidation at a new family of chiral iron and manganese catalysts with well-defined chiral topology. Universitat de Girona, 2007.

33. Costas, M.; Que, J., L., *Angew Chem. Int. Ed. Engl.* **2002,** *12*, 2179-2181.

34. Bernadou, J.; Meunier, B., *Chem. Commun.* **1998,** 2167-2173.

35. Galonic, D. P.; Barr, E. W.; Walsh, C. T.; Bollinger, J. M.; Krebs, C., *Nat. Chem. Biol.* **2007,** *3*, 113-116.

36. Goto, Y.; Matsui, T.; Ozaki, S.-i.; Watanabe, Y.; Fukuzumi, S., *J. Am. Chem. Soc.* **1999,** *121*, 9497-9502.

37. Ogliaro, F.; de Visser, S. P.; Cohen, S.; Sharma, P. K.; Shaik, S., *J. Am. Chem. Soc.* **2002,** *124*, 2806-2817.

38. Quiñonero, D.; Morokuma, K.; Musaev, D. G.; Mas-Ballesté, R.; Que, L., Jr., *J. Am. Chem. Soc.* **2005,** *127*, 6548-6549.

39. Nam, W., *Acc. Chem. Res.* **2007,** *40*, 522-531.

40. Rohde, J.-H.; Stubna, A.; Bominaar, E.; Münck, E.; Nam, W.; Que, L. J., *Inorg. Chem.* **2006,** *45*, 6435-6445.

Chapter VI

Conclusions

VI. Conclusions

This PhD thesis has been devoted to create synthetic models for O_2-processing metallopenzymes. The thesis is divided in two blocks.

In the first block new tricoordinate dicopper(I) complexes have been designed as models of dinuclear O_2 activating copper proteins. Results presented in this block highlight the importance of synergistic effects in O_2 activation by two copper(I) centers. The complexes prepared have different degree of rigidity but they posses copper(I) centers with an almost identical coordination environment. Their corresponding reaction rates for reaction with O_2 are dramatically different. We conclude that their marked different reactivity towards O_2-activation/reduction is not dictated by the electronic or steric properties of a single site, but instead by the ability of two metal ions to act cooperatively. Thus, the synergic interplay of the two copper ions allows to overcome the disfavored single-electron reduction of the O_2 molecule by a single copper site. Results are reminiscent with the recent observation that the active site of tyrosinase accommodates important changes in the Cu···Cu distance during the catalytic cycle, suggesting that cooperation between the two copper sites is needed to achieve O_2 activation at this site.

$Cu^{III}_2(\mu\text{-}O)_2$ species are formed in the reaction of our dicopper complexes and O_2, and the present work also demonstrate that they are capable of performing a biologically relevant transformation: the *ortho*-hydroxylation of phenolates to give catechols. This reaction occurs through the formation of a phenolate adduct of the bis(μ-oxo) core and posterior electrophilic attack on the aromatic ring. These results unambiguously indicate that, despite not being detected in biological systems, the bis(μ-oxo) core is competent for performing the *ortho*-hydroxylation of phenols. The main peculiarity of the system reported here is that exclusive formation of a bis(μ-oxo)dicopper(III) species is observed, before and after phenolate binding to the Cu_2O_2 site. This observation may be relevant to the mechanism of action of tyrosinase.

In the second block of this thesis a new family of mononuclear non-heme iron(II) complexes has been prepared as models for O_2-activating non-heme iron enzymes. The iron complexes contain an oxidatively robust tetradentate ligand (N_4) based on a triazacyclonane ring derivatized with a methylpyridine arm, so that two *cis* labile positions are available for interaction with exogenous ligands.

These complexes are functional models of the family of Rieske dioxygenases. They catalyze the stereospecific hydroxylation of alkanes using H_2O_2 as the oxidant, with excellent efficiencies. The catalytic epoxidation and *cis*-dihydroxylation of olefins is successfully achieved with remarkable efficiencies, and the diol:epoxide ratio obtained is highly dependent on the structure of the specific catalyst. Mechanistic probes clearly point towards the mediation of highly selective metal centered species with relevance to the active species involved in non-heme iron enzymes.

The detailed study of alkane hydroxylation and alkene oxidation performed by means of isotopic labeling studies provides strong support for the proposal that reactions occur through the mediation of $N_4Fe^V(O)(OH)$ species formed by water-assisted lysis of a N_4Fe^{III}-OOH precursor. On one hand, in alkane hydroxylation the reaction is initiated by hydrogen-atom abstraction by the high valent $N_4Fe^V(O)(OH)$ species. Following this event, the incipient alkyl radical can rebound with any of the two hydroxyl ligands of the newly formed $N_4Fe^{IV}(OH)_2$ species. Steric interactions between the α position of the pyridine ring and the carbon centered radical determine the relative energies of the trajectories of the two rebound steps. As a result, the α position of the pyridine ring determines the level of oxygen from water that ends up into the oxidized products. On the other hand, for olefin epoxidation and *cis*-dihydroxylation labeling studies strongly suggest the implication of two non-equivalent isomers of the $N_4Fe^V(O)(OH)$ species. These new mechanistic considerations are unprecedented and they give a new twist to the mechanistic landscape of non-heme systems. Thus, the presence of two labile sites in a *cis* configuration in non-heme systems is more than just a structural feature but also an important point to give a markedly different reactivity in comparison to heme enzymes.

The ability of Fe^{III}-OOH species to perform substrate oxidation is a matter of debate. In the systems studied here it is detected that an oxidant precedent to the $Fe^V(O)(OH)$ cannot oxidize alkanes and olefins but it is competent for sulfide oxidation. We formulate the new oxidant as a N_4Fe^{III}-OOH species. This observation contrasts with heme systems in which it has been demonstrated that the Fe^{III}-OOH intermediate (the so called Compound 0) is not competent as an oxidant because O-O breakage is much faster than substrate oxidation. Again, a new interesting difference between heme and non-heme enzymes arises.

The involvement of iron(IV)-oxo species in several non-heme iron oxygenases has been demonstrated over the last five years. In this work we have synthesized a novel iron(IV)-oxo species which, analogously to natural systems, is capable of exchanging its oxo group with water. Moreover, it is competent to perform biologically relevant transformations such as hydrogen-atom abstraction of C-H bonds and oxygen-atom transfer to sulfides. Finally, reaction of the iron(IV)-oxo species with anionic ligands (X) such as halides has allowed preparation of $N_4Fe^{IV}(O)(X)$ species where the oxo group and the X ligand are in a relative *cis*- position. These new species are synthetic models for the active species operating in α-ketoglutarate-dependent oxygenases and halogenases.

Appendix

Appendix I. Synthesis of Pytacn ligands

This Annex corresponds to the experimental section for the preparation of the ligands reported in this thesis.

1. Synthetic routes used to prepare Pytacn ligands

Scheme 1. Schematic representation of the ligands synthesized.

R = iPr	R' = H	R'' = H	**Py(iPr)₂tacn**
R = iPr	R' = Me	R'' = H	**6Me-Py(iPr)₂tacn**
R = Me	R' = H	R'' = H	**PyMe₂tacn**
R = Me	R' = Me	R'' = H	**6Me-PyMe₂tacn**
R = Me	R' = F	R'' = H	**6F-PyMe₂tacn**
R = Me	R' = H	R'' = Me	**4Me-PyMe₂tacn**
R = Me	R' = Me	R'' = Me	**4,6Me₂-PyMe₂tacn**

pinene-PyMe₂tacn
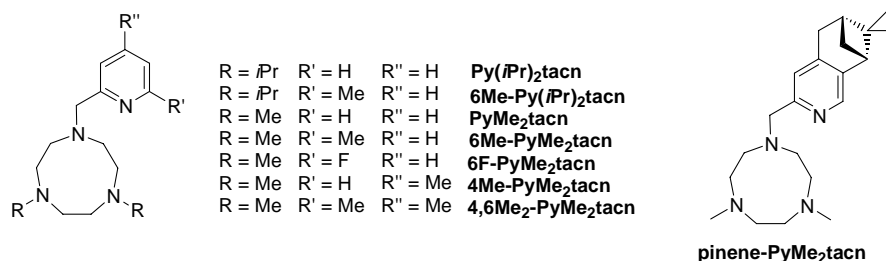
Scheme 2. Schematic representation of the synthetic route for the preparation of Pytacn ligands.
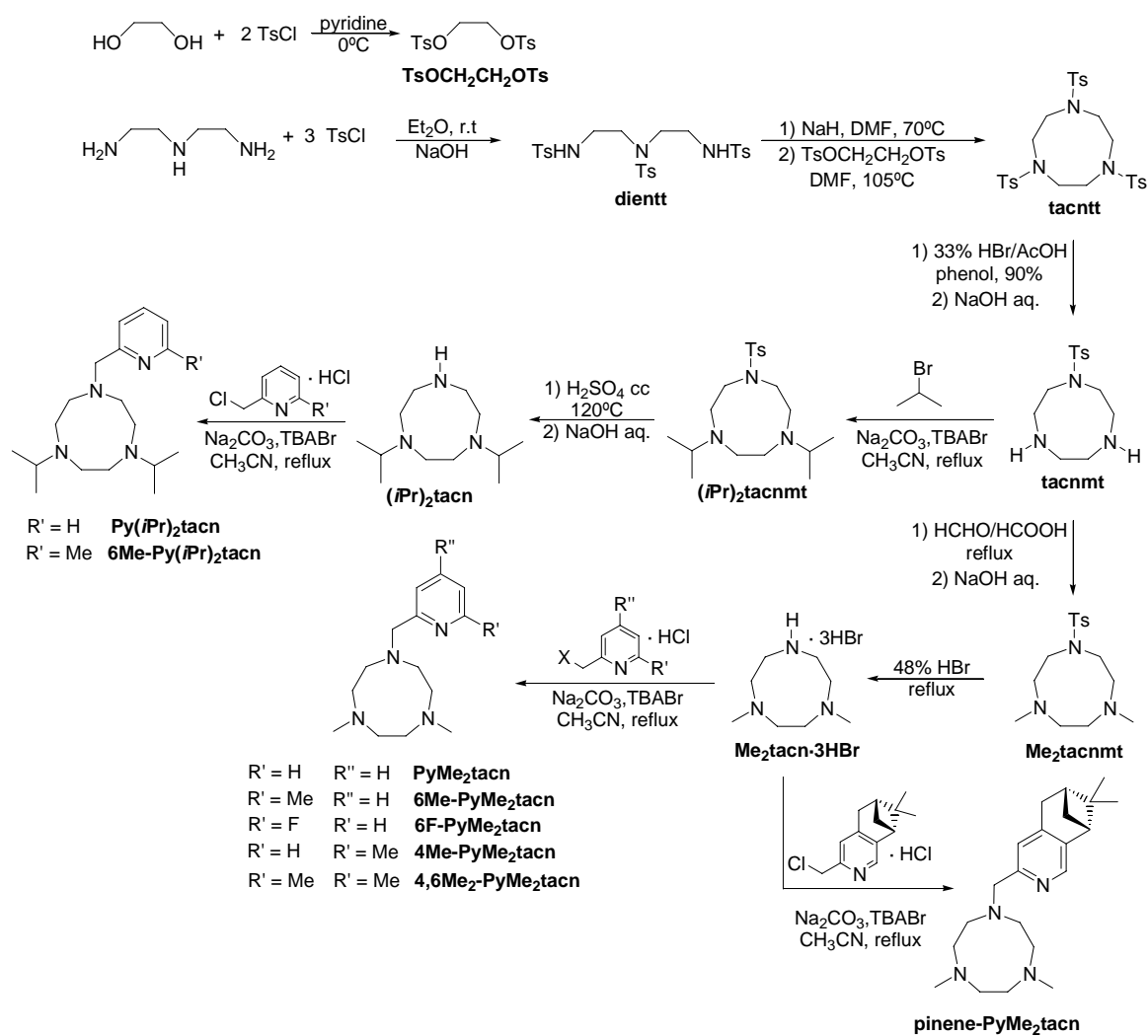
2. Synthesis of pyridine synthons

Synthesis of 2-chloromethyl-6-methylpyridine hydrochloride, 6Me-PyCH₂Cl
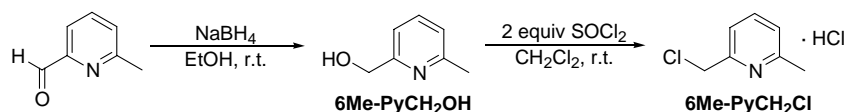
6-Methyl-2-pyridinemethanol, 6Me-Py-alcohol. 6-Methyl-2-pyridine-carboxaldehyde (1.52 g, 12.5 mmols) was dissolved in absolute ethanol (30 mL) and NaBH$_4$ (1 g, 25 mmols) was directly added as a solid in little portions. The mixture was stirred for 4 hours at room temperature and then 10 mL of water were cautiously added in order to destroy the unreacted NaBH$_4$. After 10 minutes of stirring the solvent was removed under reduced pressure and 10 mL of water were added to the resulting white residue. The mixture was extracted with 3 x 20 mL CH$_2$Cl$_2$, the combined organic phases were dried with anhydrous MgSO$_4$ and the solvent was removed under reduced pressure to yield 1.44 g of the desired product (11.7 mmols, 93 %). ^{1}H-NMR (CDCl$_3$, 200 MHz, 300K) δ, ppm: 7.56 (t, J = 7.6 Hz, 1H, py-**H**$_\gamma$), 7.07 – 7.02 (m, 2H, py-**H**$_\beta$), 4.72 (s, 2H, py-**CH$_2$**), 4.04 (br.s, 1H, O**H**), 2.55 (s, 3H, **CH$_3$**).

2-Chloromethyl-6-methylpyridine hydrochloride, 6Me-PyCH₂Cl. 6Me-PyCH$_2$OH (1.44 g, 11.7 mmols) was dissolved in CH$_2$Cl$_2$ (20 mL). SOCl$_2$ (1.7 mL, 23.3 mmols) was cautiously added dropwise and the mixture was stirred overnight at room temperature. The solvent was removed by bubbling N$_2$ into the crude mixture (gaseous HCl is formed during this process and extreme caution must be taken) and a white solid was obtained. This product was suspended in 20 mL of diethyl ether and stirred for one hour to give a fine solid which was then filtered, washed with 2 x 10 mL of diethyl ether and dried under vacuum. 1.94 g of a white solid were obtained (10.9 mmols, 93 %). FT-IR (ATR) ν, cm^{-1}: 1635, 1402 (py). ^{1}H-NMR (CDCl$_3$, 200 MHz, 300K) δ, ppm: 8.33 (t, J = 7.8 Hz, 1H, py-**H**$_\gamma$), 7.91 (d, J = 7.8 Hz, 1H, py-**H**$_\beta$), 7.66 (d, J = 7.8 Hz, 1H, py-**H**$_\beta$), 5.28 (s, 2H, py-**CH$_2$**), 3.03 (s, 3H, **CH$_3$**). ^{13}C-NMR (CDCl$_3$, 50 MHz, 300K) δ, ppm: 154.48, 151.78 (py**C**$_q$), 145.44 (py**C**$_\gamma$), 126.87, 124.15 (py**C**$_\beta$), 39.35 (py-**CH$_2$**-Cl), 19.45 (py-**CH$_3$**).

Synthesis of 2-fluoro-6-bromomethylpyridine, 6F-PyCH₂Br
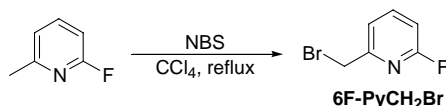
2-Fluoro-6-bromomethylpyridine, 6F-PyCH₂Br. Commercially available 2-fluoro-6-bromomethyl (2.00 g, 18.0 mmols) was dissolved in CCl$_4$ (80 mL). NBS (3.6 g, 20.2 mmols) was directly as a solid, and the medium was refluxed for 6 h in the presence of benzoyl peroxide (120 mg). The solvent was then evaporated and a white solid together with a yellow oil was obtained. This residue was treated with 10 mL of a 1:1 CH$_2$Cl$_2$:hexane and filtered off to remove the white solid. The resulting yellow solution was taken to dryness and the resultant yellow oil was purified by means of chromatography on silica gel using CH$_2$Cl$_2$:hexane 1:1 as the eluent. The desired product was

collected as the second fraction. Evaporation of solvent yielded 1.08 g (5.7 mmols, 32 %) ^{1}H-NMR (CDCl$_3$, 200 MHz, 300K) δ, ppm: 7.80 (dd, J = 7.6 Hz, J = 8.0 Hz, 1H, py-**H**$_\gamma$), 7.33 (dd, J = 7.4 Hz, J = 2.2 Hz, 1H, py-**H**$_\beta$), 6.87 (dd, J = 8.2 Hz, J = 2.8 Hz , 1H, py-**H**$_\beta$), 4.47 (s, 2H, py-**CH$_2$**-Br). ^{13}C-NMR (CDCl$_3$, 50 MHz, 300K) δ, ppm: 162.86 (d, J^{CF} = 239.5 Hz, py**C**$_q$-F), 155.53 (d, J^{CF} = 13.1 Hz, py**C**$_q$-CH$_2$-Br), 141.99 (d, J^{CF} = 7.7 Hz, py**C**$_\gamma$), 120.63 (d, J^{CF} = 4.2 Hz, py**C**$_\beta$), 109.05 (d, J^{CF} = 36.4 Hz, py**C**$_\beta$), 32.23 (py-**C**H$_2$-Br).

Synthesis of (*R*)-4,5-Pineno-2-picolylchloride hydrochloride, pinene-PyCH$_2$Cl

pinene-PyCH$_2$OH   **pinene-PyCH$_2$Cl**
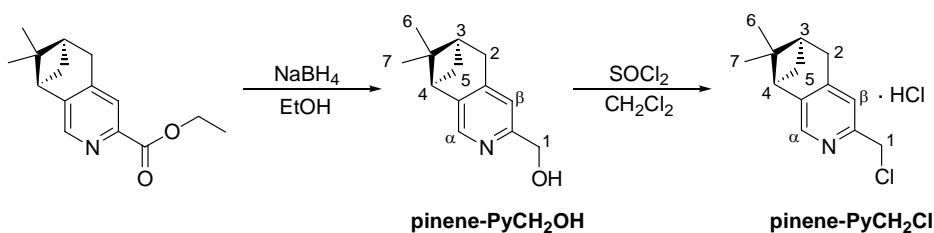
(*R*)-4,5-Pineno-2-picolylalcohol, pinene-PyCH$_2$OH. (*R*)-4,5-pineno-2-picolyl ethyl ester (3.65 g, 14.9 mmols) was dissolved in absolute ethanol (60 mL). NaBH$_4$ (2.15 g, 50.7 mmols) was added as a solid and the solution was placed under N$_2$ and refluxed for 3h. The reaction mixture was then cooled to room temperature and H$_2$O (10 mL) and HCl 2M (10 mL) were added. The mixture was stirred for 10 min and it was basified to pH = 14 with a concentrated NaOH solution (12 M). The mixture was extracted with CHCl$_3$ (3 x 100 mL). The organic phases were combined and washed with H$_2$O (100 mL), dried over MgSO$_4$ and filtered. The solvent was removed under reduced pressure to obtain the alcohol as a dark brown oil that was directly used for the next step. ^{1}H-NMR (CDCl$_3$, 200 MHz, 300K) δ, ppm: 8.10 (s, 1H, py-**H**$_\alpha$), 7.06 (s, 1H, py-**H**$_\beta$), 4.73 (s, 2H, **H**$_1$), 2.99 (d, J = 2.2 Hz, 2H, **H**$_2$), 2.83 (m, 1H, **H**$_4$), 2.71 (m, 1H, **H**$_{11}$ exo), 2.33 (m, 1H, **H**$_3$), 1.44 (s, 3H, **H**$_6$), 1.23 (d, J = 9.4 Hz, 1H, **H**$_{11}$ endo), 0.65 (s, 3H, **H**$_7$). ^{13}C-NMR (CDCl$_3$, 50 MHz, 300K) δ, ppm: 156.85, 145.44, 144.44, 141.29, 119.81, 64.11, 44.34, 39.97, 39.16, 32.71, 31.82, 25.92, 21.30.

(*R*)-4,5-pineno-2-picolylchloride hydrochloride, pinene-PyCH$_2$Cl. Pinene-PyCH$_2$OH (2.8 g, 13.8 mmol) was dissolved in anhydrous CH$_2$Cl$_2$ (60 mL). Thionyl chloride (10 mL, 135.7 mmols) dissolved in CH$_2$Cl$_2$ (10 mL) was added dropwise and the resulting mixture was stirred overnight. The solvent was removed under a stream of N$_2$. The residue was washed with ether (100 mL) and then dissolved in ethanol (60 mL) and stirred for 24 hours. The solvent was removed under vacuum to afford a dark brown oil that crystallized upon standing in the fridge. The product was used in the next step without additional purification (3.5 g, 13.6 mmols, 98 %). ^{1}H-NMR (CDCl$_3$, 200 MHz, 300K) δ, ppm: 8.24 (s, 1H, py-**H**$_\alpha$), 7.79 (s, 1H, py-**H**$_\beta$), 5.11 (s, 2H, **H**$_1$), 3.23 (d, J = 2.2 Hz, 2H, **H**$_2$), 3.04 (m, 1H, **H**$_4$), 2.82 (m, 1H, **H**$_5$ exo), 2.41 (m, 1H, **H**$_3$), 1.44 (s, 3H, **H**$_6$), 1.21 (d, J = 9.4 Hz, 1H, **H**$_5$ endo), 0.62 (s, 3H, **H**$_7$). ^{13}C-NMR (CDCl$_3$, 50 MHz, 300K) δ, ppm: 157.90, 149.03, 146.47, 135.46, 125.8, 44.30, 39.58, 39.03, 38.82, 34.21, 30.90, 25.29, 21.38.

Synthesis of 2-chloromethyl-4-methylpyridine hydrochloride, 4Me-PyCH$_2$Cl
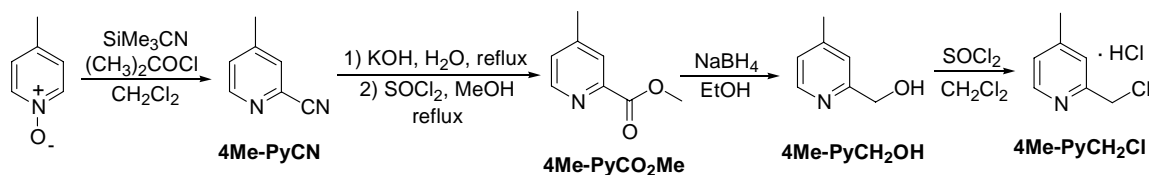
4-Methyl-pyridine-2-carbonitrile, 4Me-PyCN. 4-methylpyridine-N-oxide (7 g, 64 mmols) was placed in a round bottom flask, dissolved in dry dichloromethane (50 mL), and placed under a N$_2$ atmosphere. Trimethylsilyl cyanide (10.26 mL, 7.7 g, 77 mmols) was added dropwise. After 30 minutes, dimethyl carbamoyl chloride (7.1 mL, 8.22 g, 77 mmols) was added dropwise. The resulting mixture was stirred overnight. At this point, the reaction was quenched by addition of saturated aqueous NaHCO$_3$ (30 mL), and the organic fraction was extracted with dichloromethane (2 x 50 mL). The combined organic layers were washed with H$_2$O (50 mL), saturated aqueous NaHCO$_3$ (50 mL) and H$_2$SO$_4$ 1M (50 mL). The resulting organic fraction was dried over MgSO$_4$ and filtered and the solvent was removed under reduced pressure to yield the desired product as a white solid (6.7 g, 57 mmols, 89%). FT-IR (ATR) ν, cm^{-1}: 3505, 3049, 2233 (CN), 1598, 1506, 1408, 838. ^{1}H-NMR (CDCl$_3$, 200 MHz, 300K) δ, ppm: 8.58 (d, J = 5 Hz, 1H, py-**H**$_\alpha$), 7.53 (m, 1H, py-**H**$_\beta$), 7.33 (m, 1H, py-**H**$_\beta$), 2.43 (s, C**H**$_3$, 3H).

4-Methyl-pyridine-2-carboxylic acid methyl ester, 4Me-PyCO$_2$Me. Potassium hydroxide (6.4 g, 114 mmols) was placed in a round bottom flask, and dissolved in water (60 mL). 4Me-PyCN (6.7 g, 57 mmols) was then suspended in this solution, and the mixture was refluxed during 1h, at which time a clear yellow-orange solution had formed. The solution was stirred at 40 ºC for two days, and after cooling to room temperature, H$_2$SO$_4$ cc (6.1 mL) diluted in water (20 mL) was carefully added. The solution was then neutralized to pH = 7 by careful addition of saturated aqueous NaHCO$_3$. The white solid that appeared was filtered off. The solvent from the filtrates was removed under reduced pressure and the resulting solid was extracted with AcOEt (2 x 50 mL) and absolute EtOH (2 x 50 mL). The filtrates were dried over MgSO$_4$ and filtered. The solvent was removed under vacuum to obtain 3.26 g of the carboxylic acid product as an oily solid that was used without further purification. The carboxylic acid was dissolved in dry methanol (50 mL), and SOCl$_2$ (4 mL) was added dropwise (caution, reaction is very exothermic). The resulting mixture was then refluxed during 16h. At this time, it was allowed to cool down to room temperature, and the solvent was removed under vacuum. The residue was treated with saturated aqueous NaHCO$_3$ (75 mL), and extracted with dichloromethane (3 x 50 mL). The organic phases were combined, dried over MgSO$_4$, filtered and the solvent was removed under reduced pressure to obtain the product as a pale yellow oil (2.05 g, 13.6 mmol, 24%). ^{1}H-NMR (CDCl$_3$, 200 MHz, 300K) δ, ppm: 8.59 (d, 1H, J = 4.8 Hz, py-**H**$_\alpha$), 7.97 (s broad, 1H, py-**H**$_\beta$), 7.29 (d, J = 4.8 Hz, 1H, py-**H**$_\beta$), 4.01 (s, 3H, CO$_2$C**H**$_3$), 2.44 (s, 3H, py**CH**$_3$).

4-methyl-2-picolylalcohol, 4Me-PyCH$_2$OH. 4Me-PyCO$_2$Me (2.05 g, 13.57 mmols) was placed in a round bottom flask and dissolved in dry methanol (50 mL). The mixture was placed under N$_2$, and NaBH$_4$ (3 g) was carefully added in small portions. The resulting mixture was stirred under N$_2$ at room temperature for 24h. After this time, a second portion of NaBH$_4$ (1 g) was slowly added in small

portions and the mixture was stirred for further 12h at under N_2. 1 M HCl (10 mL) was added and the mixture was stirred for 30 min. The solvent was removed under reduced pressure and the resulting residue was treated with saturated aqueous $NaHCO_3$ (50 mL), and extracted with CH_2Cl_2 (3 x 50 mL). The combined organic layers were dried over $MgSO_4$, filtered and the solvent was removed under reduced pressure to obtain a pale yellow oil. (1.67 g, 13.56 mmols, 99%). ^{1}H-NMR ($CDCl_3$, 200 MHz, 300K) δ, ppm: 8.40 (d, J = 5.0 Hz, 1H, py-H_α), 7.04 (m, 2H, py-H_β), 4.72 (s, 2H, CH_2OH), 2.36 (s, 3H, CH_3).

2-Chloromethyl-4-methylpyridine hydrochloride, 4Me-PyCH$_2$Cl. 4Me-PyCH$_2$OH (1.67 g, 13.6 mmols) was placed in a round bottom flask and dissolved in dry CH_2Cl_2 (25 mL). $SOCl_2$ (4 mL) was added dropwise and the resulting mixture was stirred under N_2 overnight. After that time, methanol (10 mL) was added carefully and the resulting mixture was placed under a stream of N_2 until all solvent evaporated. The oily residue was then treated with diethyl ether (70 mL) which caused the formation of a solid. This compound was filtered and the desired product was obtained as a white-cream solid (1.98 g, 11.12 mmols, 82%). ^{1}H-NMR (D_2O, 200 MHz, 300K) δ, ppm: 8.63 (d, J = 5.8 Hz, 1H, py-H_α), 8.00 (s, 1H, py-H_β), 7.89 (d, J = 5.8 Hz, 1H, py-H_β), 5.00 (s, CH_2Cl, 2H), 2.71 (s, 3H, CH_3). ^{13}C-NMR (D_2O, 50 MHz, 300K) δ, ppm: 162.34 (pyC_α-CH_2Cl), 149.29 (pyC_α-H), 140.68 (pyC_γ-CH_3), 127.69, 127.20 (pyC_β), 40.04 (py-CH_2Cl), 21.65 (py-CH_3).

Synthesis of 2-chloromethyl-4,6-dimethylpyridine hydrochloride, 4,6Me$_2$-PyCH$_2$Cl
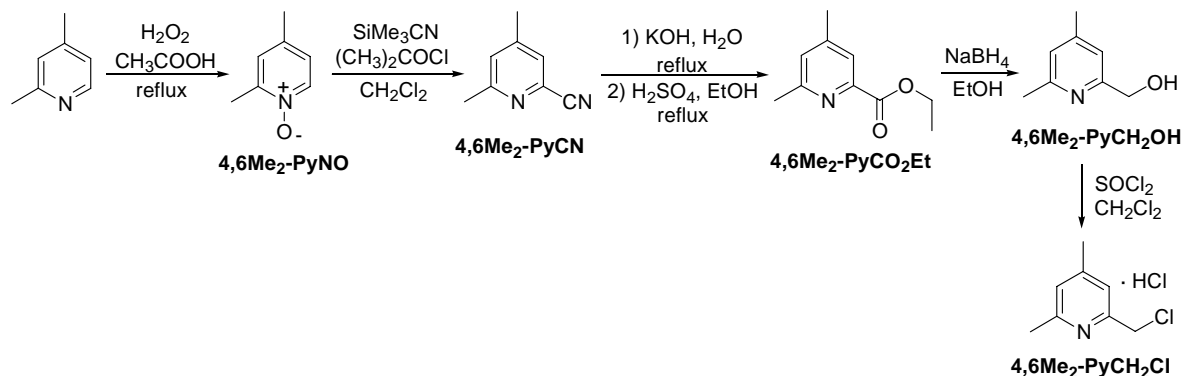
2,4-dimethylpyridine-N-oxide, 4,6Me$_2$-PyNO. 2,4-Lutidine (30 g, 0.28 mols) was placed in a 250 mL round flask, and acetic acid (100 mL) was carefully added. H_2O_2 30% (30 mL) was carefully added to the mixture which was refluxed for 12h. After this time, a second portion of H_2O_2 30% (30 mL) was added and the mixture was further refluxed for additional 12h. After this time, the acetic acid was removed under reduced pressure. $CHCl_3$ (100 mL) and Na_2CO_3 (5 g) were added over the mixture which was stirred for an hour to destroy any remaining peroxide. The solvent was removed under reduced pressure and the remaining residue was distilled under vacuum. After initial distillation of residual acetic acid and lutidine, the desired product was collected as the fraction that distilled at 149-151 ºC as a pale yellow oil (24.9 g, 0.20 mols, 71%). ^{1}H-NMR ($CDCl_3$, 200 MHz, 298K) δ, ppm: 7.99 (d, J = 6.6 Hz, 1H, py-H_α), 6.92 (s, 1H, py-H_β), 6.80 (dd, J = 6.6 Hz, J = 2.2 Hz, 1H, py-H_β), 2.34 (s, 3H,

CH$_3$), 2.17 (s, 3H, CH$_3$). ^{13}C-NMR (CDCl$_3$, 50 MHz, 298K) δ, ppm: 147.91, 138.40, 136.74 (py**C**$_q$ and py**C**$_\gamma$), 126.89, 124.07 (py**C**$_\beta$), 19.91, 14.41 (py-**CH**$_3$).

4,6-dimethyl-pyridine-2-carbonitrile, 4,6Me$_2$-PyCN. 4,6Me$_2$-PyNO (7 g, 56.8 mmols) was placed in a round bottom flask, dissolved in dry dichloromethane (75 mL), and placed under a N$_2$ atmosphere. Trimethylsilyl cyanide (7.56 mL, 5.62 g, 56.7 mmols) was added dropwise. After 15 minutes, dimethyl carbamoyl chloride (5.22 mL, 6.1 g, 56.7 mmol) was carefully added and the resulting mixture was stirred overnight. At this point, the reaction was quenched by addition of saturated aqueous NaHCO$_3$, and the organic fraction extracted with dichloromethane (2 x 50 mL). The organic phase was then washed with saturated aqueous NaHCO$_3$ (50 mL) and H$_2$SO$_4$ 1M (50 mL). Finally, it was dried over MgSO$_4$ and filtered and the solvent was removed under reduced pressure to yield the product as a white solid (5.6 g, 42.4 mmol, 75%). ^{1}H-NMR (CDCl$_3$, 200 MHz, 298K) δ, ppm: 7.34 (s, 1H, py-**H**$_\beta$), 7.20 (s, 1H, py-**H**$_\beta$), 2.56 (s, 3H, CH$_3$), 2.38 (s, 3H, CH$_3$). ^{13}C-NMR (CDCl$_3$, 50 MHz, 298K) δ, ppm: 160.23 (py**C**$_\alpha$-CH$_3$), 148.61 (py**C**$_\gamma$-CH$_3$), 132.98 (py**C**$_\alpha$-CN), 127.63, 126.63 (py**C**$_\beta$), 117.51 (py**C**N), 24.11, 20.67 (py-**CH**$_3$).

4,6-Dimethyl-pyridine-2-carboxylic acid ethyl ester, 4,6Me$_2$-PyCO$_2$Et. Potassium hydroxide (5 g, 89 mmols) was placed in a round bottom flask, and dissolved in water (100 mL). 4,6Me$_2$-PyCN (5.6 g, 42.4 mmol) was then suspended in this solution, and the mixture was refluxed during 4h, at which time a clear yellow-orange solution had formed. The solution was cooled down to room temperature and acidified with a mixture of H$_2$SO$_4$ cc (5 mL) diluted in water (20 mL). The solvent was removed under vacuum, and the residue was taken in absolute ethanol (80 mL). H$_2$SO$_4$ cc (20 mL) was then carefully added (caution, the solution becomes very hot) and the resulting suspension was refluxed during 16h. After that time, it was allowed to cool down to room temperature and it was dropped over hexanes (200 mL). The aqueous phase was taken to basic pH with a saturated aqueous solution of Na$_2$CO$_3$, and the organic phase collected. The aqueous layer was further extracted with hexanes (2 x 100 mL). The combined organic fractions were dried over MgSO$_4$, filtered and the solvent was removed under reduced pressure to obtain the product as a pale yellow oil (4.1 g, 22.88 mmols, 54%). ^{1}H-NMR (CDCl$_3$, 200 MHz, 298K) δ, ppm: 7.63 (s, 1H, py-**H**$_\beta$), 7.15 (s, 1H, py-**H**$_\beta$), 4.45 (q, J = 7.2 Hz, 2H, C**H$_2$**CH$_3$), 2.61 (s, 3H, CH$_3$), 2.38 (s, 3H, CH$_3$), 1.43 (t, J = 7.2 Hz, 3H, CH$_2$**CH$_3$**). ^{13}C-NMR (CDCl$_3$, 50 MHz, 298K) δ, ppm: 165.64 (**C**=O), 158.72 (py**C**$_\alpha$-CH$_3$), 148.24 (py**C**$_\gamma$-CH$_3$), 147.67 (py**C**$_\alpha$-CO$_2$Et), 127.41, 123.33 (py**C**$_\beta$), 61.74 (**C**H$_2$CH$_3$), 24.39, 20.80 (py-**CH**$_3$), 14.27 (CH$_2$**CH**$_3$).

4,6-dimethyl-2-picolylalcohol, 4,6Me$_2$-PyCH$_2$OH. 4,6Me$_2$-PyCO$_2$Et (4.1 g, 22.9 mmols) was placed in a round bottom flask and dissolved in absolute ethanol (80 mL) and NaBH$_4$ (5 g) was slowly added in small portions. The resulting mixture was stirred under N$_2$ at room temperature for two days. After this time, HCl cc (1 mL) was added and the mixture was stirred for 1 h. The solvent was removed under reduced pressure and the resulting residue was treated with saturated aqueous NaHCO$_3$ (50 mL), and extracted with CH$_2$Cl$_2$ (3 x 50 mL). The organic layers were combined, dried over MgSO$_4$, filtered and the solvent was removed under vacuum to obtain a pale yellow old that solidified upon applying vacuum (2.86 g, 20.8 mmol, 91%). ^{1}H-NMR (CDCl$_3$, 200 MHz, 298K) δ, ppm: 6.87 (s broad, 2H, py-**H**$_\beta$), 4.67 (s, 2H, C**H$_2$**OH), 3.27 (s broad, 1H, O**H**), 2.50 (s, 3H, CH$_3$), 2.31 (s, 3H, CH$_3$). ^{13}C-

NMR (CDCl$_3$, 50 MHz, 298K) δ, ppm: 158.11 (py**C**$_\alpha$-CH$_3$), 157.01 (py**C**$_\alpha$-CH$_2$OH), 148.15 (py**C**$_\gamma$-CH$_3$), 122.82, 118.41 (py**C**$_\beta$), 63.91 (**C**H$_2$OH), 23.84, 20.85 (py-**C**H$_3$).

2-Chloromehtyl-4,6-dimethylpyridine hydrochloride, 4,6Me$_2$-PyCH$_2$Cl. 4,6Me$_2$-PyCH$_2$OH (2.85 g, 20.8 mmols) was placed in a round bottom flask and dissolved in dry CH$_2$Cl$_2$ (50 mL). SOCl$_2$ (5 mL) was added dropwise and the resulting mixture was stirred under N$_2$ overnight. After that time, methanol (15 mL) was carefully added and the resulting mixture was placed under a stream of N$_2$ until all the solvent evaporated. The oily residue was then taken in diethyl ether (100 mL) and stirred which gave suspend solid. This product was filtered and the product was isolated as a white-cream solid (3.90 g, 20.3 mmol, 98%). ^{1}H-NMR (D$_2$O, 200 MHz, 298K) δ, ppm: 7.76 (s, 1H, py-**H**$_\beta$), 7.67 (s, 1H, py-**H**$_\beta$), 4.90 (s, 2H, py**C**H$_2$Cl), 2.74 (s, 3H, **C**H$_3$), 2.61 (s, 3H, **C**H$_3$). ^{13}C-NMR (D$_2$O, 50 MHz, 298K) δ, ppm: 161.49, 153.72 (py**C**$_\alpha$), 148.48 (py**C**$_\gamma$-CH$_3$), 127.72, 125.12 (py**C**$_\beta$), 39.82 (py-**C**H$_2$Cl), 21.38, 18.63 (py-**C**H$_3$).

3. Synthesis of 1-(*p*-toluensulfonyl)-1,4,7-triazacyclononane, tacnmt
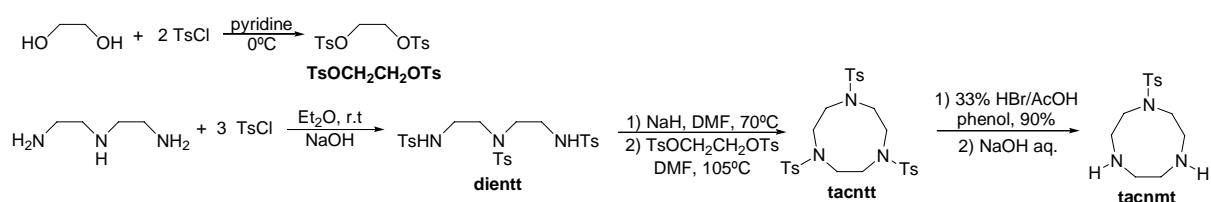
N,N',N''-tris(*p*-toluensulfonyl)diethylentriamine, dientt. A solution of *p*-toluenesulfonyl chloride (120 g, 0.63 mols) in diethyl ether (600 mL) was added dropwise to a stirred solution of diethylenetriamine (20.7 g, 0.20 mols) and NaOH (24 g, 0.60 mols) in water (200 mL). After sitrring for 2 hours at room temperature methanol was added and a white fine precipitate appeared. The product was filtered and washed with water and methanol. Finally the white solid was dried under vacuum to obtain 62.64 g of the desired product (0.11 mols, 55 %). Anal. Calcd for C$_{25}$H$_{31}$O$_6$N$_3$S$_3$ (MW = 565.73 g/mol): C, 53.08; H, 5.52; N, 7.43; S, 17.00 %. Found: C, 52.93; H, 5.53; N, 7.34; S, 16.68 %. FT-IR (ATR) ν, cm^{-1}: 3286 (N-H), 1322, 1154 (R-SO$_2$-N). ^{1}H-NMR (CDCl$_3$, 200 MHz, 300K) δ, ppm: 7.80 (d, J = 8.4 Hz, 4H, Ar**H**), 7.65 (d, J = 8.4 Hz, 2H, Ar**H**), 7.37 – 7.32 (m, 6H, Ar**H**), 5.19 (br s, 2H, N**H**), 3.23 – 3.16 (m, 8H, N-C**H$_2$**-C**H$_2$**-N), 2.47 (s, 9H, Ar-C**H$_3$**). ^{13}C-NMR (CDCl$_3$, 50 MHz, 300K) δ, ppm: 144.16, 143.59 (**ar C**-CH$_3$), 136.63, 134.65 (**ar C**-SO$_2$-), 129.95, 129.78, 127.26, 127.11 (**ar C**-H), 50.82 (C-**C**H$_2$-TsN-**C**H$_2$-C), 42.57 (TsHN-**C**H$_2$-CH$_2$), 21.48 (Ar-**C**H$_3$). ESI-MS (m/z): 565.9 [M+H]$^+$, 411.7 [M-Ts]$^+$, 582.8 [M+NH$_4$]$^+$.

1,2-di(*p*-toluensulfonyloxi)ethane, TsOCH$_2$CH$_2$OTs. Solid *p*-toluenesulfonyl chloride (80 g, 0.42 mols) was added in portions to a stirred solution of ethane-1,2-diol (12.45 g, 0.20 mols) in pyridine (125 mL) at 0ºC (in an ice bath). After leaving at room temperature for 1 day ice was added and the solution was left stirring for about 2 hours. A white precipitated was formed and it is filtered with water, ethanol and diethyl ether and air-dried. The product was recrystallized from hot acetone (125 mL) with the addition of ether (125 mL). 56.03 g of a crystalline white solid were obtained (0.15 mols, 75 %).

Anal. Calcd for $C_{16}H_{18}O_6S_2$ (MW = 370.44 g/mol): C, 51.88; H, 4.90; S, 17.31 %. Found: C, 51.70; H, 4.89; S, 17.20 %. FT-IR (ATR) ν, cm^{-1}: 1357, 1174 (R-SO$_2$-N). ^{1}H-NMR (CDCl$_3$, 200 MHz, 300K) δ, ppm: 7.80 (d, J = 8.2 Hz, 4H, Ar**H**), 7.38 (d, J = 8.2 Hz, 4H, Ar**H**), 4.24 (s, 4H, O-C**H$_2$**-C), 2.50 (s, 6H, Ar-C**H$_3$**). ^{13}C-NMR (CDCl$_3$, 50 MHz, 300K) δ, ppm: 145.21 (**arC**-CH$_3$), 132.36 (**arC**-SO$_2$-), 129.90, 127.92 (arom.), 66.61 (**C**H$_2$O), 21.62 (Ar-**C**H$_3$). ESI-MS (m/z): 370.7 [M+H]$^+$, 198.4 [M-TsOH]$^+$, 387.7 [M+NH$_4$]$^+$.

1,4,7-tri(*p*-toluensulfonyl)-1,4,7-triazacyclononane, tacntt. Sodium hydride (6.7 g of 60% suspension in oil) was added in little portions to a stirred solution of dientt (28.3 g, 0.05 mols) in dry dimethylformamide (550 mL) to form the disodium salt. After main effervescence (due to H$_2$ evolution) the solution was brought to 70ºC, and on cessation of hydrogen evolution the excess NaH was filtered off under an inert atmosphere by means of a cannula. The resulting yellow solution was stirred at 105ºC under an inert atmosphere and a solution of TsOCH$_2$CH$_2$OTs (18.5 g, 0.05 mols) in dry dimethylformamide (200 mL) was added over a period of 2 hours. The solution was stirred at 105ºC for a further 2 hours. After reduction of volume to 200 mL, gradual addition of water (1.5 L) gave a flocculent white precipitate. This was filtered off, washed with water, ethanol and diethyl ether, and dried at 100ºC. Recrystallization from chloroform (60 mL) and gradual addition of ethanol (250 mL) afforded 25.03 g of tacntt as a white crystalline solid (42.3 mmols, 84 %). Anal. Calcd for $C_{27}H_{33}O_6N_3S_3$ (MW = 591.77 g/mol): C, 54.80; H, 5.62; N, 7.10; S, 16.25 %. Found: C, 54.57; H, 5.89; N, 6.74; S, 15.70 %. FT-IR (ATR) ν, cm^{-1}: 2925 (C-H)$_{sp3}$, 1318, 1149 (R-SO$_2$-N). ^{1}H-NMR (CDCl$_3$, 200 MHz, 300K) δ, ppm: 7.70 (d, J = 8.1 Hz, 6H, Ar**H**), 7.32 (d, J = 8.1 Hz, 6H, Ar**H**), 3.42 (s, 12H, N-C**H$_2$**-C), 2.43 (s, 9H, Ar-C**H$_3$**). ^{13}C-NMR (CDCl$_3$, 50 MHz, 300K) δ, ppm: 143.85 (**arC**-CH$_3$), 134.59 (**arC**-SO$_2$-), 129.83, 127.45 (**arC**-H), 51.82 (N-**C**H$_2$-C), 21.46 (Ar-**C**H$_3$). ESI-MS (m/z): 591.9 [M+H]$^+$, 608.9 [M+NH$_4$]$^+$.

1-(*p*-toluensulfonyl)-1,4,7-triazacyclononane, tacnmt. tacntt (24.6 g, 41.6 mmols) and phenol (35.2 g, 374 mmols) were mixed in a 500 mL flask. A solution of HBr in acetic acid (33%, 380 mL) was added with extreme care as an important evolution of HBr$_{(g)}$ takes place. The mixture was gently heated with stirring to 90ºC which caused the complete dissolution of all the starting reactives giving rise to the formation of a dark solution. A colorless precipitate of 1-(*p*-toluensulfonyl)-1,4,7-triazacyclononane·2HBr appeared within 2-4 h. After heating for 36 h, the mixture was cooled to room temperature and filtered. The solid was washed with diethyl ether (125 mL) and then dissolved in aqueous NaOH 1M (320 mL). The resultant pink aqueous mixture was then extracted with CH$_2$Cl$_2$ (3 x 190 mL) and the organic extracts dried with anhydrous MgSO$_4$, filtered and evaporated under reduced pressure. Drying the resultant oil under vacuum afforded 9.88 g of the pure product (34.9 mmols, 84 %). Anal. Calcd for $C_{13}H_{21}O_2N_3S$ (MW = 283.39 g/mol): C, 55.10; H, 7.47; N, 14.83; S, 11.31 %. Found: C, 54.49; H, 7.41; N, 14.71; S, 11.38 %. FT-IR (ATR) ν, cm^{-1}: 3302 (N-H), 2914, 2855 (C-H)$_{sp3}$, 1328, 1152 (R-SO$_2$-N). ^{1}H-NMR (CDCl$_3$, 200 MHz, 300K) δ, ppm: 7.70 (d, J = 8.2 Hz, 2H, Ar**H**), 7.34 (d, J = 8.2 Hz, 2H, Ar**H**), 3.23 - 3.18 (m, 4H, TsN-C**H$_2$**-CH$_2$-NH), 3.12 - 3.09 (m, 4H, TsN-CH$_2$-C**H$_2$**-NH), 2.90 (s, 4H, HN-C**H$_2$**-C**H$_2$**-NH), 2.44 (s, 3H, Ar-C**H$_3$**), 1.85 (s, 2H, N**H**). ^{13}C-NMR (CDCl$_3$, 50 MHz, 300K) δ, ppm: 143.16 (**arC**-CH$_3$), 135.60 (**arC**-SO$_2$-), 129.59, 127.16 (**arC**-H), 53.91 (TsN-**C**H$_2$-C), 49.63, 49.46 (**C**H$_2$-NH-**C**H$_2$), 21.41 (Ar-**C**H$_3$). ESI-MS (m/z): 283.7 [M+H]$^+$.

4. Synthesis of 1,4-diisopropyl-1,4,7-triazacyclononane, (*i*Pr)₂tacn.

tacnmt   (*i*Pr)₂tacnmt   (*i*Pr)₂tacn
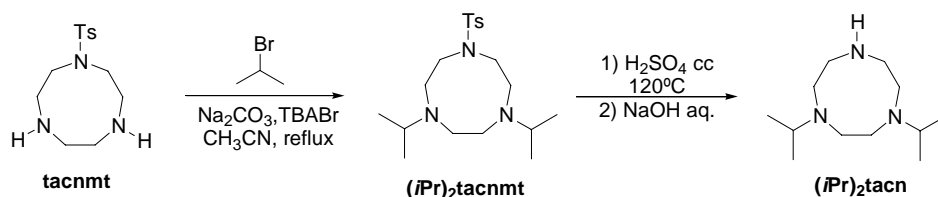
1,4-diisopropyl-7-(p-toluensulfonyl)-1,4,7-triazacyclononane, (*i*Pr)₂tacnmt. tacnmt (9.78 g, 34.5 mmols), 2-bromopropane (26.10 mL, 276.2 mmols) and anhydrous acetonitrile (50 mL) were mixed in a 100 mL flask. Na_2CO_3 (14.57 g) and tetrabutylammonium bromide, TBABr (0.08 g) were added directly as solids and the resulting mixture was heated at reflux under N_2 for 18 hours. After cooling to room temperature, the yellow mixture was filtered and the filter cake was washed with CH_2Cl_2. The combined filtrates were evaporated under reduced pressure to yield a pale-brown oil with a small amount of a white solid. This residue was redissolved in CH_2Cl_2 (25 mL) and then washed with 1M NaOH (25 mL). The organic layer was removed and the aqueous phase was extracted with CH_2Cl_2 (3 x 10 mL). The combined organic layers were dried over anhydrous $MgSO_4$ and the solvent was removed under reduced pressure to yield 12.33 g of a pale brown-solid (33.5 mmols, 97 %). Anal. Calcd for $C_{19}H_{33}O_2N_3S$ (MW = 367.55 g/mol): C, 62.09; H, 9.05; N, 11.43; S, 8.72 %. Found: C, 61.96; H, 9.63; N, 11.18; S, 7.99 %. FT-IR (ATR) ν, cm^{-1}: 2962 – 2814 (C-H)$_{sp3}$, 1335,1156 (R-SO$_2$-N). ^{1}H-NMR (CDCl$_3$, 200 MHz, 300K) δ, ppm: 7.68 (d, J = 8.0 Hz, 2H, Ar**H**), 7.28 (d, J = 8.0 Hz, 2H, Ar**H**), 3.32-3.28 (m, 4H, TsN-C**H₂**-CH₂-N), 2.88-2.84 (m, 4H, TsN-CH₂-C**H₂**-N), 2.78 (heptet, J = 6.6 Hz, 2H, N-C**H**-(CH₃)₂), 2.46 (s, 4H, N-C**H₂**-C**H₂**-N), 2.41 (s, 3H, Ar-C**H₃**), 0.93 (d, J = 6.6 Hz, 12H, CH-(C**H₃**)₂). ^{13}C-NMR (CDCl$_3$, 50 MHz, 300K) δ, ppm: 142.59 (**ar**C-CH₃), 136.63 (**ar**C-SO₂-), 129.42, 127.11 (arom.), 53.65 (TsN-**C**H₂-C + N-**C**H-(CH₃)₂), 52.30, 50.32 (iPrN-**C**H₂-C), 21.39 (Ar-**C**H₃), 18.23 (CH-(**C**H₃)₂). ESI-MS (m/z): 367.7 [M+H]$^+$.

1,4-diisopropyl-1,4,7-triazacyclononane, (*i*Pr)₂tacn. (*i*Pr)₂tacnmt (9.45 g, 26 mmols) was dissolved in concentrated sulfuric acid (96 %, 35 mL). The dark solution was heated at 120ºC for 24 hours. After cooling to room temperature, the dark mixture was poured into crushed ice (70 g) and 3 M NaOH (ca. 400 mL) was cautiously added while cooling the mixture in an ice bath until the pH of the mixture exceeded 11. The mixture was extracted with CH_2Cl_2 until the organic extracts were colorless. The organic phases were mixed and after drying with anhydrous $MgSO_4$, the solvent was removed under reduced pressure to yield 5.5 g of brown oil (26 mmols, > 99 %). FT-IR (ATR) ν, cm^{-1}: 3404 (N-H), 2964 – 2871 (C-H)$_{sp3}$. ^{1}H-NMR (CDCl$_3$, 200 MHz, 300K) δ, ppm: 3.75 (br.s, 1H, N**H**), 2.86 (heptet, J = 6.6 Hz, 2H, N-C**H**-(CH₃)₂), 2.68-2.66 (m, 4H, TsN-C**H₂**-CH₂-NH), 2.61-2.55 (m, 4H, TsN-CH₂-C**H₂**-NH), 2.49 (s, 4H, HN-C**H₂**-C**H₂**-NH), 1.00 (d, J = 6.6 Hz, 12H, N-CH-(C**H₃**)₂). ^{13}C-NMR (CDCl$_3$, 50 MHz, 300K) δ, ppm: 52.48 (N-**C**H-(CH₃)₂), 45.96, 43.84, 43.43 (N-**C**H₂-**C**H₂-N), 18.65. ESI-MS (m/z): 213.6 [M+H]$^+$.

5. Synthesis of 1,4-dimethyl-1,4,7-triazacyclononane trihydrobromide, Me₂tacn·3HBr

tacnmt   Me₂tacnmt   Me₂tacn·3HBr
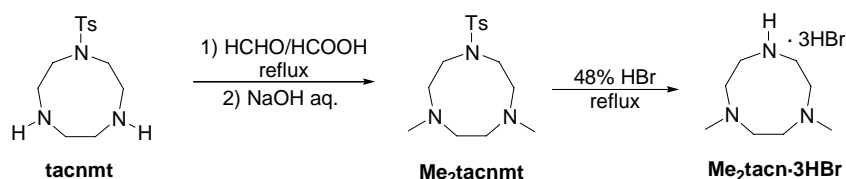
1,4-dimethyl-7-(*p*-toluenesulfonyl)-1,4,7-triazacyclononane, Me₂tacnmt. tacnmt (8.5 g, 30 mmols) was dissolved in 37 % formaldehyde (25 mL) and 98 % formic acid (25 mL) and the resulting orange solution was refluxed for 24 h. After cooling to room temperature, 10 mL HCl cc were added and the mixture was left stirring for 10 min. The solvent was removed under vacuum and a small amount of water (10 mL) was added to the resulting residue. The solution was brought to pH > 14 by addition of NaOH 4 M. This caused the slow formation of a white precipitate corresponding to the desired product. After stirring for 20 h at room temperature, filtration of the mixture gave a white precipitate which was dissolved in 50 mL CH₂Cl₂ giving a pale yellow solution which was treated with 50 mL NaOH 4 M. The aqueous layer was further extracted with 2x50 mL CH₂Cl₂. The combined organic layers were dried over anhydrous MgSO₄ and the solvent was removed under reduced pressure to yield 8.3 g of a crystalline white solid (27 mmols, 90 %). ^{1}H-NMR (CDCl₃, 200 MHz, 300K) δ, ppm: 7.67 (d, J = 8.2 Hz, 2H, Ar**H**), 7.30 (d, J = 8.2 Hz, 2H, Ar**H**), 3.27 – 3.23 (m, 4H, N-C**H₂**-CH₂), 2.92 – 2.88 (m, 4H, N-C**H₂**-CH₂), 2.69 (s, 4H, N-C**H₂**-CH₂), 2.42 (s, 3H, Ar-C**H₃**), 2.39 (s, 6H, N-C**H₃**).

1,4-dimethyl-1,4,7-triazacyclononane trihydrobromide, Me₂tacn·3HBr. Me₂tacnmt (8.6 g, 27 mmols) was dissoleved in 48 % HBr (86 mL) and refluxed for 48 h. After cooling at room temperature, the solvent of the black crude mixture was removed under reduced pressure. Addition of acetone (100 mL) and stirring for 3 hours afforded a fine pale precipitate which was filtered off and washed with acetone. The resulting pale grey solid was dissolved with boiling water (75 mL) and filtered. The solvent from the yellow filtrates was removed under reduced pressure and the resulting residue was treated with absolute ethanol (100 mL). A fine pale yellow precipitated appeared which was filtered off and dried under vacuum to yield 5.3 g of the desired product (13 mmols, 49%). ^{1}H-NMR (D₂O, 200 MHz, 300K) δ, ppm: 3.49 – 3.42 (m, 4H, N-C**H₂**-CH₂), 3.33 – 3.30 (m, 4H, N-C**H₂**-CH₂), 3.22 (s, 4H, N-C**H₂**-CH₂), 2.80 (s, 6H, N-C**H₃**).

6. Synthesis of the final Pytacn ligands

1,4-diisopropyl-7-(2-pyridylmethyl)-1,4,7-triazacyclononane, Py(*i*Pr)₂tacn. 2-Picolyl chloride hydrochloride (0.39 g, 2.3 mmols), (*i*Pr)₂tacn (0.50 g, 2.3 mmols) and anhydrous acetonitrile (10 mL) were mixed in a 25 mL flask. Na₂CO₃ (1 g) and tetrabutylammonium bromide, TBABr (0.04 g) were
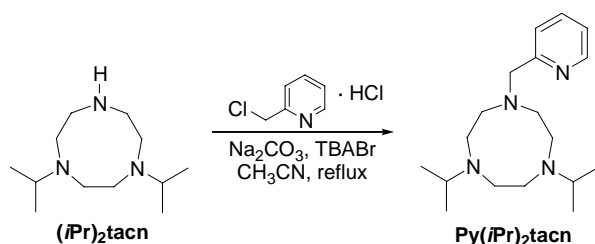
(*i*Pr)₂tacn   Py(*i*Pr)₂tacn

added directly as solids and the resulting mixture was heated at reflux under N₂ for 18 hours. After cooling to room temperature, the yellow mixture was filtered and the filter cake was washed with CH₂Cl₂. The combined filtrates were evaporated under reduced pressure. To the resulting residue,

1M NaOH (20 mL) was added and the mixture was extracted with CH_2Cl_2 (4 x 15 mL). The combined organic layers were dried over anhydrous $MgSO_4$ and the solvent was removed under reduced pressure to yield 0.59 g of a brown oil (1.9 mmols, 83 %). FT-IR (ATR) ν, cm^{-1}: 2964 – 2845 (C-H)$_{sp3}$, 1591, 1362 (py). ^{1}H-NMR (CDCl$_3$, 200 MHz, 300K) δ, ppm: 8.55 (d, J = 6.0 Hz, 1H, py**H**$_\alpha$), 7.66 – 7.62 (m, 2H, py**H**$_\beta$ + py**H**$_\gamma$), 7.17 – 7.13 (m, 1H, py**H**$_\beta$), 3.87 (s, 2H, py-C**H**$_2$), 3.00 – 2.85 (m, 6H, N-C**H**-(CH$_3$)$_2$ + N-C**H**$_2$-CH$_2$), 2.70 – 2.63 (m, 8H, N-C**H**$_2$-CH$_2$), 0.99 (d, J = 6.6 Hz, 12H, CH-(C**H$_3$**)$_2$). ESI-MS (m/z): 305.1 [M+H]$^+$.

1,4-diisopropyl-7-(6-methyl-2-pyridylmethyl)-1,4,7-triazacyclononane, 6Me-Py(*i*Pr)$_2$tacn. 6Me-PyCH$_2$Cl (0.98 g, 5.5 mmols), (*i*Pr)$_2$tacn (1.18 g, 5.5 mmols) and anhydrous acetonitrile (30 mL) were mixed in a 50 mL flask. Na$_2$CO$_3$ (2.4 g) and tetrabutylammonium bromide, TBABr (0.04 g) were added
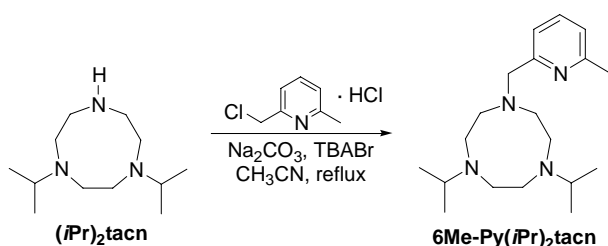
directly as solids and the resulting mixture was heated at reflux under N$_2$ for 18 hours. After cooling to room temperature, the yellow mixture was filtered and the filter cake was washed with CH$_2$Cl$_2$. The combined filtrates were evaporated under reduced pressure. To the resulting residue, 1M NaOH (30 mL) was added and the mixture was extracted with CH$_2$Cl$_2$ (3 x 20 mL). The combined organic layers were dried over anhydrous MgSO$_4$ and the solvent was removed under reduced pressure to yield 1.74 g of a pale yellow oil (5.5 mmols, > 99 %). FT-IR (ATR) ν, cm^{-1}: 2953 – 2853 (C-H)$_{sp3}$, 1455 (py). ^{1}H-NMR (CDCl$_3$, 200 MHz, 300K) δ, ppm: 7.53 (t, J = 7.6 Hz, 1H, py**H**$_\gamma$), 7.39 (d, J = 7.6 Hz, 1H, py**H**$_\beta$), 7.48 (d, J = 7.4 Hz, 1H, py**H**$_\beta$), 3.82 (s, 2H, py-C**H**$_2$), 2.96 – 2.83 (m, 6H, N-C**H**-(CH$_3$)$_2$ + N-C**H**$_2$-CH$_2$), 2.62 (m, 8H, N-C**H**$_2$-CH$_2$), 2.53 (s, 3H, py-C**H$_3$**), 0.97 (d, J = 6.6 Hz, 12H, CH-(C**H$_3$**)$_2$). ^{13}C-NMR (CDCl$_3$, 50 MHz, 300K) δ, ppm: 160.65, 157.24 (py**C**$_q$), 136.34 (py**C**$_\gamma$), 120.94, 119.69 (py**C**$_\beta$), 64.02 (py-**C**H$_2$-N), 55.63 54.71, 52.77, 52.41 (N-**C**H$_2$-C + N-**C**H-(CH$_3$)$_2$), 24.39 (py-**C**H$_3$), 18.33 (CH-(**C**H$_3$)$_2$). ESI-MS (m/z): 319.3 [M+H]$^+$.
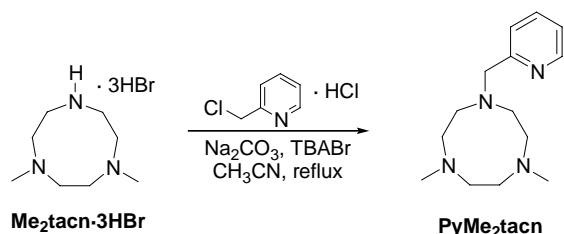
1,4-dimethyl-7-(2-pyridylmethyl)-1,4,7-triazacyclononane, PyMe$_2$tacn. 2-Picolyl chloride hydrochloride (0.43 g, 2.6 mmols), Me$_2$tacn·3HBr (1.02 g, 2.6 mmols) and anhydrous acetonitrile (35 mL) were mixed in a 50 mL flask. Na$_2$CO$_3$ (1.90 g) and tetrabutylammonium bromide, TBABr (0.04 g)

were added directly as solids and the resulting mixture was heated at reflux under N$_2$ for 20 hours. After cooling to room temperature, the resulting yellow mixture was filtered and the filter cake was washed with CH$_2$Cl$_2$. The combined filtrates were evaporated under reduced pressure. To the resulting residue, 1M NaOH (30 mL) was added and the mixture was extracted with CH$_2$Cl$_2$ (3 x 20 mL). The combined organic layers were dried over anhydrous MgSO$_4$ and the solvent was removed under reduced pressure. The resulting residue was treated with n-pentane (50 mL) and stirred for 12 hours. The mixture was filtered and the solvent from the yellow filtrates was removed under reduced

pressure to yield 0.55 g of a pale yellow oil (2.2 mmols, 86 %). FT-IR (ATR) ν, cm^{-1}: 2922 – 2759 (C-H)$_{sp3}$, 1589, 1453 (py).^{1}H-NMR (CDCl$_3$, 200 MHz, 300K) δ, ppm: 8.52 (d, J = 4.8 Hz, 1H, py$\mathbf{H}_\alpha$), 7.66 (t, J = 7.8 Hz, 1H, py$\mathbf{H}_\gamma$), 7.48 (d, J = 7.8 Hz, 1H, py$\mathbf{H}_\beta$), 7.15 (m, 1H, py$\mathbf{H}_\beta$), 3.85 (s, 2H, py-C$\mathbf{H_2}$), 2.86 – 2.80 (m, 8H, N-C$\mathbf{H_2}$-CH$_2$), 2.71 – 2.65 (m, 4H, N-C$\mathbf{H_2}$-CH$_2$), 2.37 (s, 6H, N-C$\mathbf{H_3}$). ^{13}C-NMR (CDCl$_3$, 50 MHz, 300K) δ, ppm: 160.37 (py$\mathbf{C}_q$), 148.87 (py$\mathbf{C}_\alpha$) 136.18 (py$\mathbf{C}_\gamma$), 123.22, 121.75 (py$\mathbf{C}_\beta$), 64.61 (py-C$\mathbf{H_2}$-N), 57.06, 56.86, 55.94 (N-C$\mathbf{H_2}$-C), 46.54 (N-C$\mathbf{H_3}$). ESI-MS (m/z): 249.2 [M+H]$^+$.

1,4-dimethyl-7-(6-methyl-2-pyridylmethyl)-1,4,7-triazacyclononane, 6Me-PyMe$_2$tacn. 6Me-PyCH$_2$Cl (0.44 g, 2.5 mmols), Me$_2$tacn·3HBr (1.00 g, 2.5 mmols) and anhydrous acetonitrile (30 mL) were mixed in a 50 mL flask. Na$_2$CO$_3$ (1.85 g) and tetrabutylammonium bromide, TBABr (0.04 g) were
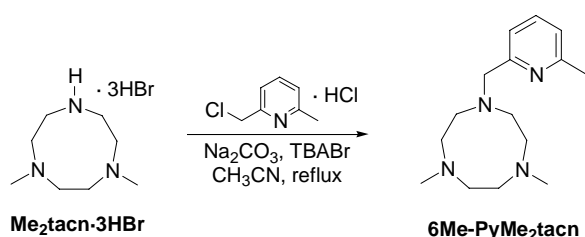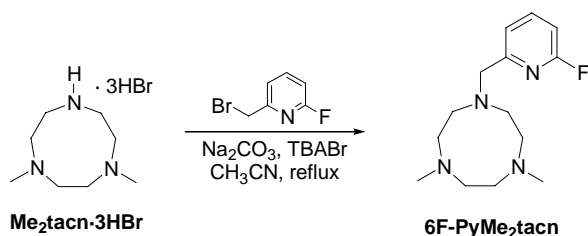

Me$_2$tacn·3HBr   **6Me-PyMe$_2$tacn**

added directly as solids and the resulting mixture was heated at reflux under N$_2$ for 15 hours. After cooling to room temperature, the resulting yellow mixture was filtered and the filter cake was washed with CH$_2$Cl$_2$. The combined filtrates were evaporated under reduced pressure. To the

resulting residue, 1M NaOH (30 mL) was added and the mixture was extracted with CH$_2$Cl$_2$ (3 x 20 mL). The combined organic layers were dried over anhydrous MgSO$_4$ and the solvent was removed under reduced pressure. The resulting residue was treated with n-pentane (50 mL) and stirred for 12 hours. The mixture was filtered and the solvent from the yellow filtrates was removed under reduced pressure to yield 0.60 g of a pale yellow oil (2.3 mmols, 92 %). FT-IR (ATR) ν, cm^{-1}: 2960 – 2802(C-H)$_{sp3}$, 1578, 1456, 1358 (py). ^{1}H-NMR (CDCl$_3$, 200 MHz, 300K) δ, ppm: 7.54 (t, J = 7.6 Hz, 1H, py$\mathbf{H}_\gamma$), 7.29 (d, J = 7.4 Hz, 1H, py$\mathbf{H}_\beta$), 7.00 (d, J = 7.4 Hz, 1H, py$\mathbf{H}_\beta$), 3.82 (s, 2H, py-C$\mathbf{H_2}$), 2.84 – 2.79 (m, 8H, N-C$\mathbf{H_2}$-CH$_2$), 2.68 – 2.66 (m, 4H, N-C$\mathbf{H_2}$-CH$_2$), 2.53 (s, 3H, py-C$\mathbf{H_3}$), 2.36 (s, 6H, N-C$\mathbf{H_3}$). ^{13}C-NMR (CDCl$_3$, 50 MHz, 300K) δ, ppm: 159.85, 157.41 (py$\mathbf{C}_q$), 136.38 (py$\mathbf{C}_\gamma$), 121.16, 119.93 (py$\mathbf{C}_\beta$), 64.83 (py-C$\mathbf{H_2}$-N), 57.20, 57.06, 56.28 (N-C$\mathbf{H_2}$-C), 46.65 (N-C$\mathbf{H_3}$), 24.38 (py-C$\mathbf{H_3}$). ESI-MS (m/z): 263.1 [M+H]$^+$.

1,4-dimethyl-7-(6-fluoro-2-pyridylmethyl)-1,4,7-triazacyclononane, 6F-PyMe$_2$tacn. 6F-PyCH$_2$Br (0.31 g, 1.6 mmols), Me$_2$tacn·3HBr (0.66 g, 1.6 mmols) and anhydrous acetonitrile (25 mL) were mixed in a 50 mL flask. Na$_2$CO$_3$ (1.25 g) and tetrabutylammonium bromide, TBABr (0.03 g) were

Me$_2$tacn·3HBr   **6F-PyMe$_2$tacn**

added directly as solids and the resulting mixture was heated at reflux under N$_2$ for 20 hours. After cooling to room temperature, the resulting yellow mixture was filtered and the filter cake was washed with CH$_2$Cl$_2$. The combined filtrates were evaporated under reduced pressure. To the

resulting residue, 1M NaOH (15 mL) was added and the mixture was extracted with CH$_2$Cl$_2$ (3 x 10 mL). The combined organic layers were dried over anhydrous MgSO$_4$ and the solvent was removed under reduced pressure. The resulting residue was treated with n-pentane (50 mL) and stirred for 12

hours. The mixture was filtered and the solvent from the yellow filtrates was removed under reduced pressure to yield 0.42 g of a pale yellow oil (1.6 mmols, 99 %). FT-IR (ATR) ν, cm^{-1}: 2922 – 2760 (C-H)$_{sp3}$, 1604, 1451, 1367 (py). ^{1}H-NMR (CDCl$_3$, 200 MHz, 300K) δ, ppm: 7.78 (dd, J = 7.4 Hz, J = 2.2 Hz, 1H, py-**H**$_\gamma$), 7.41 (dd, J = 7.4 Hz, J = 2.6 Hz, 1H, py-**H**$_\beta$), 6.81 (dd, J = 8.0 Hz, J = 2.8 Hz , 1H, py-**H**$_\beta$), 3.84 (s, 2H, py-C**H$_2$**), 2.90 – 2.84 (m, 4H, N-C**H$_2$**-CH$_2$), 2.81 (s, 4H, N-C**H$_2$**-CH$_2$), 2.73 – 2.69 (m, 4H, N-C**H$_2$**-CH$_2$), 2.40 (s, 6H, N-C**H$_3$**). ^{13}C-NMR (CDCl$_3$, 50 MHz, 300K) δ, ppm: 162.82 (d, J^{CF} = 237.0 Hz, py**C**$_q$-F), 159.81 (d, J^{CF} = 12.4 Hz, py**C**$_q$-CH$_2$), 141.00 (d, J^{CF} = 7.7 Hz, py**C**$_\gamma$), 120.12 (d, J^{CF} = 4.2 Hz , py**C**$_\beta$), 107.02 (d, J^{CF} = 36.7 Hz , py**C**$_\beta$), 63.53 (py-**C**H$_2$-N), 57.17, 57.04, 55.99 (N-**C**H$_2$-C), 46.67 (N-**C**H$_3$). ESI-MS (m/z): 267.1 [M+H]$^+$

Preparation of pinene-PyMe$_2$tacn. Pinene-PyCH$_2$Cl (388 mg, 1.50 mmols), Me$_2$tacn·3HBr (547 mg, 1.37 mmols) and anhydrous acetonitrile (20 mL) were mixed in a 50 mL flask. Na$_2$CO$_3$ (0.95 g) and tetrabutylammonium bromide, TBABr (0.04 g) were added directly as solids and the resulting mixture

Me$_2$tacn·3HBr → **pinene-PyMe$_2$tacn**
Na$_2$CO$_3$, TBABr
CH$_3$CN, reflux

was heated at reflux under N$_2$ for 20 hours. After cooling to room temperature, the resulting yellow mixture was filtered and the filter cake was washed with CH$_2$Cl$_2$. The combined filtrates were dried over anhydrous MgSO$_4$, filtered and evaporated under reduced pressure. The resulting residue was treated with n-pentane (50 mL) and stirred for 12 hours. The mixture was filtered and the solvent from the yellow filtrates was removed under reduced pressure to yield 255 mg of a pale yellow oil. A second pentane extraction afforded additional 127 mg. Combined yield (382 mg, 1.11 mmols, 81%). ^{1}H-NMR (CDCl$_3$, 200 MHz, 300K) δ, ppm: 8.07 (s, 1H, py-**H**$_\alpha$), 7.28 (s, 1H, py-**H**$_\beta$), 3.83 (s, 2H, **H$_1$**), 3.00-3.98 (m, 3H, **H$_2$**, **H$_4$**), 2.88-2.84 (m, 9H, N-C**H$_2$**-CH$_2$, **H$_5$** exo), 2.75-2.73 (m, 4H, N-C**H$_2$**-CH$_2$), 2.40 (s, 6H, N-C**H$_3$**), 2.35 (m, 1H, **H$_3$**), 1.43 (s, 3H, **H$_6$**), 1.21 (d, 1H, **H$_5$** endo), 0.65 (s, 3H, **H$_7$**). ^{13}C-NMR (CDCl$_3$, 50 MHz, 300K) δ, ppm: 161.28 (py**C**$_q$), 144.95 (py**C**$_\alpha$), 144.73, 140.59 (py**C**$_q$), 122.60 (py**C**$_\beta$), 64.42 (**C$_1$**), 56.93, 56.82, 55.62 (N-**C**H$_2$-C), 46.40 (N-**C**H$_3$), 44.28, 40.06 (**C$_3$**, **C$_4$**), 39.19 (**C$_8$**), 32.76, 31.85 (**C$_2$**, **C$_5$**) 25.96 (**C$_6$**), 21.29 (**C$_7$**). ESI-MS (m/z): 343.3 [M+H]$^+$.

1,4-dimethyl-7-(4-methyl-2-pyridylmethyl)-1,4,7-triazacyclononane, 4Me-PyMe$_2$tacn. 4Me-PyCH$_2$Cl (0.35 g, 2.0 mmols), Me$_2$tacn·3HBr (0.79 g, 2.0 mmols) and anhydrous acetonitrile (25 mL) were mixed in a 50 mL flask. Na$_2$CO$_3$ (1.47 g) and tetrabutylammonium bromide, TBABr (0.03 g) were

Me$_2$tacn·3HBr → **4Me-PyMe$_2$tacn**
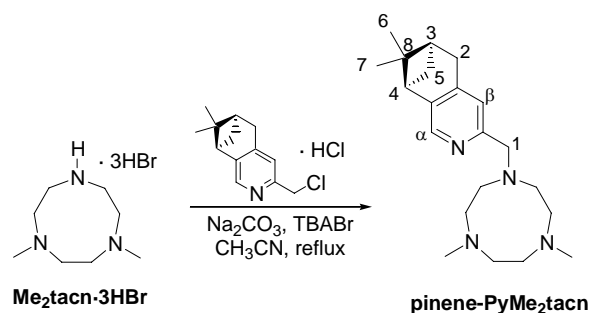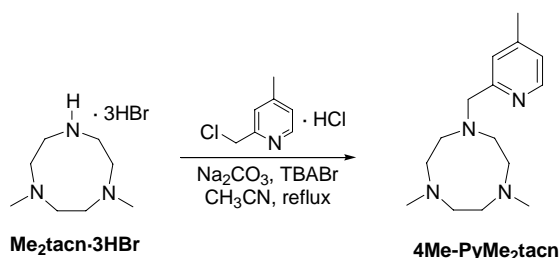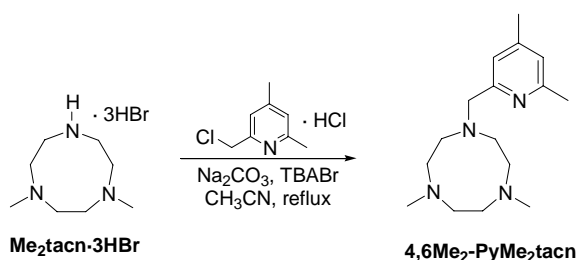Na$_2$CO$_3$, TBABr
CH$_3$CN, reflux

added directly as solids and the resulting mixture was heated at reflux under N$_2$ for 16 hours. After cooling to room temperature, the resulting yellow mixture was filtered and the filter cake was washed with CH$_2$Cl$_2$. The combined filtrates were evaporated under reduced pressure. To the resulting residue, 1M NaOH (30 mL) was added and

the mixture was extracted with CH_2Cl_2 (3 x 10 mL). The combined organic layers were dried over anhydrous $MgSO_4$ and the solvent was removed under reduced pressure. The resulting residue was treated with hexane (70 mL) and stirred for 12 hours. The mixture was filtered and the solvent from the yellow filtrates was removed under reduced pressure to yield 0.35 g of a pale yellow oil (1.6 mmols, 67 %). ^{1}H-NMR (CDCl$_3$, 200 MHz, 300K) δ, ppm: 8.37 (d, J = 5.0 Hz, 1H, py**H**$_α$), 7.29 (s, 1H, py**H**$_β$), 6.96 (d, J = 5.0 Hz, 1H, py**H**$_β$), 3.81 (s, 2H, py-C**H$_2$**), 2.84 – 2.79 (m, 8H, N-C**H$_2$**-CH$_2$), 2.69 – 2.67 (m, 4H, N-C**H$_2$**-CH$_2$), 2.36 (s, 6H, N-C**H$_3$**), 2.35 (s, 3H, py-C**H$_3$**). ^{13}C-NMR (CDCl$_3$, 50 MHz, 300K) δ, ppm: 160.01 (py**C**$_q$), 148.62 (py**C**$_α$), 147.16 (py**C**$_q$), 124.04, 122.77 (py**C**$_β$), 64.35 (py-**C**H$_2$-N), 57.11, 56.96, 55.81 (N-**C**H$_2$-C), 46.55 (N-**C**H$_3$), 21.06 (py-**C**H$_3$). ESI-MS (m/z): 263.3 [M+H]$^+$.

1,4-dimethyl-7-(4,6-dimethyl-2-pyridylmethyl)-1,4,7-triazacyclononane,   4,6Me$_2$-PyMe$_2$tacn.
4,6Me$_2$-PyCH$_2$Cl (0.32 g, 1.7 mmols), Me$_2$tacn·3HBr (0.67 g, 1.7 mmols) and anhydrous acetonitrile (25 mL) were mixed in a 50 mL flask. Na$_2$CO$_3$ (1.24 g) and tetrabutylammonium bromide, TBABr (0.03 g) were added directly as solids and the resulting mixture was heated at reflux under N$_2$ for 16 hours. After cooling to room temperature, the resulting yellow mixture was filtered and the filter cake was washed with CH_2Cl_2. The combined filtrates were evaporated under reduced pressure. To the resulting residue, 1M NaOH (30 mL) was added and the mixture was extracted with CH_2Cl_2 (3 x 20 mL). The combined organic layers were dried over anhydrous $MgSO_4$ and the solvent was removed under reduced pressure. The resulting residue was treated with hexane (70 mL) and stirred for 12 hours. The mixture was filtered and the solvent from the yellow filtrates was removed under reduced pressure to yield 0.31 g of a pale yellow oil (1.1 mmols, 67 %). ^{1}H-NMR (CDCl$_3$, 200 MHz, 300K) δ, ppm: 7.05 (s, 1H, py**H**$_β$), 6.75 (s, 1H, py**H**$_β$), 3.71 (s, 2H, py-C**H$_2$**), 2.78 – 2.71 (m, 8H, N-C**H$_2$**-CH$_2$), 2.62 – 2.57 (m, 4H, N-C**H$_2$**-CH$_2$), 2.41 (s, 3H, py-C**H$_3$**), 2.29 (s, 6H, N-C**H$_3$**), 2.23 (s, 3H, py-C**H$_3$**). ^{13}C-NMR (CDCl$_3$, 50 MHz, 300K) δ, ppm: 159.61, 157.13 (py**C**$_{α,q}$), 147.26 (py**C**$_{γ,q}$), 122.17, 120.85 (py**C**$_β$), 64.47 (py-**C**H$_2$-N), 57.24, 57.11, 55.98 (N-**C**H$_2$-C), 46.67 (N-**C**H$_3$), 24.19, 20.95 (py-**C**H$_3$). ESI-MS (m/z): 277.3 [M+H]$^+$.

Me$_2$tacn·3HBr   **4,6Me$_2$-PyMe$_2$tacn**

Appendix II. Evans' method

The Evans' method allows the measurement of the magnetic susceptibility of substances in solution by nuclear magnetic resonance and thus the calculation of the number of unpaired electrons in paramagnetic complexes. The Evans' method[1] is based on the frequency shift of the NMR signal of a reference compound occasioned by the magnetic field of a co-dissolved paramagnetic compound. In our case, CH_2Cl_2 was used as the internal reference in CD_3CN solutions. A coaxial NMR tube is required for these measurements. The inner tube contains the deuterated solvent together with the reference compound, while the outer tube contains in addition a known amount of the substance of which the paramagnetic moment is to be determined.

The frequency shift of the reference signal between the inner and outer tubes ($\Delta\nu$) produced by the presence of the paramagnetic compound, is used to calculate the mass magnetic susceptibility χ_g ($cm^3 \ g^{-1}$) according to equation 1,[2]

$$\chi_g = -3 \ \Delta\nu / 4\pi \cdot \nu_0 \cdot c + [\ \chi_0 + \chi_0 \ (\ \rho_0 - \rho_s \ ) / c \ ] \qquad (1)$$

where $\Delta\nu$ is the frequency shift in Hz of the reference compound, ν_0 is the spectrometer frequency in Hz, c is the concentration of the complex in $g \cdot cm^{-3}$, χ_0 is the mass susceptibility of the solvent in $cm^3 \cdot g^{-1}$, and ρ_0 and ρ_s are the densities of the solvent and solution, respectively. The term in square brackets disappears because, at the concentrations used (10 – 15 mM), the solution density was approximated as $\rho_s = \rho_0 + c$, and the mass magnetic susceptibility simplifies to

$$\chi_g = -3 \ \Delta\nu / 4\pi \cdot \nu_0 \cdot c \qquad (2)$$

It is important to notice that the original Evans' technique was developed for the cylindrical sample axis perpendicular to the magnetic field,[1] whereas modern instruments generally have magnetic fields parallel to the sample tube axis. For this reason, a factor of $3/4\pi$ appears in equation 1 rather than the original $3/2\pi$.[3]

The chemical shift defined as the difference between the resonance frequency of the nucleus (ν) and a standard ($\nu_{standard}$) with respect to the spectrometer frequency (ν_0) can be used. The chemical shift (δ) is measured in ppm and it is defined as described in equation 3,

$$\delta = (\nu - \nu_{standard}) \cdot 10^6 / \nu_0 \quad (3)$$

This allows the conversion of the $\Delta\nu/\nu_0$ term into,

$$\Delta\nu/\nu_0 = \Delta\delta \cdot 10^{-6} \qquad (4)$$

where $\Delta\delta$ is the difference in the chemical shift of the reference compound between the inner and outer tubes measured in ppm.

Substitution of equation 4 into equation 2 gives equation 5,

$$\chi_g = -3 \ \Delta\delta \cdot 10^{-6} / 4\pi \cdot c \qquad (5)$$

By multiplying the χ_g values by the molecular weight, M ($g \cdot mol^{-1}$), the molar magnetic susceptibility χ_m ($cm^3 \cdot mol^{-1}$) is obtained according to equation 6.

$$\chi_m = \chi_g \cdot M \qquad (6)$$

χ_m is corrected for the diamagnetic contributions of ligands, counterions and metal core electrons using the sum of tabulated Pascal's constants[4] to give a corrected molar susceptibility χ_m':

$$\chi_m' = \chi_m + \Sigma\chi_\alpha \qquad (7)$$

where $\Sigma\chi_\alpha$ is the sum of Pascal's constants in $cm^3 \cdot mol^{-1}$ of the diamagnetic species in the sample.

χ_m' is used to calculate the effective magnetic moment μ_{eff} (in MB) using equation 8,

$$\mu_{eff} = 2.828 \, (\chi_m' \cdot T)^{1/2} \quad (MB) \quad (8)$$

where T is the temperature in K.

Sample preparation

NMR samples for susceptibility measurements using the Evans' method were prepared using special coaxial insert tubes purchased from Wilmad Glass Co. An exact amount of the iron complex (3 – 4 mg) was dissolved in 0.4 mL CD_3CN containing 2 μL of CH_2Cl_2 and the resulting solution was placed in the outer tube of the coaxial tube. The inner tube contained the reference solution prepared by adding 1 μL of CH_2Cl_2 in 0.2 mL CD_3CN. ^1H-NMR spectra of the samples showed two different signals for CH_2Cl_2 corresponding to inner and outer tubes. The difference in the chemical shift between the two peaks ($\Delta\delta$ in ppm) was used to determine the effective magnetic moment (μ_{eff}) following the equations described above.

References

1. Evans, D. F., *J. Chem. Soc.* **1959,** 2003-2005.
2. Bryliakov, K. P.; Duban, E. A.; Talsi, E. P., *Eur. J. Inorg. Chem.* **2005,** 72-76.
3. Naklicki, M. L.; White, C. A.; Plante, L. L.; Evans, C. E. B.; Crutchley, R. J., *Inorg. Chem.* **1998,** *37*, 1880-1885.
4. Drago, R. S., *Physical Methods for Chemists.* 2nd ed.; Surfside Scientific Publishers: Gainesville, 1992.